THE BELT OF SCHUPPEN OF NAGALAND AND IMPLICATIONS ON THE TECTONIC FRAMEWORK OF THE INDO-MYANMAR RANGES

KENEISAZO NAGI

DEPARTMENT OF GEOLOGY

NAGALAND UNIVERSITY

KOHIMA CAMPUS, MERIEMA – 797004

2025

THE BELT OF SCHUPPEN OF NAGALAND AND IMPLICATIONS ON THE TECTONIC FRAMEWORK OF THE INDO-MYANMAR RANGES

BY

KENEISAZO NAGI

Submitted in partial fulfilment of the requirement of the

Degree of Doctor of Philosophy in Geology

of Nagaland University

2025

PLAGIARISM-FREE UNDERTAKING

Name of Research Scholar	Mr. Keneisazo Nagi
Ph.D. Registration Number	Ph.D/GEL/00090 of 30th August, 2017
Title of Ph.D. thesis	The Belt of Schuppen of Nagaland and Implications on the Tectonic Framework of the Indo-Myanmar Ranges
Name & Institutional Address of the Supervisor	Dr. C. M. Khuman, Department of Geology, Nagaland University, Kohima Campus, Meriema - 797004
Name of the Department & School	Department of Geology / School of Sciences
Date of submission	28 February 2025
Date of plagiarism check	28 February 2025
Percentage of similarity detected by the DrillBit software	9%

I hereby declare / certify that the Ph.D. thesis submitted by me is complete in all respects, as per the guidelines of the Nagaland University. I also certify that the thesis (soft copy) has been checked for plagiarism using DrillBit plagiarism detection software. It is also certified that the contents of the electronic version of the thesis are the same as the final hard copy of the thesis. A copy of the report generated by the DrillBit plagiarism detection software is also enclosed.

Date: (Name and Signature of the Scholar)

Place:

Name & Signature of the Supervisor with sea

NAGALAND UNIVERSITY

February 2025

DECLARATION

I, Mr. Keneisazo Nagi, hereby declare that the subject matter of this thesis is the record of work done by me and that the contents of this thesis did not form basis of the award of any previous degree to me or to the best of my knowledge to anybody else. It is also declared that the thesis has not been submitted by me for any research degree in any other University/Institute.

This thesis is submitted to the Nagaland University, in partial fulfilment for the degree of Doctor of Philosophy in Geology.

Candidate

Head Supervisor

NAGALAND UNIVERSITY

Chabungbam Mangi Khuman
Assistant Professor
Department of Geology

Kohima Campus, Meriema - 797004

Mobile 8789899916
E-mail mangikhuman@yahoo.com
mangikhuman@nagalanduniversity.ac.in

CERTIFICATE

The thesis presented by Mr. Keneisazo Nagi, M.Sc in Geology., bearing Registration No. Ph.D/GEL/00090 (30th August 2017) embodies the results of investigations carried out by him under my supervision and guidance.

I certify that this work has not been presented for any degree elsewhere and that the candidate has fulfilled all conditions laid down by the University.

Place: KOHIMA
Date: 28 Feb 2025

CH. MANGI KHUMAN
Supervisor

Department of Earth Sciences
Manipur University
Chanchipur, Imphal-795 003, Manipur India.

Prof. Soibam Ibotombi
Mobile : 9436028012
E-mail : ibotombi2002@ yahoo.co.uk
soibamibotombi@gmail.com

CERTIFICATE

The thesis presented by Mr. Keneisazo Nagi, M.Sc. in Geology, bearing Registration No. Ph.D/GEL/00090 (30th August 2017) embodies the results of investigations carried out by him under my co-supervision and guidance.

I certify that this work has not been presented for any degree elsewhere and that the candidate has fulfilled all conditions laid down by the Nagaland University.

Place: IMPHAL
Date: 28 February 2025

PROF. SOIBAM IBOTOMBI
Co-Supervisor

ACKNOWLEDGEMENT

At the very outset, I, Thank the Almighty God for all his abundant blessings through my research work which has made this academic pursuit possible.

I am immensely grateful and indebted to my supervisor Dr. Ch. Mangi Khuman who has been an excellent mentor, for his tireless effort to guide me both on and off the field motivating and encouraging me to do better not just in this research but in every aspect of life, without whom this thesis would be in shambles. My deepest gratitude to Professor Soibam Ibotombi, my co-supervisor for his valuable input for the improvement of the thesis. I am also grateful to him for his help in arranging the use of resources at Manipur University.

I am extremely grateful to Professor Santosh Kumar Singh for his motivation, and unwavering support, under whose headship granted me an extension period enabling me to complete this thesis. I am also very thankful to him for allowing me to the use resources of the Department of Geology, Nagaland University.

My heartfelt gratitude to Professor Vikoleno Rino Professor S.K. Srivastava Nagaland University and Professor Maibam Bidyananda of Manipur University for allowing me the use of microscope for Photomicrographs. I am also thankful to Miss Akham Thajamambi, research scholar, at Manipur University for her assistance in this matter.

My heartfelt thanks also go out to Dr. Yengkhom Raghumani Singh, Professor, Manipur University for allowing me the use of his lab for the preparation of ICPMS samples and Mr. Ajoy Kumar, research scholar at Manipur University for assisting in this matter.

My special thanks to Dr. Temsulemba Walling, and Professor G.T Thong for their constant guidance, support, encouragement and motivation. My batch mates Miss Diezeneino Meyase, Dr Mehilo Apon, Dr Akhrulu Vero, Miss Hievinu Olivia Richa,

Miss Mademshila Jamir, Miss Vilavonuo Keditsu, your constant guidance, encouragement and support is deeply appreciated and I am forever indebted to you all.

I am very grateful to Khundrakpam Kumarjit Singh and Mr. Thokchom Nilamani Singh, research Scholar for your assistance in fieldwork and contributions in carrying out the palaeostress analysis.

Special thanks to Mr. Arenlong Aier, Mr. Notoka K., Miss Thejavinuo Mere, Miss W. Liyung Nekong, Miss Bendangtola Longchar, Miss Temjeninla Longkumer, and Miss Sentisenla Jamir, all field enthusiast and research scholars at the Department of Geology Nagaland University. Special thanks to Mr. Arite Khape for his help with the improvement of the graphics and images in the thesis and to all my Seniors, Juniors and friends whose names could not be mentioned, you have my deepest gratitude for your support and encouragement.

I am forever grateful to Mrs. Kshetrimayum Nirmala, wife of Dr. Mangi for always caring for me like her own son in all my visit to Manipur. Your help and care meant I could work without any worry.

Finally, yet not the least, to my parents and siblings, my uncles, aunts and relatives, thank you for your unwavering love, support and encouragement. You have stood with me in difficult times and have been a support system I, can always lean on throughout this endeavour.

PREFACE

The rugged landscape of high mountainous terrain to low lying plains is a sight of beauty and awe. Geologists have always been mesmerized by these structures and have strived to understand the various processes and factor responsible for the formation and origin of these beautiful structures. Schuppen structure refers to an imbricate structure (like stacking of books on a shelves). In the field the study area which is a part of the Belt of Schuppen of Nagaland, different lithological units are juxtaposed in an imbricate manner up against each other.

An attempt has been made in this study to explain the geological field setting observed, resulting due to the orogenesis of the Indo-Myanmar Ranges. Petrography and Geochemical studies are carried out to determine the source of the sediments, calculation of the palaeostress using software and stereonet are some of the techniques applied to understand the present-day field setting of the Belt of Schuppen.

The thesis is compiled as a series of 7 chapters. Chapter 1 gives an introduction to the proposed study area, a general overview including the location map of the study area. The previous work done in the area, the objectives and methodology of the study is also mentioned in this chapter. Chapter 2, Covers the geology of the state and the study area. The various lithological group and formations found are explained in this chapter. Chapter 3 comprises the petrographic and geochemical studies. The various plots of the modal analysis can be found this chapter. Chapter 4 is about the various observations and field settings of the studied section *viz.* Pimla to Old Jalukie, Chumukedima to Piphema and Nuiland to Zhadima. The various structural, geological map and geological profile sections are explained in this chapter. Chapter 5 and 6 gives the structural aspects of the study. Chapter 5, explains the stress condition of the Belt of Schuppen. Various plots and stereographical projections indicating the palaeostress of the study area can be found in this chapter. Chapter 6 shows the method and calculations applied for the calculation of shortening in the study area. Finally, in the last chapter various inferences from the above chapters are discussed and the results of the study is summarized to form the conclusion.

CONTENTS

		Page No
Declaration		i
Certificate		ii
Acknowledgement		iii
Preface		iv
Contents		v-ix
List of figures		x-xiii
List of tables		xiv
Particulars of candidate		xv
Bio data of the candidate		xvi-xvii
CHAPTER 1: INTRODUCTION		**1-24**
1.1	Indo-Myanmar Ranges	1
1.2	Belt of Schuppen of Nagaland	4
	1.2.1 Previous Works and Review of Literature	7
1.3	General Account of Nagaland	9
	1.3.1 Geography	10
	1.3.2 Climate	10
1.4	Study Area	11
1.5	Objectives	13
1.6	Methodology	13
	1.6.1 Field Work	14
	1.6.2 Geological Mapping	15
	1.6.3 Laboratory Analysis	16
	1.6.3.1 Stereographic Projections	17
	1.6.3.2 Map Preparation	18
	1.6.3.3 Cross Sectional Profiles	19
	1.6.4 Shortening Calculation	19
	1.6.5 Inductively Coupled Plasma - Mass Spectrometry (ICP -MS)	20
	1.6.5.1 Sample Preparation	21

1.6.6 Petrography 22
1.6.6.1 Preparation of Thin Section 22
1.6.6.2 Modal Analysis 22

CHAPTER 2: GEOLOGICAL TECTONIC SETTING 25-36
2.1 Lithostratigraphy of Metamorphic Complex 26
2.1.1 Nimi Formation 27
2.1.2 Saramati Formation 27
2.1.3 Pokhungri Formation 27
2.2 Lithostratigraphy of Ophiolite Melange Zone 27
2.2.1 Jopi Formation/ Pokphur Formation 28
2.3 Cenozoic Stratigraphic Sequence 28
2.3.1 Disang Group 29
2.3.2 Barail Group 29
2.3.3 Surma Group 30
2.3.4 Tipam Group 30
2.3.5 Dupitila Group 31
2.3.6 Dihing formation 31
2.4 Geo-Tectonic subdivision of Nagaland 31
2.4.1 Belt of Schuppen 31
2.4.2 Inner Fold Belt 35
2.4.3 Ophiolite Belt 36
2.4.4 Metamorphic Belt 36

CHAPTER 3: PETROGRAPHY AND GEOCHEMISTRY 37-48
3.1 Petrography 39
3.2 Trace and Rare Earth Elements Geochemistry 43

CHAPTER 4: FIELD SETTING AND GEOLOGICAL PROFILES 49-83
4.1 Niuland - Zhadima Section 50
4.2 Chumukedima - Piphema Section 58
4.3 Pimla - Old Jalukie Section 72

CHAPTER 5: JOINTS, CONJUGATE FRACTURE AND SLICKENSIDE ANALYSIS **84-119**

5.1 Joint Analysis 86

5.2 Conjugate Fracture Analysis 102

5.3 Slickenside Analysis 113

CHAPTER 6: SHORTENING CALCULATION **120-131**

CHAPTER 7: DISSCUSSION AND CONCLUSION **132-144**

7.1 Discussion 132

7.2 Conclusions 142

BIBLIOGRAPHY **145-154**

LIST OF FIGURES

Figure 1.1 Dextral Shear Deformation mechanism of the IMR (after Soibam, 2006).

Figure 1.2 H.M. Cadel's Experiment as shown by Peach and Horne (1907)

Figure 1.3 The different thrust sheets (shown in different colours) of the Belt of Schuppen (modified after Evan 1932)

Figure 1.4 Map of Nagaland Showing the 17 districts of Nagaland along with the districts (Shaded portion) where the study is carried out (Map Source: Internet, Wikipedia).

Figure 1.5 (a) Location Map showing the three studied section on the map of Nagaland (b) Base Map of Niuland – Zhadima Section (c) Base Map of Pimla – Old Jalukie Section (d) Base Map of Chumukedima – Piphema Section.

Figure 1.6 Flow chart showing the methodology followed for field work

Figure 1.7 Flow chart showing the methodology followed for lab work

Figure 2.1 Geological map of Nagaland (after GSI 2011)

Figure 2.2 Map showing geotectonic classification of Nagaland (after Khuman et al., 2023).

Figure 3.1 Map showing the locations from where samples have been collected.

Figure 3.2 QFR plot of sandstone samples from different points of Chumukedima - Piphema section. Only Barail and Surma Groups of rocks could be studied

Figure 3.3 QFL plot of sandstone samples from different points of Chumukedima - Piphema section. Only Barail and Surma Groups of rocks could be studied.

Figure 3.4 Spider diagrams for REE standard normalisation, (a) representative samples of shale (b) representative samples of sandstone.

Figure 3.5 Spider diagrams for UCC standard normalisation, (a) representative samples of shale; (b) representative samples of sandstone.

Figure 4.1 The dip-strike plot of the beds at different locations of the Niuland – Zhadima Section**.**

Figure 4.2 Geological and Structural Map of Niuland - Zhadima Section and Geological Profiles along AB and BC.

Figure 4.3 Cyclographic plot, Rose-, Pole- and Contour diagrams of (a) AB segment; (b) BC segment and (c) whole of Niuland - Zhadima Section

Figure 4.4 Exposure of various lithologies in Niuland – Zhadima Section (a) Tipam sandstone (b) Conglomerate bed (c) Massive sandstone in Surma (d) Sandstone – Shale alteration in Surma (e) Renji Sandstone (f) Jenam Shales.

Figure 4.5 Various structures observed in Niuland – Zhadima Section (a) Contact between Surma and Tipam (b) Slickenside in Surma sandstone (c) Shearing contact with drag folds on top of Renji sandstone (d) Cross bedding in Surma sandstone (e) Coal streak in Surma sandstone (f) Thrusting in Jenam formation crushing the materials in between the two thrust plane

Figure 4.6 Terrain map of Nagaland showing the Chumukedima - Piphema Section and the three subdivisions of the section.

Figure 4.7 The dip-strike plot of the beds at different locations of the Chumukedima - Piphema Section**; (**a) Segment I, (b) Segment II and (c) Segment III.

Figure 4.8 Geological and Structural Map of Chumukedima - Medziphema Segment (segment I) and Geological Profile along sectional line AB.

Figure 4.9 Geological and Structural Map of Medziphema – Pherima Segment (segment II) and Geological Profile along sectional line BC.

Figure 4.10 Geological and Structural Map of Pherima – Piphema Segment (segment III) and Geological Profile along sectional line CD.

Figure 4.11 Cyclographic plot, Rose-, Pole- and Contour diagrams of (a) Chumukedima - Medziphema Segment (AB) (b) Medziphema – Pherima Segment (BC) (c) Pherima – Piphema Segment (CD) and (d) whole of Chumukedima - Piphema Section.

Figure 4.12 (a) Exposure of Dihing formation (b) Exposure of Namsang Formation (c) Exposure of Girujan Clay (d) Exposure of Tipam Sandstone (e) Exposure of Surma Group. (f) Exposure of Renji formation.

Figure 4.13 (a) Ripple marks in siltstone bed (b) Thrusting in Jenam formation (c) Fold in Shale beds (d) Thrusting between Renji sandstone and Jenam shales (e) Rip up clast in Surma Sandstone (f) Normal Faulting in Jenam formation.

Figure 4.14 The dip-strike plot of the beds at different locations of the Pimla - Old Jalukie Section**.**

Figure 4.15 Geological and Structural Map of the Pimla - Old Jalukie Section.

Figure 4.16: Geological Profile along the sectional line AB of the Pimla - Old Jalukie Section.

Figure 4.17: Cyclographic plot, Rose, Pole and Contour diagrams of the Pimla - Old Jalukie Section.

Figure 4.18 (a) Exposure of Dihing? formation (b) Exposure terrace deposit over Girujan clay (c) Terrace deposit over Tipam sandstone (d) Exposure of Tipam sandstone (e) Exposure of Surma Sandstones in a river bed (f) Exposure of Jenam Formation

Figure 4.19 (a) Closure of a fold (b) Thrust contact between Laisong and Jenam formation (c) Drag fold developed in Jenam shales (d) Petrified wood (e) closure of a pair of Syncline and Anticline

Figure 5.1 Geological map of Nagaland showing the different geotectonic units and the location of the study area.

Figure 5.2 A Schematic representation of different types of joints with respect to compression direction. (a) Tensile fracture (Mode-I) and Shear fracture (Mode-II); (b) Mixed mode or Hybrid fracture (Mode-III).

Figure 5.3 Rose diagrams of beddings and joints. (a) Segment I, (b) Segment II, (c) Segment III, (d) Segment IV.

Figure 5.4 Beta diagrams of the bedding planes of the four segments of the studied section. (a) Segment I, (b) Segment II, (c) Segment III, (d) Segment IV.

Figure 5.5 Projected planes, Pi and Contour diagrams of joints. (a) Segment I, (b) Segment II, (c) Segment III, (d) Segment IV.

Figure 5.6 Relationship between the three principal stresses and conjugate shear surfaces.

Figure 5.7 Block diagrams of three classes of faults predicted by E. M. Anderson.

Figure 5.8 Pi and Contour diagrams of conjugate joints of the section: (a) Segment I, (b) Segment II, (c) Segment III, (d) Segment IV, (e) All Segments.

Figure 5.9 The equal-area stereograms show typical fault and slickenline orientation data for a set of faults within each class. For normal faults and thrust faults, the arrows on the great circles of the stereograms point in the direction of the hanging-wall motion. For strike-slip faults, the arrows on the great circles indicate the sense of shear. After Angelier (1979) in Suppe (1985).

Figure 5.10 Pole and Contour diagrams of 30 slickenside data from the study area

Figure 6.1 Simple schematic diagram showing shortening of material for calculation using Area Balancing Method (modified after Hossack 1979)

Figure 6.2 Simple schematic diagram showing how shortening can be calculated from the original length and final length using line balancing method

Figure 6.3 Photographs showing various minor structures from which shortening is calculated; (a) calculation of crustal shortening from the exposure of a thrust, (b) calculation of crustal shortening from another exposure of a thrust

Figure 6.4 Photographs showing various minor structures from which shortening is calculated; (a) and (b) calculation of crustal shortening from the exposure of two minor folds, (c) calculation of crustal shortening from a seismic profile (seismic profile from the article of Choudhuri et al., 2023).

Figure 7.1 Dextral simple-shear deformation mechanism of the rocks of the rest of Indo-Myanmar Ranges (after Soibam, 2006).

Figure 7.2 Google terrian map showing the position of Nagaland in the IMR

Figure 7.3 Schematic model showing the southern part (South of 26º N) of the Belt of Schuppen

LIST OF TABLES

Table 1.1 Plate motion at various points in and around Manipur (after Soibam, 2006).

Table 2.1 Generalised lithostratigraphic succession of the Belt of Schuppen of Nagaland (after GSI 2011).

Table 3.1 Table showing the modal proportion of Quartz, Feldspar and Rock Fragments / Lithic Fragments

Table 3.2 Table Showing REE in Sandstones and Shale samples

Table 3.3 Table Showing UCC elements in Sandstones and Shale samples

Table 4.1 Bedding attitudes at various stations of Niuland - Zhadima Section.

Table 4.2 Summary of Rose and Pole diagrams of Fig. 4.3

Table 4.3 Bedding attitudes at various stations of Chumukedima - Piphema Section

Table 4.4 Summary of Rose and Pole diagrams of Fig. 4.11

Table 4.5 Bedding attitudes at various stations of Pimla - Old Jalukie Section.

Table 4.6 Summary of Rose and Pole diagrams of Fig. 4.17.

Table 5.1 Attitudes of joints from different locations of Chumukedima – Piphema Section.

Table 5.2 Data of 75 conjugate fracture pairs collected from different locations of Chumukedima – Piphema section

Table 5.3 Values of the three principal stresses of the segments- I, II, III, IV and I-IV.

Table 5.4 Slickensides data from different stations of Chumukedima – Piphema section

Table 5.5 The values of the three principal stresses found out from the slickenside data.

Table 6.1 Calculated shortening from various structures

PARTICULARS OF CANDIDATE

NAME OF THE CANDIDATE	: Mr. Keneisazo Nagi
DEGREE	: Ph.D
DEPARTMENT	: Geology
TITLE OF THESIS	: The Belt of Schuppen of Nagaland and Implication on the Tectonic Framework of the Indo- Myanmar Ranges
DATE OF ADMISSION	: 30th August 2017
APPROVAL OF RESEARCH PROPOSAL	: 16th August 2018

Biodata of the Candidate

Research paper published

- Ch. Mangi Khuman, **Keneisazo Nagi**, Soibam Ibotombi, H. Sanatomba, Arenlong Aier, & Notoka, K. (2023). Structural and Geotechnical Approach of Characterization of the Causes of Meriema Landslide Along the Kohima–Wokha Road Section of the National Highway No. 61, Near Nagaland University-Kohima Campus Approach Road Junction, Nagaland, India (pp. 19–45). https://doi.org/10.1007/978-981-99-6395-9_2

Presentation of paper

- *"*Virtual National Seminar on Sedimentation, Tectonics and Metallogeny of North – East India. North-Eastern Hill University, Shillong and Geological Society of India (21st to 23rd September 2020.
- "*The Belt of Schuppen of Nagaland in the tectonic framework of the Indo-Myanmar Ranges*". National Conference on Current Understanding from Indian Sedimentary Basins and Road Ahead & 38th convention of Indian Association of Sedimentologists (IAS). Department of Geology, Centre for advance Studies, University of Delhi. (9th to 11th December 2022).

Workshops and Seminar/Webinars attended

- National Workshop on Sequence Stratigraphy and Basin Analysis, Department of Geology, Nagaland university, Kohima campus, Meriema (26th to 30th November 2018)
- "Geo-Sciences for Society". 4th National Geo-Research Scholars Meet 2020. Organised by Wadia Institute of Himalayan Geology, Dehradun (23rd to 24th June 2020)
- "Recent Advances in Geosciences" national Workshop conducted by Department of Geosciences, Dr. Ambedkar University , Etcherla, Srikakulam on 31st July 2020
- "Recent Earthquakes in Indo-Burmese Ranges" organised by Department of Geology, Pachhunga University College, Aizwal, Mizoram (6th and 7th August 2020)

- e-training on “Earthquake versus landslide with special reference to Mizoram” webinar conducted by Mizoram University on 13th August 2020
- “Fundamentals of Structural Geology”. conducted by RTD, SR, GSITI, Hyderabad (12.08.2020 to 14.08.2020)
- e-Training on “Basic Training Course on Earthquake Geology, Active Fault Mapping and Seismo-tectonic Studies”. Conducted by RTD, CR, GSITI, Nagpur (17.08.2020 to 21.08.2020)
- e-Training on “Fundamentals of Mapping in Tertiary Terrain” exclusively for SC and ST conducted by RTD, NER, GSITI, Shillong from 24.08.2020 to 26.08.2020
- e-Training on “Fundamentals of Palaeontology” conducted by RTD, ER, GSITI, Kolkata (10.09.2020 to 12.09.2020.)
- e-Training on “Basics of Geographical Information System and its Applications” conducted by CGMT Division of GSI Training Institute, Hyderabad from 17.09.2020 to 19.09.2020
- *“*Virtual National Seminar on Sedimentation, Tectonics and Metallogeny of North – East India. Organised by North-Eastern Hill University, Shillong and Geological Society of India (21st to 23rd September 2020.
- e-Training on “Transect Mapping in the Nagaland-Manipur Ophiolite Belt” conducted by RTD, NER, GSITI, Shillong from 05.10.2020 to 09.10.2020.
- “Global Seismology and Tectonics”. International Virtual Workshop organised by the Geoscience & Technology Division, CSIR-NEIST, Jorhat, Assam, India (20th to 30th September 2021.
- “Local Groundwater Related Issues and Participatory Groundwater Management. Online Training course held at Department of Geology, Nagaland University, Kohima, Nagaland organised by Central Ground Water Board, North Eastern Region, Guwahati. (28th February 2022)
- National Conference on Current Understanding from Indian Sedimentary Basins and Road Ahead & 38th convention of Indian Association of Sedimentologists (IAS). Department of Geology, Centre for advance Studies, University of Delhi. (9th to 11th December 2022.

Chapter 1
Introduction

The present work entitled "*The Belt of Schuppen of Nagaland and Implications on the Tectonic Framework of The Indo-Myanmar Ranges*" encompasses a wide spectrum of interdisciplinary areas mainly of structure, tectonics, stratigraphy and sedimentary petrology. The problem for the proposed research work is to find out the extent of the basin in which the sediments were deposited; and how the basin ultimately subjected to compression leading to the generation of the present day field setting of the belt in due course of the orogenesis and evolution of the Indo-Myanmar Ranges (which was earlier known as the Indo-Burmese Ranges). Let me begin with the very concept about the Indo-Myanmar Ranges.

1.1 Indo-Myanmar Ranges

Geologists have always been fascinated by the geology of the North-East India in general and the tectonics of the Indo-Myanmar Ranges (IMR) in particular. Their tectonic setting and evolution have been a source of curiosity. The orogen is one of the most structurally and tectonically complex regions of the world, overloaded with various complicated geological structures such as strike slip faults, thrusts, etc., many of which have to be inferred as they are not day-lighted as one would see in the textbook styles or because they are covered by the lush vegetation of the area. The complexity is also occasionally compounded by various joint planes extending over a large stretch which can be easily confused with bedding planes unless examined and judged with a certain degree of expertise.

The approximately 1200 km long narrow sigmoidal belt, Indo-Myanmar Ranges (IMR), linking the Arunachal Himalaya to the north and Andaman-Nicobar Islands to the south, has three distinct segments from south to north viz Arakan Yoma, Chin Hills and Manipur-Naga Hills, each of about 400km length (Brunnschweiler 1966). There are a number of opinions about the generation of the IMR. The IMR owes its orogeny to the continental–continental collision (Acharyya et al., 1986) between the Indian and Eurasian plates (Molnar and Tapponier, 1975; Aier et al., 2011). The Myanmar continental micro-plate from the East overrides the eastern fringe of the Indian continental plate (N. C.

Ghose et al., 2014; Singh, 2017), causing the various structural arrangements observed today and resulting in it being one of the most seismically active regions in the world (Tapponnier et al., 1986.; Singh 2017).

Analysis of plate kinematics in and around Manipur by Soibam (2006) reveals that the structural and tectonic features of the Indo-Myanmar Ranges (IMR) have been evolved as a result of interaction between the Indian and Myanmar plates rather than Indian and Eurasia plates or Myanmar and Eurasian. Soibam (2006), also computed plate motion in and around in Manipur using rotation vectors given by various workers (e.g. De Mets et al, 1990; Minster and Jordan, 1978; Curry et al, 1976), which is shown the Table 1.1.

Table 1.1: Plate motion at various points in and around Manipur (after Soibam, 2006).

Plate pairs	24°N, 93°E	22°N, 93°E	25°N, 94.5°E	26°N, 94°E
${}_{E}V_{I}$	5.45cm.yr^{-1} N17.7°E	5.47cm.yr^{-1} N18.6°E	5.49cm.yr^{-1} N17.9°E	5.46cm.yr^{-1} N17.3°E
${}_{E}V_{M}$	3.50cm.yr^{-1} N9°W	3.54cm.yr^{-1} N12.1°W	3.34cm.yr^{-1} N6.3°W	3.36cm.yr^{-1} N
${}_{M}V_{I}$	2.71cm.yr^{-1} N50°E	2.92cm.yr^{-1} N53°E	2.75cm.yr^{-1} N46°E	2.59cm.yr^{-1} N44°E

Note: I - India, E - Eurasia, M – Myanmar

From the analysis it is observed that relative motion of Indian plate with respect to Eurasian plate (${}_{E}V_{I}$) is almost parallel to NNE, the tectonic strike of the region and, therefore, such a motion cannot produce compression structures which are parallel to the motion. Similarly, ${}_{E}V_{M}$ is towards N only slightly different from the regional strike and so, may not be responsible for the evolution of structural and tectonic features of the region. Thus, ${}_{M}V_{I}$, which moves towards NE, induces a dextral shear couple deformation mechanism of the region to produce the tectonic features of the study area in particular and the Indo-Myanmar Ranges in general. Such a deformation mechanism caused the rocks of the region to have been compressed in the WNW-ESE (E-W) and extended in the NNE-SSW (N-S) directions (Fig. 1.1). And such a deformation mechanism is responsible for evolution of the Indo-Myanmar Hill Ranges leading to the present

juxtaposition of the litho-units of the region in due course of subduction orogenesis on account of subduction of the Indian plate below the Myanmar micro-plate.

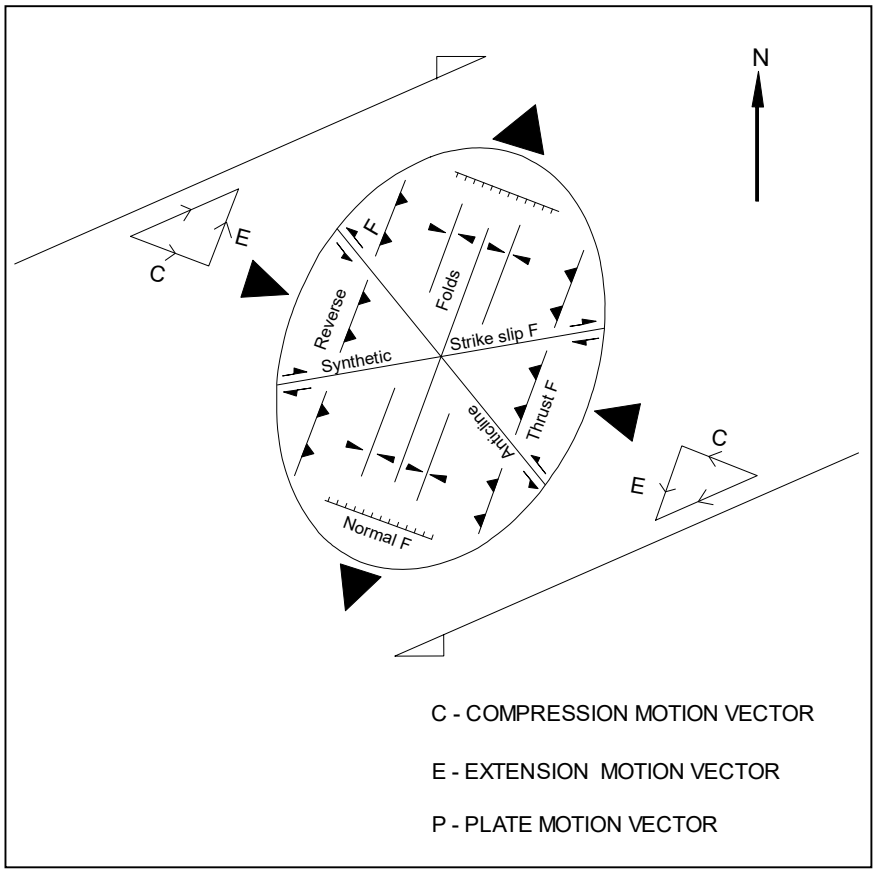

Fig. 1.1: Dextral Shear Deformation mechanism of the IMR (after Soibam, 2006).

The Manipur-Naga Hills segment is the northernmost part of the IMR. The state of Nagaland lies in the northern part of the Manipur-Naga Hills segment. Nagaland, for the most part, is hilly, except for the low-lying alluvial tracts bordering the Assam valley. The constituent ranges of the Naga Hills are characterized by intense folding and thrusting, and these are the result of the various phases of the Tertiary orogenic upheavals of the IMR. There is an imbricate system on the western part of the Manipur-Naga Hills segment of the IMR in the form of a long narrow belt. The belt could be observed as a series of thrusts stacked upon one another, forming an imbricate structure designated as the Belt of Schuppen.

1.2 Belt of Schuppen of Nagaland

The Schuppen Structure, or Schuppenstruktur, was first used by Eduard Seuss (1885) to describe structures in the Alps where several thrusts were observed stacked upon each other. Henry Cadel (1889) performed an experiment that recreated a group of thrusts stacked upon one another. He also termed it Schuppenstruktur, inspired by the usage of the term by Eduard Seuss. Based on his experiment, workers like Peach and Horne (1907) described and illustrated an array of steeply dipping minor thrusts (Fig. 1.2) detached on the basal surface (Sole Thrust). This concept later came to be known as Thin Skin Tectonics.

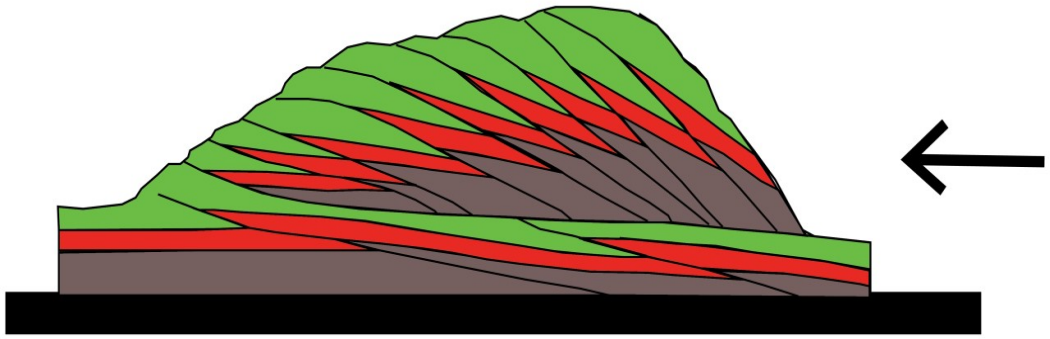

Fig. 1.2: Schematic diagram of H.M. Cadel's Experiment as shown by Peach and Horne (1907).

W.H. Hobbs (1893) used the term Weather-board Structure to describe the structures of the Housatonic valley lying west of Mount Washington, where he observed rocks that undergo sharp compression formed folds that found relief of pressure in the slight dislocations or thrusts and produced the Schuppenstruktur. He later opted to use the term imbricate structure, on the suggestion of a Mr Bernard Hobson. An imbricate structure in Geology is used to describe structures consisting of a series of overlapping rock slices separated by steeply inclined subparallel reverse faults and bounded above and below by major low-angle thrust surfaces, resembling an arrangement of house roof tiles overlapped one above the other. The word imbricate originates from the Latin *imbricare*, which means 'to form like a gutter tile' (Oxford Universal Dictionary).

The Schuppen Belt of Nagaland (Fig. 1.3) has been defined as a narrow linear belt of about 350 km stretch and a major portion of it passes along the hill ranges bordering the alluvium plains of Assam. The litho-units in the Schuppen Belt are juxtaposed against each other along various imbricate thrust sheets, the oldest being in the east and the youngest in the west (Evans 1932). The major limiting thrusts are the Disang thrust on the east and the Naga thrust on the west. It has been reported that in some sections across the Belt of Schuppen in Nagaland there are about eight thrust namely Naga Thrust, Changpang Thrust, Lakhuni Thrust, Konkan Thrust, Chongliyimsen Thrust, Piphema Thrust, Chaneh Thrust and Disang Thrust (Ghosh et al 2014). All the thrusts of the belt are dipping towards SE. The BoS starts from upper Assam in the north and ends where the Disang thrust merged with the E-W trending Dauki fault near Haflong in Lower Assam in the south. Sedimentary sequences in the belt range in age from Eocene-Oligocene to Plio-Pleistocene and are characterized mainly by those of the Groups of Barail, Surma, Tipam and Dupitila (in the chronological order of oldest to youngest). The Barail Group comprises flysch sediments while the rest are mollassic sediments. The mollasse sediments except in some horizons of Surma Group are poorly consolidated making successful petrographic study of all the arenaceous components challenging.

The recognition of the types of litho-units in the field is not easy, since they are not in sequential order. The litho-characters of the sediments particularly of Tipam sandstones and Surma sandstone are also very similar making it extremely difficult to differentiate it. The majority of the rocks are soft, closely jointed, and weathered. The area is also thickly vegetated covering most of the structural elements, so the confirmation and inference of a thrust is carried out using evidence of juxtaposition of different litho-unit. Most of the litho-units exposed across the belt are poorly consolidated. Thus, a successful petrographic study of all the arenaceous components becomes challenging.

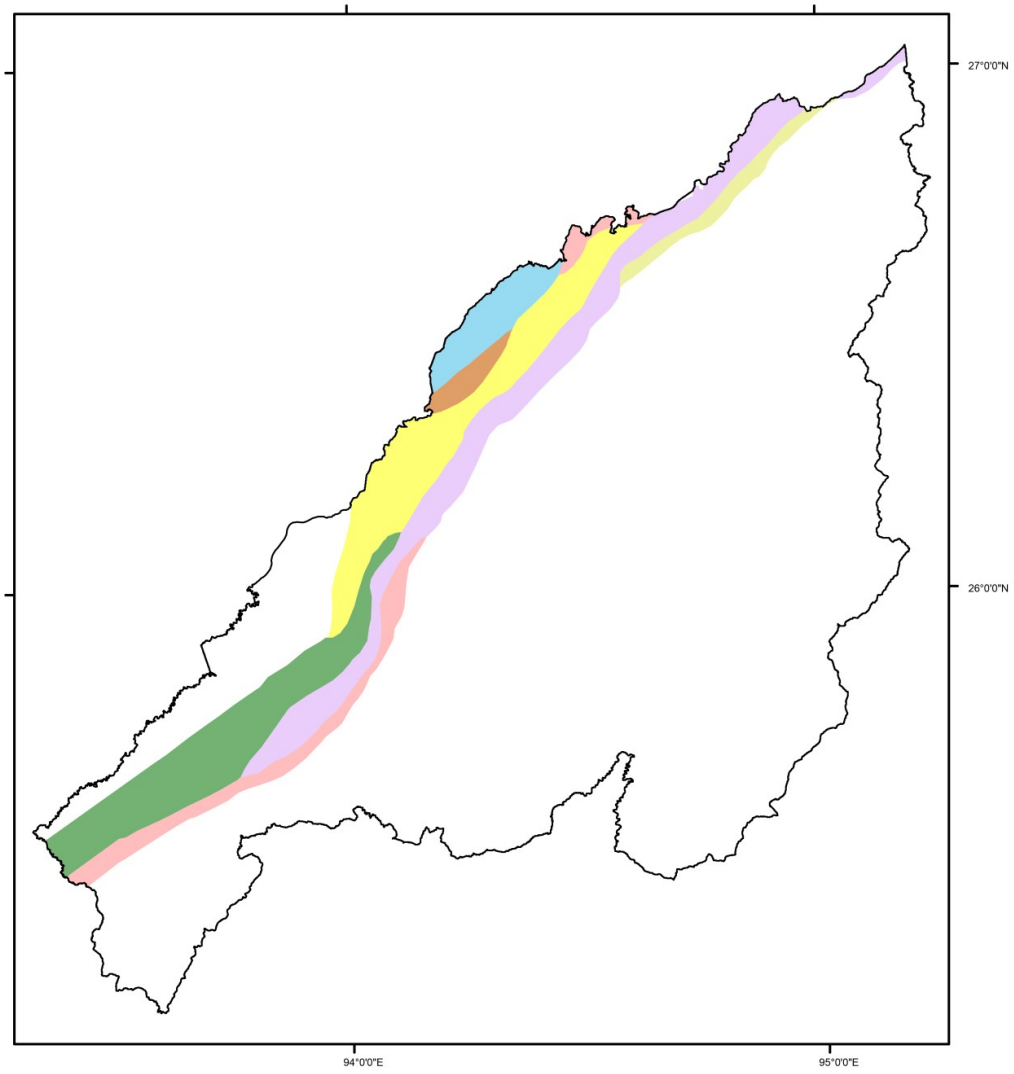

Fig. 1.3: The different thrust sheets (shown in different colours) of the Belt of Schuppen of Nagaland (after Evan 1932).

There have been growing recent international scientific interests in the geology and tectonics of the Indo-Myanmar Ranges (IMR). Soon after the concept of ocean floor subduction became accepted, the International SETAR Workshop (SETAR – Studies in East Asian Tectonics and Resources) in Bangkok in 1974 identified the Indo-Myanmar transect as the prime project in East Asia for understanding the structural and tectonic evolution of active convergent continental margin. Fieldwork in this transect was never carried out for political reasons, rather than funding reasons. Interest in the mountain ranges' evolution has continued to grow with the realization that they are probably one of

the best global examples of a relatively un-eroded but high-relief forearc ridge situated between a subducting sediment-filled remnant ocean basin (Bengal Delta) and well-preserved forearc basin (Chindwin-Minbu), all of it above sea level. The mountain range is thus turning out to be a superb natural museum for geo-scientific research. This is in addition to their potential for revealing the structural processes linking the Himalayas, through the oil and natural bearing collision zone in the Naga Hills, to the Sunda arc.

The aim of undertaking the problem of the proposed research work entitled "*The Belt of Schuppen of Nagaland and Implications on the Tectonic Framework of the Indo-Myanmar Ranges*" is to find out the extent and environment of the basin in which the sediments were deposited; and how the basin ultimately subjected to compression leading to the generation of the present day field setting of the belt in due course of the orogenesis and evolution of the Indo-Myanmar Ranges. The study also aims to provide a logical explanation through the analytical interpretations for a clear picture about the system of forces responsible for the generation of the thrust belt. The paleo-stress conditions in rocks could be deciphered from certain geological structures. Among the different geological structures, the conjugate fractures are regarded as the most conspicuous and least complicated method of evaluation of the principal stress orientations of the stress field. Slickensides are also undoubtedly a convenient method used for the evaluation of orientations of principal stresses.

1.2.1 Previous Works and Review of Literature

The earliest and crude geological mapping in the Naga Hills was pioneered by the British army whose geological observations were published partly in the official report of Topographical Survey for 1872-73 as cited by R.D. Oldham (1883). Oldham (1883) himself gave a detailed report on the geology of the Naga Hill which includes parts of Nagaland. Mallet (1876) gave a comprehensive account of the Nazira coal field. The Systematic geological mapping of different parts in Nagaland; Jalukie Tuensang, Mokokchung, Zunheboto, Wokha, Kohima, and Phek were carried out by Chakradhar and Gaur (1985); Saxena and Yedekar (1979); Bhattacharyya and Sanawal (1985); Srivastava (1983); Devdas and Gandhi (1986); Sarma, H. (1985); Sarma and Bhartiya (1978); Saxena et. al., (1981): geologists of the Geological Survey of India.

The Regional geology and tectonic setting of North-east India, Naga Hills, were published by Roy and Kacker (1980, 1986); and Acharyya et. al., (1986). Mitchel and McKerrow (1975); Molnar and Tapponier, 1975; Bhattacharjee (1997). Acharyya (2010) described the sedimentation, tectonic evolution and regional setting of the Indo-Myanmar ranges.

Geological mapping of Ophiolites was carried out by many workers like Singh et al. (1983) and Bhattacharjee (1991). The emplacement history and tectonic evolution of the Naga ophiolites were studied by Acharyya et. al., (2007); Ghose and Agrawal (1989); Jain and Bhowmik (2016). The ophiolites, on the Manipur side of the Indo-Myanmar range, its field setting and petro-tectonic significance on the IMR were carried out by Khuman et. al. (2010). Ibotombi et. al (2012), worked on the structure and Fareeduddin and Dilek (2015); on the petrology of the Ophiolites. Bhattacharyya and Sanawal (1985) gave an early description of the Naga Metamorphics. Vidyadharan et. al., (1986) gave the distribution and description of the major rock types in the Ophiolites and Naga Metamorphics.

Structural accounts of the Belt of Schuppen of Nagaland have been well documented in the works of Evans (1932, 1964), Evans and Mathur (1964). Ranga Rao and Murthy (1980) researched the origin of Naga Thrust, and Srinivasan (2007) gave a regional configuration and seismic pattern of the Belt of Schuppen. The mapping of the belt of Schuppen using geospatial technology was carried out by Ghose et. al., (2010). Balanced cross section and the structural evolution on the Northern part of the Belt of Schuppen in the upper Assam and Arunachal Pradesh in a doctoral thesis of D.P. Monica Saini (2021). The Geomorphic evolution of the Medziphema intermontane in the Belt of Schuppen was accomplished by Aier et. al., (2011).

Ichnological studies in the upper Disang of Nagaland were carried out by Singh et. al (2019). The study of the late quaternary deformation in part of the Belt of Schuppen was brought about by Moiya et. al., (2020). Geotechnical investigations of landslides in various areas of Nagaland have been carried out by Jamir et. al (2022), Apon et., al., (2024), and Notoka et.al., (2025). A structural approach to the cause of the landslide was carried out by Khuman et. al. (2023).

1.3 General Account of Nagaland

Nagaland, the 16th state of India is located in the North-Eastern part of India. It shares its border with Assam to the West, Arunachal Pradesh and parts of Assam to the North, Myanmar to the East, and Manipur to the South. Nagaland attained its statehood on the 1st of December 1963. It has an area spanning 16,579 sq. km (C. Jamir et al., 2012), with a population of approximately 19.79 lakh as per the 2011 census of India. With the addition of Meluri the state of Nagaland now has 17 administrative districts (Fig. 1.4). The districts are Chumukedima, Dimapur, Kiphire, Kohima, Longleng, Meluri, Mokokchung, Mon, Niuland, Noklak, Peren, Phek, Shamator, Tuensang, Tseminyü, Wokha and Zünheboto occupied by 17 major tribes along with other subtribes.

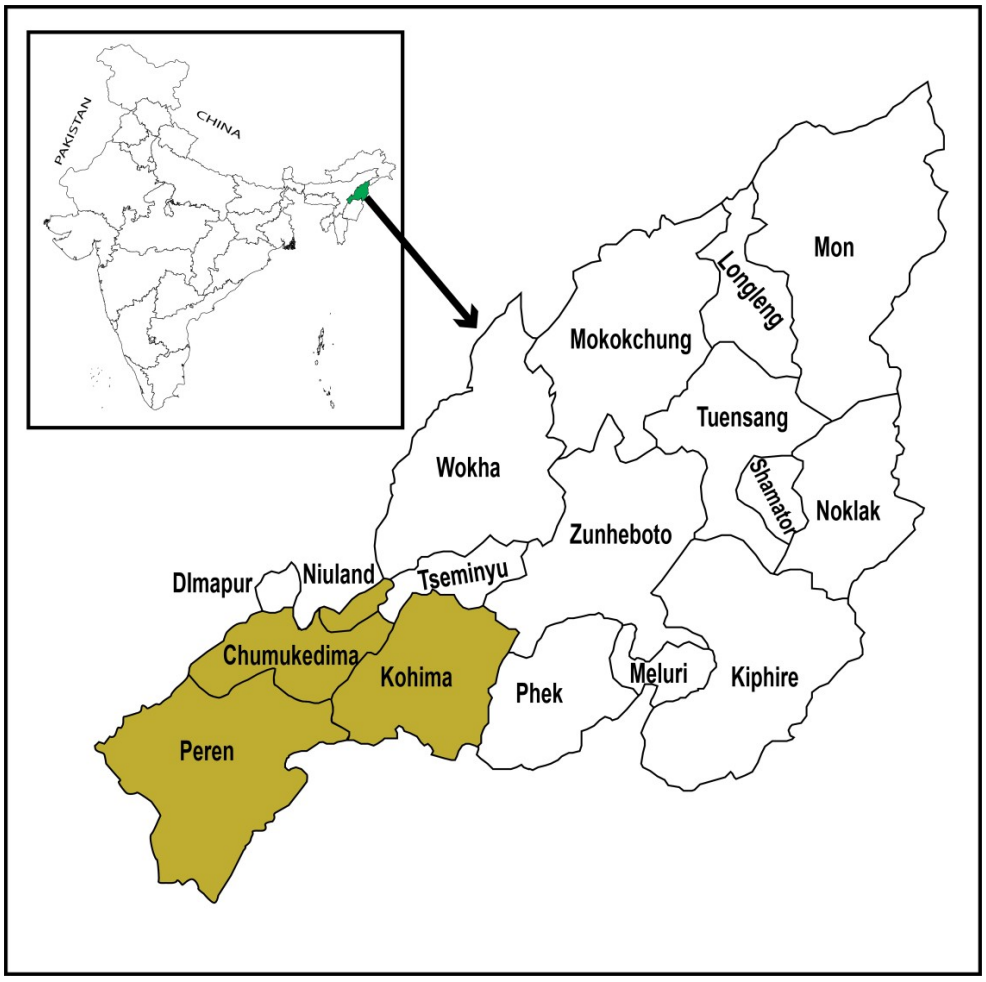

Fig. 1.4: Map of Nagaland Showing the 17 districts of Nagaland along with the districts (Shaded portion) where the study is carried out (Map Source: Wikipedia).

Christianity has had an immense influence on the people of Nagaland and the present day Christian population accounts 87.93% of total population (2011 census). Pre-British era, each village was individually its own republic and had its unique system of social and political administration governed by its unique separate laws and customs. A transition from the age-old traditional governance, laws and customs was observed with the coming of Christianity, brought about by the British.

1.3.1 Geography

Geographically, Nagaland lies between the Assam plains in the West and the Central Myanmar basin to the East, forming the North-Western part of the Indo-Myanmar ranges (D.R. Nandy, 2001). Geomorphologically the areas show terrains of alluvial plains having elevation between 150 to 200 msl, moderate hills between 500 to 800 msl, and high hills above 800 msl.

The rock types control the topography in the belt of Schuppen. Anticlinal hills in the Surma and Tipam formations near the Naga Thrust indicate immature topography (Chakradhar and Gaur, 1985). The hills in Nagaland are generally of heights ranging between 1000 m to 2000 m but, at points in the Patkai range, exceed 3000 m, with the highest peak in Nagaland, Mount Saramati, recording a height of 3840 m, acting as a natural barrier between Nagaland and Myanmar (Evan 1964; A. Balasubramanium, 2017).

The subjugation of the rocks in Nagaland to a roughly E-W compressional stress has resulted in several NE – SW trending folds and faults in the region. The orientation of the folds has guided the drainage of Nagaland, and most rivers have an NE – SW alignment. However, the anticlines do not necessarily represent the hills, nor do the synclines form the stream courses (K. R., Dikshit and J. K., Dikshit, 2014).

1.3.2 Climate

Due to its proximity to the tropics, Nagaland, to a large extent, shows characteristics of a tropical climate. The temperature in the summer ranges from 23º to 40º C, while the temperature in the winter rarely drops below 4º C, though frost is

common at the higher elevations. The state is affected by three seasons: summer, rainy and winter. However, there is a drastic difference in the climatic conditions between the plains and the mountainous region of the state.

Nagaland has a monsoon type of climate with annual average rainfall between 180 cm to 250 cm and receives most of the rainfall during summer, from May to September, with the highest rainfall in June and July. The average temperature decreases with the increase in elevation. Humidity levels are generally high in Nagaland. Rainfall in the region is affected by the proximity to the Bay of Bengal and Brahmaputra and the disposition of other orographic features (K. R., Dikshit and J. K., Dikshit, 2014).

1.4 Study Area

The belt is a narrow stretch running almost in NNE-SSW direction on the western part of Nagaland and crosses the districts of Peren, Chumukedima, Niuland, Wokha, Mokokchung and Mon districts. The study area lies between 25°35' - 26° N latitudes and 93°36' - 94° 05'E longitudes, which covers the southern part of the BoS that lies south of N 26° latitude. The study is carried out along 3 different transverse sections: Niuland – Zhadima section, Pimla – Old Jalukie section and Chumukedima – Piphema, from north to the south, in the Southern part of the Belt of Schuppen exposed in Nagaland (Fig. 1.5a).

Base maps of the study area (Figs. 1.5 b, c, and d) are prepared using Google Earth Imagery, Digital elevation model from Bhuvan, referring to Survey of India toposheet (83 G/9, 83 G/10, 83 G/13 83, G/14, 83 K/1, 83 K/2).

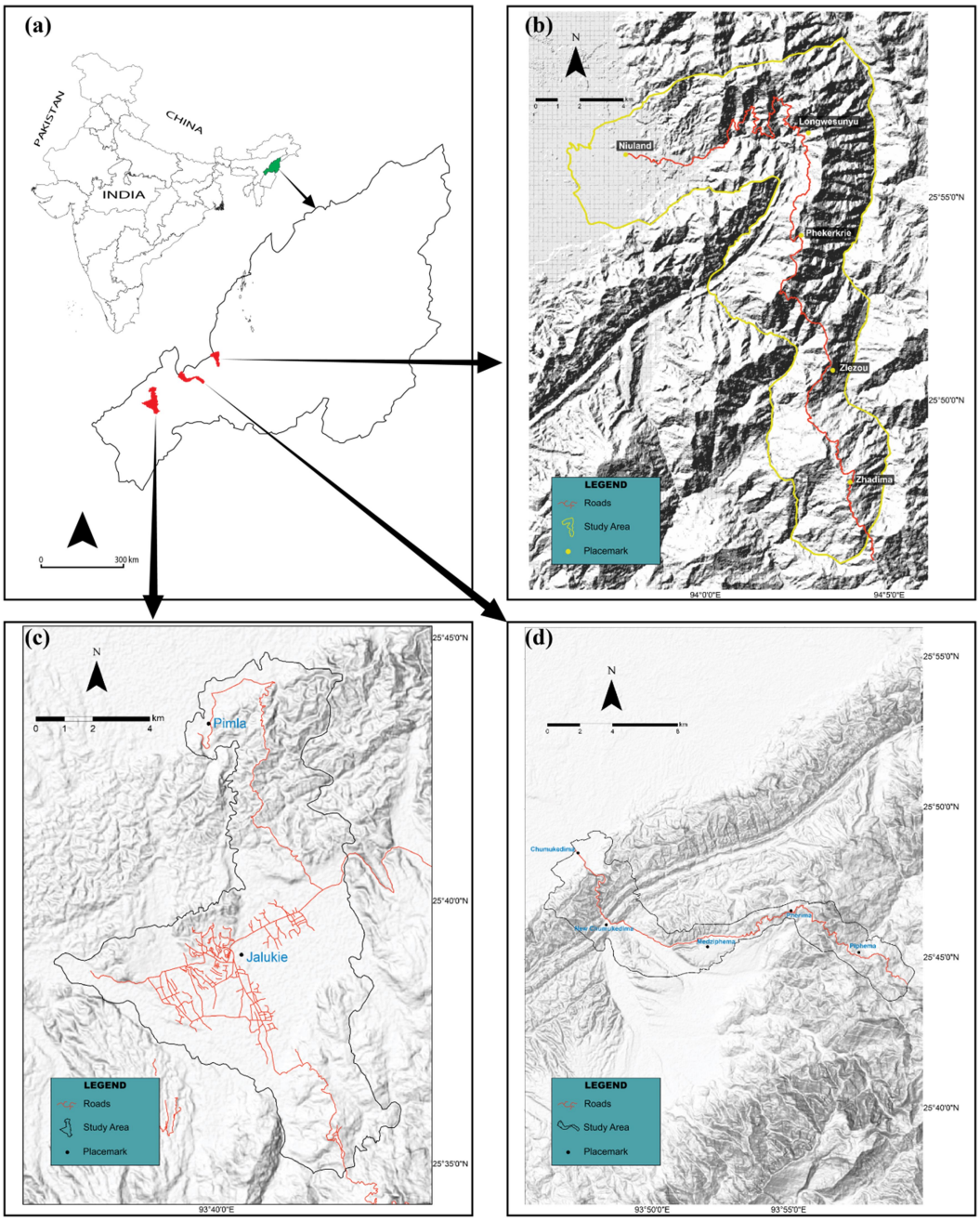

Fig. 1.5: (a) Location Map showing the three studied sections of the southern part of BoS of Nagaland

(b) Base Map of Niuland – Zhadima Section

(c) Base Map of Pimla – Old Jalukie Section

(d) Base Map of Chumukedima – Piphema Section.

1.5 Objectives

The research topic entitled "The Belt of Schuppen of Nagaland and Implication on the Tectonic Framework of the Indo-Myanmar Ranges" is dedicated to ascertaining the extent and how the basin was ultimately subjected to compression leading to the generation of the present-day field setting of the Belt of Schuppen in due course of the orogenesis and evolution of the Indo-Myanmar Range (IMR). The research work also attempts to explain why the belt is restricted, particularly in this area and not along the entire hill range.

Cross-sections are carried across the strike and crustal shortening of the basin is calculated. This calculation may give clues about the role of some of the significant structural lineaments (like the Dauki fault) of the region in the evolution and orogenesis of the Belt of Schuppen.

An attempt is made to decrypt the encrypted geological and tectonic imprints in the joints of the rocks as using it as a tool to understand the system of forces responsible for the generation of these failure planes in relation to the orogenesis of the IMR, to bring out the tectonics of generation of the imbricate thrusts system of the Belt of Schuppen from a residual basin at the later stage of orogenesis of the IMR.

The objectives of the problem of the proposed work are summarised as follows:

- To study the extent of the original basin
- To estimate the quantum of crustal shortening
- To examine the evolution of the Schuppen Belt vis a vis orogenesis of the Indo-Myanmar Ranges

1.6 Methodology

The methodology chiefly involved a series of fieldwork and laboratory studies, over which a number of lithological and structural data and samples were collected, then processed and interpreted.

For a structural geologist, rock beddings and joints are among the important structural elements observed in the field and their structural data such as dip amount, dip directions and strikes of these planes should be recorded properly. These data are used for preparation of various structural plots such as rose diagram, pole diagram etc., which can give the regional trend of the rocks in an area, or presence of folded strata, the principle compression direction or the plunge of synclines and anticlines etc.

The dip amount and orientation of the fault planes and the trend and plunge of various slickenside lineation, observed is recorded along with their pitch or rake. This provides useful information for determination of the palaeostress. Conjugate joints are another type of structural elements which are produced as a result of the stress condition in the region and thus, should be recorded accurately. Corroborated with the slickenside data, conjugate data give good idea of the stress regime in a particular area.

Sedimentary structures like ripple marks, flame structures cross beddings or sole marks etc. also should not be ignored as they are good indicators of whether a bed is overturned or not.

Field photographs are just as important and proper records should be made. Care should be taken that the photos are click from a perpendicular to the exposure to avoid tilting of the images; proper lighting and exposure adjustment will give good photographs of the exposures. These photos can later use be used for references or calculation purposes such as calculation of shortening.

1.6.1 Field Work

To map the different structures and lithology manifested across the Belt of Schuppen Field works were carried out systematically through the completion of the work across the Belt of Schuppen, traversing along 4 different sections. Namely:

1. Pimla to Jalukie Section
2. Chumukedima to Piphema Section
3. Niuland to Zhadima Section

Out of the 3 sections the Chumukedima – Piphema section is selected as an index section and the maximum studies are carried out and data as well as samples are collected at maximum points in this section so as the results of which could help in the interpretation of the geological features in other areas of the southern part of BoS.

Structural geology is highly depended on field observation and correct identification of the lithological and structural units. Intensive fieldwork was carried out to collect a number of structural observations which were later substantiated by various structural analyses of the data in the lab to understand the tectonic setting of the Belt of Schuppen and its implication on the orogenesis of the Indo Myanmar Ranges.

1.6.2 Geological Mapping

Geological map is prepared by traversing along the road sections, the road cut provide good exposure for the study. Base map of Study areas (Pimla – Old Jalukie Section, Chumukedima – Piphema Section, Niuland – Zhadima Section) were prepared after referring Topographic Maps of Survey of India (83 G/9, 83 G/10, 83 G/13 83, G/14, 83 K/1, 83 K/2) on a 1:50,000 Scale and Google Earth Imagery.

In the field all planer surfaces are measured as attitudes in Strike, Dip Amount and Dip Direction and all linear features are measured as attitudes in Strike, trend and plunge along with its Pitch or Rake in the field. A Brunton Compass helps a geologist to measure the strike, dip amount and dip direction of bedding, joints plane or fault plane. It can also be used to measure attitudes of lineation such as the trend and plunge.

The strike of a planer surface is a line where the bedding plane intersects with the horizontal plane. To measure the attitudes of the planer feature, place the edge of the compass parallel to the identified strike line on the bedding surface and bring the bull's eye leveling bubble in the brunton compass to the center. The bearing at either end of the compass needle gives the value of the strike, normally the bearing closer to the north pointing needle is recorded. Now place the edge of the brunton compass perpendicular to the strike line and using the lever on the back move the clinometer so that the bubble in the clinometer level is brought to the center. The angle indicated by the clinometer scale is the measured dip amount of the planer feature. For measuring the dip direction point

the fold out pointer to the direction of the dip. The dip direction is recorded as pointing in a particular directional quadrant (eg. NE, SW etc.), or as an azimuth shown by the north pointing needle (Spencer, 1993) of the compass (eg., 032º, 325º etc).

Slickenside lineation are produced during the motion between two beds therefore it can gives a sense of motion i.e. whether the hanging wall have moved up (thrusted) or down (normal fault) in relation to the hanging wall or whether they have moved sinisterly or dextrally in case of a strike-slipping across the fracture plane. The pitch or rakes of slickenside also known sometimes as slickenline are measured using a protractor laid flat on the fracture plane with the lineation. Place the protractor with the base parallel to strike line and count the angles between the strike line and the lineation, this value gives the rake or pitch of the linear feature. Use the brunton compass to measure the direction of the rake or pitch. The end of the strike line toward which the rake or pitch is measured should also be recorded.

The location of each station point was recorded using a Global Positioning System (GPS) a Garmin Montana 680, which provide up to a 3 meter horizontal accuracy. Field Photographs were taken using a Nikon Camera, which could later be used for references and calculation of shortening across the section. Field notes were made which includes the structural attitudes, lithology observed in the area, field sketches and photo numbers of all the photos taken at each station, lithological or structural contacts, corresponding to its respective locations. Representative samples were collected at strategic locations for the preparation of Thin Sections for Petrography study and ICP-MS samples for Geochemical Study.

1.6.3 Laboratory Analysis

The various data collected from the field are analyzed and validated, to generated data which will contribute to the interpretation of the present day setting observed in the field. The use of computer software is encouraged for quicker calculation and plotting in this day and age, as such structural plots like pole diagram, contour diagrams and rose diagrams are generated using GEOrient 9.4.0, Stereonet 11.6.0, and digitized using Adobe Illustrator 2022. Palaeostress analysis is carried out using Stereonet 11.6.0 and Win Tensor 5.9.2. The three stress direction σ_1, σ_2, σ_3, were calculated using these

softwares whose representative poles and contour diagrams were also prepared using the above mentioned softwares.

1.6.3.1 Stereographic Projection

Stereographic projections are one of the basic tools utilized for structural analysis. While rose diagrams are used to show the various strike orientation of the beds stereographic projections are used to show the variations in the dip of the bed. The dip and strike of Bedding, Joints including conjugate joints, fault planes is projected on a Stereonet using Stereonet 11.6.0. When working with a huge amount of data it is difficult to represent the orientation of all the data. Thus, normal to the plane known as pole is calculated. The poles of all the beds are used for preparing pole diagrams and contour plots. The β axis and π girdle were calculated from these diagram.

The procedure for plotting on a Stereonet is explained below

Plotting a plane

Place a tracing paper on top of a printed equal area stereonet. Count off the strike bearing and mark it on the primitive circle. Rotate the tracing paper to bring the marking to the North position. Count the dip amount based on the dip direction along the east west diameter, from primitive circle toward the center of the stereonet and marking it. Tracing the great circle where both the markings coincide gives a cyclographic trace that projects the plane. Poles to the plane are projected by counting 90º away from the cyclographic traces of the plane. (Marshak and Mitra 1988).

Plotting the rake on a plane

The plane is projected using the procedure as mentioned above. The strike line is brought to the North – South. The rake is measured depending on which side of the strike the linear feature is making an angle with the strike (normally the acute angle side), therefore count the amount of rake inward from the direction of the strike it was measured along the north south great circle. This position is the plot of the rake (Marshak and Mitra 1988).

Determination of principle stress direction

The principle stress directions are determined using Conjugate fracture and slickelines.

a) From Conjugate Fracture

The attitudes of the two planes of the conjugate fractures are plotted as mentioned above. The point of intersection of the two planes is the position of sigma 2. Bring the position of the sigma 2 at the equator of the stereonet and count 90 toward the centre and trace the great circle to draw a plane perpendicular to sigma 2. The intersection point of the acute angle bisector of the two conjugate planes and the plane perpendicular to sigma 2 is the position of the sigma 1. Count 90º from the position of sigma 1 on the same plane to get the position of sigma 3, (Marshak and Mitra 1988). The sigma 3 point coincides with the intersection point of obtuse angle bisector and the sigma 1 plane.

b) From Slickenside/Slickenlines

Plot the attitude of the fault plane as mentioned above and the rake is plotted on the plane as mentioned above. Align the great circle trace projecting the fault plane and count 90 from the position of the lineation, this point is the sigma 2 position. Draw a plane which has sigma 2 as its pole by tracing a great circle. Counting 30 from the slickenline and another 60 from the slickenline to find the position of sigma 1 and sigma 3 respectively (Marshak and Mitra 1988). The direction in which it is counted to determine the position of sigma 1 and sigma 3 is dependent on the sense of motion on the fault plane.

1.6.3.2 Map Preparation

Geological maps and profile sections were prepared with the help of softwares like ArcGIS 10.7 and Adobe Illustrator 2022 for drawing and digitizing purposes. The latitude and longitude of each station along with structural data such as the dip amount and dip direction are imported and projected on the ArcMap interface of ArcGIS 10.7., using appropriate symbols and colour to depict various structures and lithology. The various lithology and their contacts, i.e. either normal stratigraphic contact or tectonic contacts are drawn as shapefiles with the help of field observations recorded, to prepare the geological map of the study area. Create proper legend to explain the symbols used,

indicate the north direction, place a map scale and bound the map with a grid showing the latitude and longitudes (Fossen 2016. McClay 2013, Spencer 2017).

1.6.3.3 Cross Sectional profiles

Cross Sectional profiles are not only a representation of the various exposures observed in the field but also a projection of those beddings into the sub-surface to a certain depth with reasonable accuracy. These are made using ArcGIS10.7 and Illustrator 2022.

Two reference points are chosen on the geological map, this will be the length of the section. A piece of paper is taken and placed across the selected section and small markings are made along the edge of the paper to indicate the position of the various elevation contours. Transfer this marking on a graph paper giving proper scale with the x-axis showing the distance between the two points and the y-axis showing the various elevation points. The markings on the piece of paper are projected to their respective height and are connected by free hand drawing.

Align another piece of paper along the selected section and marks the various lithological contacts and structural contacts. This is then transferred on to the topographic profile and the cross section is drawn referring to the geological map. (McClay 2013, Groshong 2006, Weijermars 1997).

The required topographic elevation profile is extracted from Digital Elevation Model (DEM) (Source: Bhuvan), using ArcGIS 10.7 and the cross sections are prepared from Adobe Illustrator 2022 with the help of the geological map prepared. The traditional hand draw technique of preparing cross section is applied due to lack of bore well and seismic data which many softwares utilize for automatic preparation of cross section.

1.6.4 Shortening calculation

Line balancing technique is used for calculation of the shortening in the study area from folds and thrust observed in the field. These calculations are made by direct measurements from the field photographs. The traces of the fold and faults were

measured using Surfer 21.1.158 computer software to determine the original and final length of the beds, these traces can also be measured using a thread running it along the fold and measuring its length with a scale to get a value of the original length and final length of the beddings. The use of software is preferred as it can provide a more detailed and accurate measurement.

Simple engineering strain formula states that the strain in the ratio between the change in final length and original length to the original length. This concept is applied for the estimation of shortening. Shortening is expressed in percentage as used by (Soibam 1998). A Negative value indicates shortening and positive value suggest extension.

$$e = \left(\frac{Lf - L}{Lo}\right) \times 100$$

Where e = strain (shortening or extension in percentage)

Lf = final length

Lo = original length

1.6.5 Inductively Coupled Plasma – Mass Spectrometry (ICP-MS)

33 Samples, 15 sandstone samples and 18 shales/siltstone samples were collected from the study area and prepared for ICP-MS analysis. The samples were cleaned and washed using distilled water; it was then crushed using an Agate mortar and pastel. Precautions were taken to avoid contamination of the samples.

The samples were crushed and prepared at the Laboratory of Manipur University. Acid digestion method is utilized; Hydrogen Fluoride (HF) is used to digest the silicate bearing minerals like amphiboles, quartz, feldspar etc. Nitric Acid (HNO_3) will help in digesting the salt containing iron zinc iodine etc. as with any technique certain exception are associated with it and this method does not fully dissolve resistant minerals and some secondary minerals such as Barium (Ba) in Barites, Chromium (Cr) in Chromites etc. the prepared samples were sent to Inter University Accelerator Centre (IUAC) for Analysis.

1.6.5.1 Sample Preparation

The following SOP was followed for sample preparation in the laboratory

- Rinse and wash the crucibles and measuring cylinders with Milli-Q water (Ultra-pure water).
- Measure the samples weighing between 0.100g - 0.104 g and transfer it to the crucibles (Teflon crucible).
- Prepare a solution of Hydrogen Fluoride (HF) and Nitric Acid (HNO_3) mixed in the ratio 2:1
- Pour 15to 20 ml of this mixture (HF and HNO_3) into the crucible containing the samples, then add 5 ml of Perchloric Acid ($HClO_4$)
- Keep the samples on a hot plate in moderate temperature until a paste of the solution is formed (1.5 hrs. or more). Higher temperatures hasten the process of paste formation but increase the chance of burning the sample.
- The sample is done when no liquid is left in the crucible and a brownish ring is observed on the edges of the samples
- Cool for 10 to 15 minutes and add 15-20 ml of 10% HNO_3 and reheat the samples for 10 to 15 minutes
- Cool the samples and transfer it into a 50 ml conical flask.
- Fill the conical flask with ultra-pure water till the 50 ml mark.
- Wash the crucible and repeat the process for the next sample

Precautions carried out

- Work in a closed lab where there is little chance of contamination
- All equipment should be washed using ultra-pure water.
- Teflon Crucibles are used as they have very high melting point. (326.8ºC)
- HF is not poured in glass beaker as it reacts with it.
- Wash crucibles with ultra-pure water before the start of every sample preparation
- Wear necessary protective gears (Mask, Gloves and lab Coat) while handling Chemical, like Hydrogen Fluoride which are toxic to humans.
- The sample on the hot plates should by checked periodically to avoid burning of samples

- The gloves may be dipped in water before handling the crucibles to prevent burning the gloves.
- Open the lid of the crucibles on observation of vapors. The vapors form droplets on condensation on the lids. These droplets should be allowed to coalesce and put back into the crucible.

1.6.6 Petrography

Thin section studies were carried in the Department of Geology Nagaland University using Lieca DM 2700P and photomicrographs were taken at Manipur University and Nagaland University with the same model of microscope on a Lieca K3C camera using Lieca Application Suit X 5.2.2.28326.

1.6.6.1. Preparation of Thin Section

The samples collected from the field are washed cleaned and dried, Rock chips approximately 2 cm wide are glued to a glass slide using Araldite and polishing it down to 30 μm. A rock chip from the sample is grinded using motorized grinding wheel to make it as thin as possible after which it is polished by hand using grinding powder made of silicon carbide 120 mesh sizes then slowly increasing the mesh size till 800 mesh size. Then it is finished off by polishing it with diamond paste. The polished surface can now be mounted on a glass slide using araldite as adhesive Canada balsam was used until recently. The above mention polishing techniques is repeated till the required size (30 μm) is achieved (Verma, 2023).

1.6.6.2 Modal Analysis

The various tectonic settings of a basin is a primary factor along with climate, various transport mechanism, their depositional environment etc., that affects the sandstone composition. (Dickenson et al. 1983). The modal analysis for the various samples is plotted using the Quartz (Q), Feldspar (F), and Lithic fragment (L), QFL plot provided by Dickenson and Suczek 1979. The Sandstone were classified on a Quartz (Q),

Feldspar (F), and Rock Fragment (R), QFR plot using the Folks classification (Folk 1980) About 250 to 300 grains were counted for this purpose.

The Q is the representation of all the quartz in the sample (Mono crystalline or Poly crystalline), while F is the representation of all the feldspar (Plagioclase or K-Feldspar) and similarly the L is the representation of all the lithic or rock fragments (Volcanic, Sedimentary or Meta-sedimentary) found the sample. The quartz, feldspar and lithic fragments counted from thin section are recalculated as 100 percent to classify the sandstone and plot the QFL ternary plot regardless of the matrix, cement, heavy minerals or other exotic constituent (Dickenson 1970) to determine the provenance of the samples.

To achieve the objective set to carry out the research problem entitled "*The Belt of Schuppen of Nagaland and Implications on the Tectonic Framework of the Indo-Myanmar Ranges*" the above methodologies are carried out. The methodologies discussed can be summarised as follows:

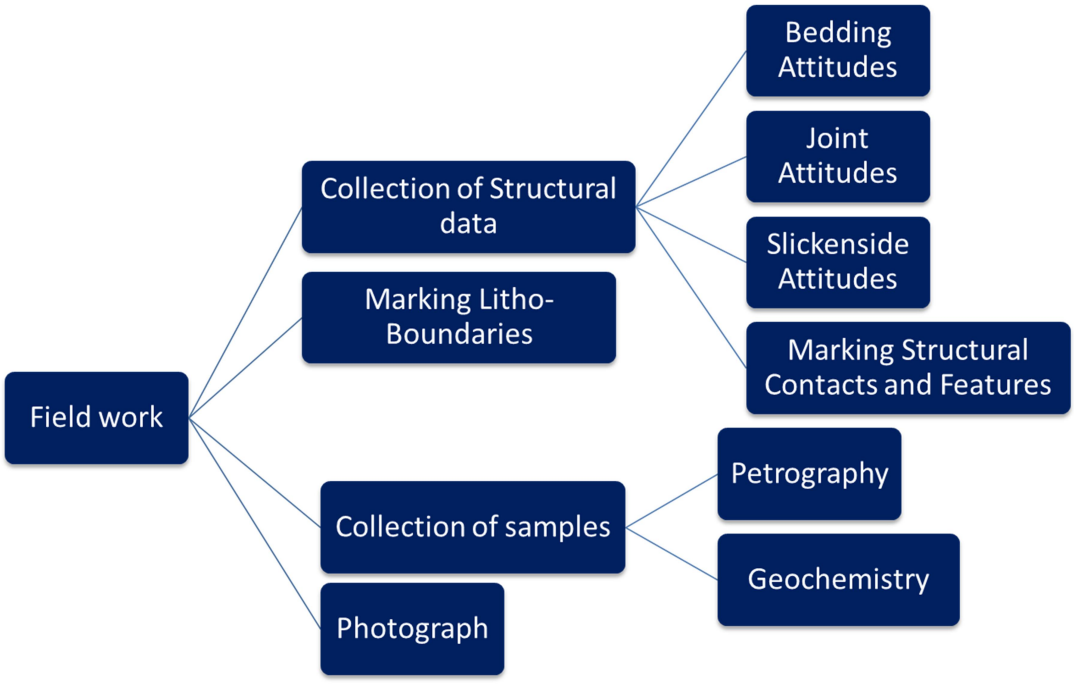

Fig. 1.6: Flow chart showing the methodology followed for field work

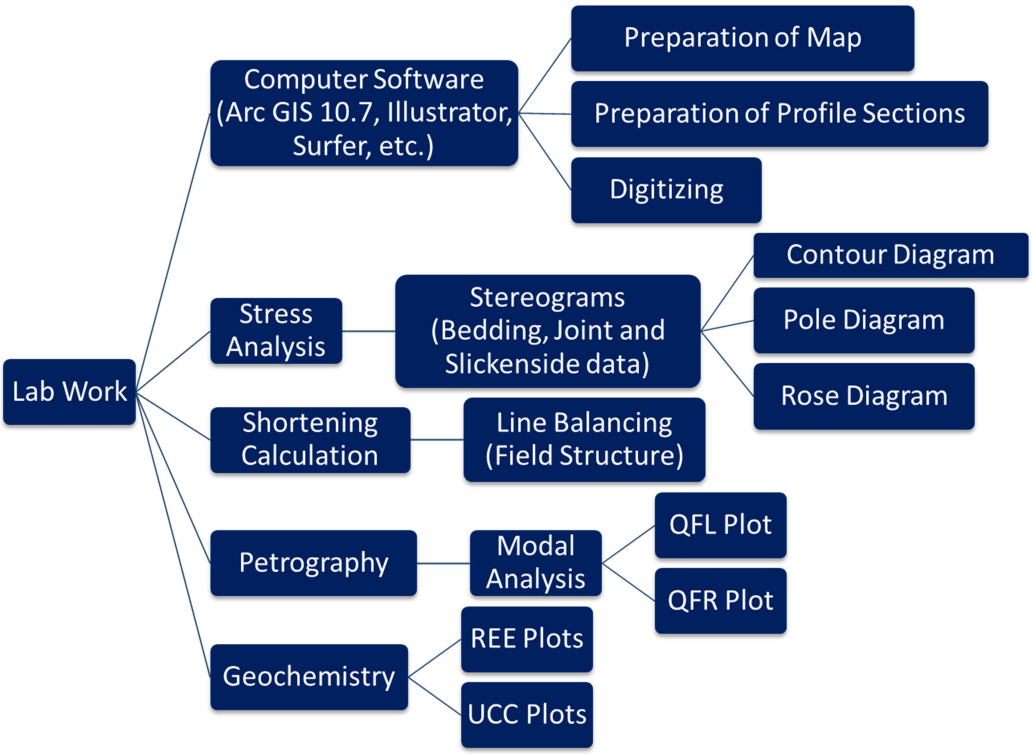

Fig. 1.7: Flow chart showing the methodology followed for lab work

Chapter 2
Geological and Tectonic Setting

The Indo-Myanmar Ranges, which is approximately 1200 km long, is a narrow sigmoidal belt linking with the Arunachal Himalaya to the north and the Andaman-Nicobar Islands to the south. It has three distinct segments from south to north viz Arakan Yoma, Chin Hills and Manipur-Naga Hills, each of about 400 km in length (Brunnschweiler, 1966). The state of Nagaland lies in the northern part of the Manipur-Naga Hills segment. Most part of Nagaland is hilly, except for the low-lying alluvial tracts bordering the plains of Assam. The approximately NNE-SSW to NE-SW trending hill ranges of the state are characterized by their varied distinctive geotectonic features (Evans, 1964). The constituent ranges of the Naga Hills are characterized by intense deformation.

Nagaland is a seismically active region (J. C. Gautam, 2007) of the Indo-Myanmar Ranges (Mathur and Evans, 1964; GSI, 2011). The orogenic belt of the Naga Hills owes its orogenesis to the subduction of the Indian plate below the Burmese plate and constitutes the northern part of the Indo-Myanmar Range (Roy and Kacker, 1980). The eastward subduction has resulted in successive under-thrusting with tectonic emplacement of the turbidites (Michell and Mckerrow, 1975).

The state of Nagaland is comprised of a wide range of litho-units in the sequence of the entire lithostratigraphic column of the earth's evolutionary history (Fig. 2.1). The different lithostratigraphic units of the state are briefly described.

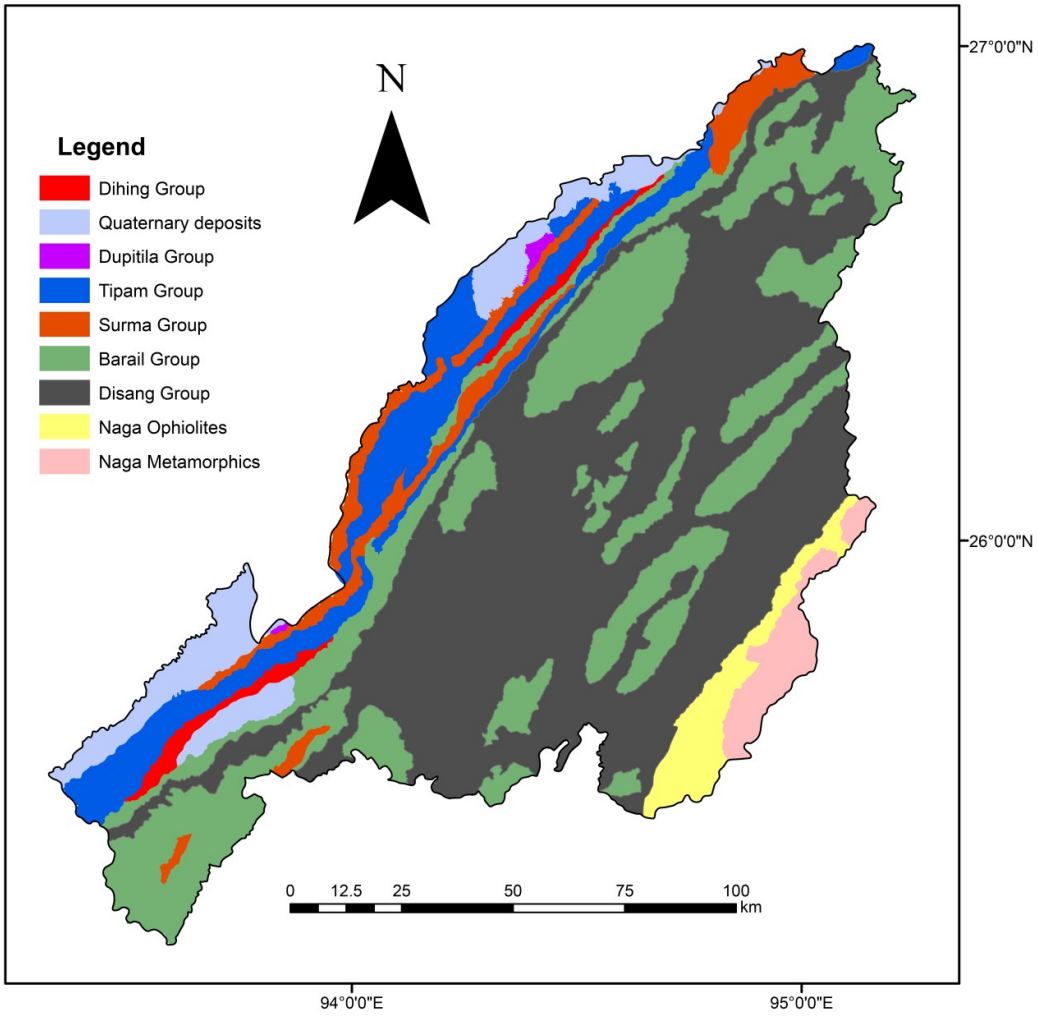

Fig. 2.1: Geological map of Nagaland (after GSI 2011)

2.1 Lithostratigraphy of Metamorphic Complex

The Naga Metamorphics are found in the eastern parts of the Naga Hills. The metamorphic complex is comprised of intensely thrusted group of metasediments. The metasediments are predominantly of low to medium grade phyllitic schist, hornblende schist, quartzite, quartz-sericite schist, mylonite, etc. (Brunnschweiler, 1966). Brunnschweiler (1966) assigned them Pre-Mesozoic or older age but Acharyya et al., (1986), however, stated them to be of Proterozoic age. The Precambrian to Palaeozoic (Bhattacharjee, 1997) meta-sediments are apparently indicative of a neritic environment (Roy and Kacker, 1980) and the absence of flysch type sediments suggests a

miogeosynclinal tectonic setting as observed in lower palaeozoic sediments of Myanmar (M. Thein, 1973). The different formations of the complex are as enumerated below.

2.1.1 Nimi Formation

The metasediments of the Nimi formation are established around Nimi village and defined by the presence of phyllite, quartz sericite schist, quartzite, and limestone intercalated with serpentine (Bhattacharyya and Sanawal, 1985). Thick limestone band with associated feldspathic quartz are common in this formation. The microcline or orthoclase feldspar in the rocks of Nimi formations suggests continental provenance (Nandy, 2001).

2.1.2 Saramati Formation

West of Saramati Mountain, a higher grade of metasediments characterised by muscovite schist, quartz-biotite schist and trending NE-SW is named the Saramati Formation. (Acharya et al., 1982; Bhattacharyya and Sanawal, 1985; Ghose and Agrawal, 1989).

2.1.3 Pokhungri Formation

The rocks of upper part of this formation are phyllitic with presence of quartz sericite schist and chlorite schist while the lower part of the formation is predominantly of quartzites meta greywacke and feldspathic sandstones. It forms a prominent zone to the eastern part of the ophiolites. Between the lower and upper parts of the Pokhungri Formation, contact seems gradational with increasing metamorphic grade from west to east (Singh et al., 1983).

2.2 Lithostratigraphy of Ophiolite Melange Zone

The Ophiolite Melange Zone comprises predominantly of broken blocks of tectonic slices representing various units of the sequence of ancient oceanic lithosphere that include the ultramafic suite, mafic dykes and sills, pillow lavas, pelagic sediments like chert and limestone, etc. in a jumbled manner (Soibam et al., 2015; Khuman and

Soibam, 2022). The Ophiolite melange zone in Nagaland has a very thick linear horizon of conglomerate lying over the ultramafics with a tectonic contact. The fossil assemblages from the associated limestone have suggested the age of the Ophiolites to be of Upper Cretaceous to Lower Eocene (Acharyya et al., 1986; Vidyadharan et al., 1986).

The Ophiolites are believed the remnants of the Tethyan oceanic crust (Roy and Kacker, 1986) and emplaced during the Indo-Australian plate, the Eurasian and Sundra plates collision (Nandy, 1982). It lies between the easterly subducting Indian oceanic lithosphere to the west and the Myanmar plate to the east (Jain and Bhowmik, 2016) and occurs as rootless bodies over flysch sediments (Bhattacharjee, 1991; *Acharyya,* 2010).

The Ophiolites are in sharp juxtaposition with the younger accretionary prism of Disang rocks (Fareeduddin and Y. Dilek, 2015; Singh et al., 1983) to the west and the older accretionary prism of Nimi Formation to the east (Roy and Kacker, 1980; Fareeduddin and Dilek, 2015; Ghose and Agrawal, 1989). The following paragraphs are briefly discussed about the litho-units of the complex.

2.2.1 Jopi Formation/ Pokphur Formation

The upper Eocene – Miocene Jopi Formation of Ophiolite-derived sediments is referred to as the Pokphur Formation by Chattopadhyay et al., 1983, Ghose and Agrawal, 1989. These are a thick sequence of conglomerate, sandstone, shale or phyllitic rocks that unconformably overlie the ophiolite melange (Fareeduddin and Dilek, 2015). The alkaline feldspar occurring with the plagioclase and ophiolite clast found in the rocks of this formation suggests oceanic provenance (Nandy, 2001).

2.3 Cenozoic Stratigraphic Sequence

The Cenozoic stratigraphic sequence encompasses the flysch sediments of the Disang and Barail Groups, the molassic sediments of the Surma, Tipam and the Dupitila Groups.

2.3.1 Disang Group

A thick sequence of grey to black shales interbedded with fine-grain sandstone and siltstone (Vidyadharan et al., 1986) defines the Disang Group of rocks. First described by Mallet (1876), the shales of this group are monotonous black splintery shales, and the sandstone becomes coarser and thicker toward the upper part (Acharyya et al., 1986). The lower formation is shale dominant with occasional occurrence of sandstones from few centimetres to few metres with increasing occurrence of sandstone toward the upper formations and gradually grades into the Barail Group of rocks (Nandy, 2001). The sediments of Disang Groups are major components of the lithounit in the central part of Nagaland.

2.3.2 Barail Group

The Barail Group of rocks displayed a lower sandstone-dominated unit and an upper argillaceous unit and was deposited in shallow marine, lagoonal or deltaic environments (Acharyya et al., 1986). The Laisong Formation is well-bedded medium-grained sandstones (Ghose et al., 2010) with bands of shales; Jenam Formation, which is more argillaceous, shales with thin wedges of sands (Ghose et al., 2010) as compared to Laisong and Renji Formations, which are arenaceous with little argillaceous are the Formations of Barails Group.

The Laisong equivalents with bedded sandstone alternating with shales and streaks of coals in upper Assam are designated Nagaon Formation (Mitra and Choudhury 1970). The Barail Group of rocks in the Belt of Schuppen are characterised mainly by the Jenam Formation. Alternating dark grey siltstone, shales, and thin sandstone bands is an identifying lithological character of Jenam Formation. This formation is correlated with the Baragolai Formation of the Upper Assam. Thick ferruginous sandstone of the Renji Formation over the Jenam Formations on the Belt of Schuppen, with its best exposures observed in the Changki village area of Mokokchung district. The equivalent formation of the Renji in Upper Assam is considered to be the Tikak Parbat Formation.

2.3.3 Surma Group

The sediments of Surma Group (lower–middle Miocene) were deposited unconformably over those of the Barails (Mathur and Evans, 1964; Acharyya et al., 1986). The sediments of Surma Group are alternations of sandstone and shale or occasionally an alternation between sandstone and thin conglomerates, common at the base (Mathur and Evans, 1964). Tidal and shallow marine conditions prevailed during the deposition of the Surma Group of rocks (Bhattacharjee, 1997).

The Surma Group of rocks was named after their type area (Surma Valley) by Evans (1932) and divided into Bhuban and Bokabil Formations based on the relative abundances of shale and sandstone as observed in the type area. The Bhuban Formation is mainly arenaceous at the basal part and argillaceous in the middle and becomes arenaceous again towards the top. The Bokabil Formation is dominantly argillaceous and comprises of soft laminated claystone, siltstone and shale alteration (Nandy 2001).

2.3.4 Tipam Group

The sediments of Tipam Group are characterised by a lower massive, friable sandstone unit known as Tipam sandstone and upper mottled clay sediments known as Girujan clay (Mathur and Evans, 1964). The sandstone of this group is greyish in unweathered rocks and brown on being weathered, medium to coarse-grained, and poorly cemented (Chakradhar and Gaur, 1985). The Tipam sediments are believed to form due to braided channel sand coalescence (Bhattacharjee, 1997).

The basal part of this group of rocks comprises of sandstone, conglomerates and occasional layers of coals with carbonaceous shales, while the upper part of the formation comprises mainly of sandstone with thin layers of argillaceous shale streaks (Nandy, 2001) designated as the Girujan clay formation. The sediments of this formation are reddish mottled sandy clay. The best exposure of the formation is observed near Bhagty town of Wokha district in the Belt of Schuppen.

2.3.5 Dupitila Group

The Namsang Formation represents the lower horizon Dupitila Group of rock. These are gritty and conglomeratic sandstones (Mathur and Evans, 1964; Roy and Kacker, 1986) overlying the Girujan Clay uncomformably. The sandstone are poorly consolidated and shale siltstones are interbedded with the pebbles beds.

2.3.6 Dihing formation

Dihing Formation is made up of thick pebble beds, thin clay, and sand without any marked consistency to the dip (Mathur and Evans, 1964). This formation overlies the Namsang Formation; the pebble beds are poorly sorted and exhibit no similarity with the regional bedding trend.

2.4 Geotectonic sub-divisions of Nagaland

The hill ranges of Nagaland have been geotectonically (morphotectonically) divided, from west to east, into three distinct longitudinal units (Mathur and Evans, 1964; Khuman et al., 2023), namely – Belt of Schuppen, the Inner Fold Belt and the Ophiolite Belt (Fig. 2.2). On the extreme east next to the ophiolite belt there is also another longitudinal unit of the exposure of metamorphic rocks (known as the Naga Metamorphics), which can be considered as a distinct geotectonic unit. Hence, it could have been better if we consider that the state is divided into four geotectonic (morphotectonic) units.

2.4.1 Belt of Schuppen

The Belt of Schuppen is the eastern margin of the Assam Shelf and a narrow linear syntectonic depositional basin bounded by the Naga Thrust to the West and the Disang Thrust to the East (Roy and Kacker, 1986), forming an imbricate thrust zone (Evan. 1932; Chakradhar and Gaur, 1985). The Naga thrust is a decollement plane developed in stages (Ranga Rao and Murthy, 1980). Toward the North East, the Mishmi Thrust prunes the Naga Thrust, and to the south west, it blends with the Dauki fault near Haflong (Roy and Kacker, 1986).

According to Evan (1964), the belt of Schuppen is an imbricate structure of about eight overthrusting sheets (Fig. 1.3) and owes its structure to the collision between the Indian plate and the Burmese plate (Roy and Kacker, 1986; Imsong et al., 2022). Regional mapping by the Geological Survey of India (GSI) and the Department of Geology and Mining Nagaland (DGM) has identified only four to five tectonic blocks (Roy and Kacker, 1986).

The major limiting thrusts are the Disang thrust on the east and the Naga thrust on the west (Evans, 1964). It has been reported that the BoS in Nagaland comprises of about six or more separate thrust sheets (Evans, 1932). Sedimentary sequences in the belt range in age from Eocene-Oligocene to Plio-Pleistocene and are characterized mainly by flysch sediments belonging to the Barail Group and molasses sediments of the Surma, Tipam and Dupitila Groups (Evans, 1932; Mathur and Evans, 1964).

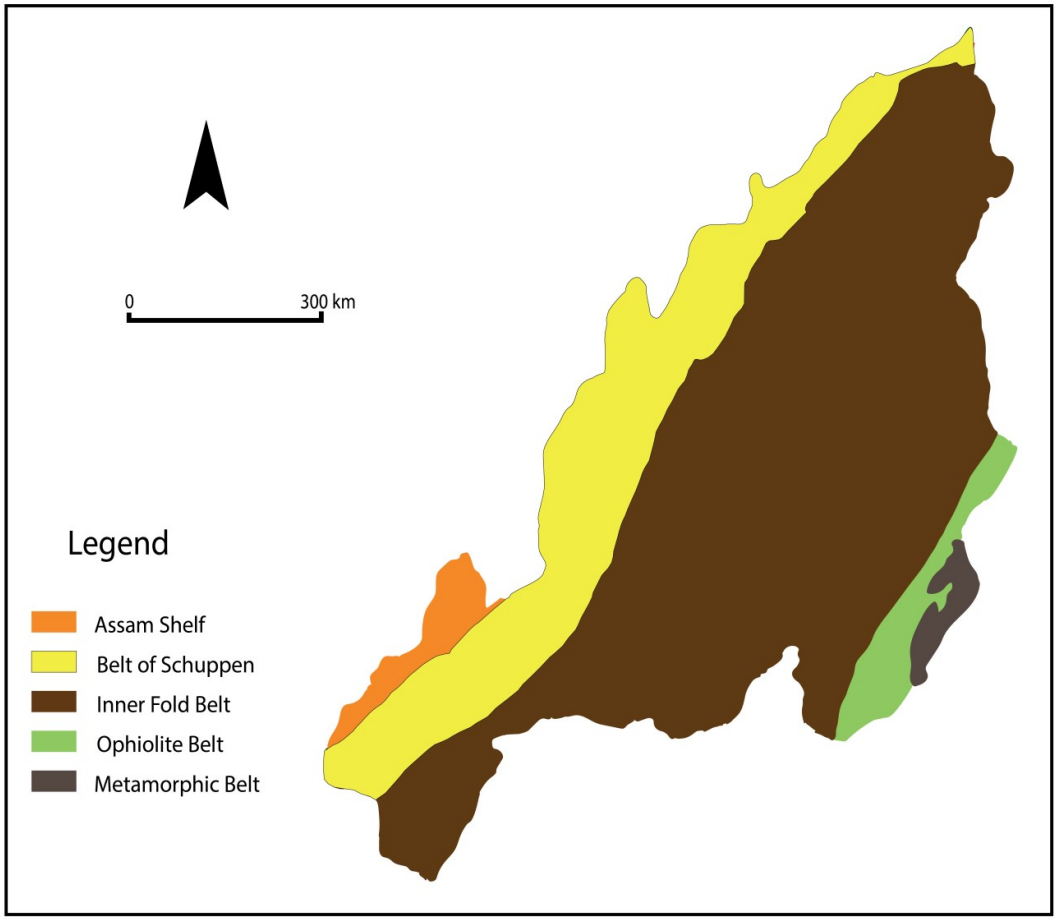

Fig: 2.2: Map showing geotectonic classification of Nagaland (after Khuman et al., 2023).

Table 2.1: Generalised lithostratigraphic succession of the Belt of Schuppen of Nagaland (after GSI 2011).

Age	Group	Subgroup	Formation	Belt of Schuppen
Recent and Pleistocene				Alluvium and Terrace deposit
Unconformity				
Plio-Pleistocene			Dihing	Conglomerates, grits, sandstone and clay beds
Unconformity				
Pliocene			Namsang	Thick beds of grits and conglomerates with occasional sandstone and claystone
Unconformity				
Miocene	Tipam		Girujan Clay	Clay, mottled sandy clay, mudstone with subordinate ferruginous sandstone
			Tipam Sandstone	Thickly-bedded, medium- to coarse-grained ferruginous sandstones with inter-band of siltstones and clay.
	Surma	Bokabil		Alternating sandstone and shale
		Bhuban	Upper Bhuban	Sandstones with subordinate siltstone and thin shale bands with a basal conglomerate
			Middle Bhuban	Siltstones and shales with subordinate sandstone often have characteristic basal conglomerates
			Unconformity	
			Lower Bhuban	Sandstones with shale, siltstone and clay with a few pebble beds and conglomerates
Unconformity				
Oligocene	Barail		Renji	Very thick sequence of hard, ferruginous, thickly-bedded sandstone with minor shale and siltstone
			Unconformity	
			Jenam	Shales, carbonaceous shales, siltstone and sandstone with a number of coal seams
			Laisong	Well bedded, laminated sandstone occasionally with alternating siltstones. Thick units of shales occur sometimes in the upper part

The general stratigraphic sequence is enumerated in Table 2.1. The youngest group of sediments found in limited areas of the study area is Namsang Formation of Dupitila Group. But, in this study area the next youngest formations found to exposed in considerably wide areas is those of Tipam Group (Table 2.1), which is found juxtaposed

with the alluvium at the extreme west of the section. It is comprised of massive gritty sandstone with no significant conglomerate horizons. The next older group of sediments is that of the Bokabil Formation of the Surma Group that are found overthrusting the Tipam (sandstone) Formation of the Tipam Group. The sediments of the Bokabil Formation are predominantly of alternating thick bands of bedded shale and almost massive sandstone. The Bokabil Formation is found to have a thick horizon of intervening conglomerate bed. The next older sediments are of the Upper Bhuban Formation. This formation is having a horizon made up of inter-bedded siltstone and sandstone, which transgresses into thickly bedded almost massive sandstone dominant horizon with subordinate poorly consolidated thick and thin shale beds. The sandstone dominant part of the sequence is comprised of a number of intervening conglomerate beds.

The Middle Bhuban Formation is predominantly of inter-bedded siltstone and shale with subordinate sandstone. The Middle Bhuban Formation is juxtaposed with older Lower Bhuban Formation. The Lower Bhuban Formation is found to have sediments of thickly bedded sandstone with siltstone and shale. The sediments belonging to the Barail Group are of the Renji, Jenam and Laisong Formations. The Renji Formation, a sequence of hard and thickly bedded sandstone with subordinate minor shale and siltstone is found to have a basal conglomerate (GSI, 2011) horizon. The Jenam Formation underlies the younger Renji Formation. In a location of the studied section the Renji Formation is found to juxtapose with Jenam Formation along a structural contact, which appear to be a shear zone. The sediments of the Laisong Formation are comprised of well bedded sandstone with alternating laminated to bedded siltstone. The Disang Group of sediments overthrust those of Barail Group along the Disang thrust.

The Jalukie-Medziphema intermontane basin (valley) is one of the prominent intermontane basins found along the entire stretch of the BoS in Nagaland. The intermontane basin, filled with terrace deposits and alluviums, has a number of protruding hillocks, which are composed mostly of very thick column of terrace-like deposits of variable sizes of particles comprising of sand, pebble, cobble and boulder. The column of such terrace-like deposit is also observed sitting on the bedrock mostly of younger formations of Tipam Group in some peripheral parts of the basin.

2.4.2 Inner Fold Belt

The Inner Fold Belt occupies the majority of the area of the state. They occur south of the Disang Thrust and are thrusted over by the ophiolites to the East (Acharyya, *2007*). The Inner Fold Belt occupies the central part of Naga Hills and extends up to Pangsu pass in Arunachal Pradesh. A large spread of Disang rocks (Mallet, 1876 and Vidyadharan et al., 1986) with isolated covers of Barail (Evans, 1932) as well as Disang-Barail Transition sequences characterizes the geological setting of this belt. The Palaeogene rocks have been folded into series of anticlines and synclines and are confined within two major tectonic zones viz. Disang thrust to the west and the Ophiolite thrust to the east.

The Inner Fold Belt is occupied by two major synclinoria, namely the Kohima synclinorium to the South and Patkai synclinorium to the North. In Kohima synclinorium the core is occupied by younger sediments of Surma Group (Oldham, 1883). The age of Disang sediments is assigned to be Upper Cretaceous to Eocene (Mallet, 1876) while that of Barail to be Upper Eocene to Oligocene (Evans, 1932). Disang Group comprises mostly of monotonous sequence of dark grey to black splintery shale in addition to intercalations of siltstone and fine to medium grained sandstone. Barail Group consists predominantly of arenaceous sediments characterized by light grey to brown, fine to medium grained sandstone with minor to considerably thick interbeds of shale. The Barail sediments are overlain by the mollasse sediments characterized as Surma (Evans, 1932) and Tipam (Mallet, 1876) Groups. Surma Group lies unconformably over Barail Group. The Tipam sediments again lie conformably over those of Surma. The age of the mollasse sediments is believed to extend from Oligocene up to Miocene (Evans, 1932 and Mallet, 1876).

The rocks here are folded with their fold axis trending NE-SW (Vidyadharan et al., 1986). Two major fold belts are observed: The Patkai synclinorium and the Kohima synclinorium (Mathur and Evan, 1964), with the Patkai synclinorium, considered the North-Eastern continuation of the Kohima synclinorium and vice versa (Roy and Kacker, 1980).

2.4.3 Ophiolite Belt

The ophiolite belt overthrusts the most predominant rock formations of the Inner Fold Belt, which are principally of turbidites flysch sediments of mainly of Tertiary age. The ophiolite belt consists predominantly of tectonic slices representing various units of the sequence of ancient oceanic lithosphere that include the ultramafic suite, mafic dykes and sills, pillow lavas, pelagic sediments like chert and limestone, etc. in a jumbled manner (Khuman and Soibam 2010; Soibam et al., 2015; Khuman and Soibam 2022) . The Ophiolite Mélange Zone consists predominantly of the main Ophiolitic body (ultramafic suite), sediments of chert and shale and various blocks of exotic rocks. The associated exotic rocks in the host of mostly of pelagic shale include a number of broken blocks of variable dimensions of dibasic dyke, pillow lava, conglomerate, gritty sandstone and rocks kindred with lava extrusion. The ultramafics having sporadic diabasic dykes cutting across them are found to have been sandwiched with pelagic shale. The ophiolite melange zone in Nagaland has a very thick linear horizon of conglomerate lying over the ultramafics with a tectonic contact. The fossil assemblages from the associated limestone have suggested an Upper Cretaceous to Lower Eocene age for the Ophiolites (Roy and Kackar, 1986; Vidyadharan et al., 1986).

2.4.4 Metamorphic Belt

The ophiolite melange zone is again overthrusted by a metamorphic complex known as the Naga metamorphics. The metamorphic complex is comprised of intensely thrusted group of metasediments, which is predominantly made up of low to medium grade phyllitic schist, hornblende schist, quartzite, quartz-sericite schist, mylonite, etc. Brunnschweiler, (1966) assigned them Pre-Mesozoic or older age but Acharyya et al., (1986), however, stated them to be of Proterozoic age.

Chapter 3
Petrography and Geochemistry

Rocks record all of the different episodes of geologic events happened at the time when they have been formed and also during their subsequent evolution. These events are implanted in them in coded form as various microscopic, mesoscopic and megascopic features. The composition of the rocks and their relationship and mode of arrangement is one of the features from which the coded information about how and where they have been formed and evolved with time can be decoded. Thus, petrology which occupies a central position in Geology is the source of our ideas about some of the episodes of the history of our planet. Petrography is the science of interpretation of information imprinted in the rocks from the composition and relationship with respect to their mode of arrangement.

Geochemistry, in the simplest terms, may be defined as the science concerned with the chemistry of the earth as a whole and of its component parts. It deals with the distribution and migration of the chemical elements within the earth in space and time. Restricting geochemistry to the spectrum of petrology, each rock may be regarded as a chemical system, in which chemical changes can be brought about by various agencies. Every such change implies a disturbance of the system either in equilibrium or non-equilibrium conditions, which is reflected in the resulting rocks. All such information is therefore imprinted in the rocks in the form of chemical codes and hence the various trends of the different parameters of the rock chemistry provide clues for the extraction of valuable information. Thus petrochemistry is an important tool to explore solutions of a wide range of petrological problems that can ultimately lead to reveal the genesis and evolution of the rocks.

The Belt of Schuppen being an imbricate belt, the litho-units are not exposed in their normal stratigraphic order. The recognition of the types of litho-units in the field is never easy, since they are not in sequential order. The litho-characters of the sediments particularly are also very similar. The majority of the rocks are soft, closely jointed and weathered. The area is also thickly vegetated. The structural contacts are generally not clearly visible. Confirmation of and inferring a particular structure needs evidence of juxtaposition of different litho-units, which finds very difficult by observation of the

litho-characters alone in the field. Moreover, most of the litho-units exposed across the belt are poorly consolidated. Thus, successful petrographic study of all the arenaceous components becomes almost impractical. Consequently, confirmation of juxtaposed litho-units from geochemical signatures becomes inevitable to be able to confirm the inferred thrusts.

Three major factors associated with sedimentary sorting may affect Trace and REE patterns in sediments: grain size contrast, general mineralogy and heavy mineral fractionation. REE abundance in various grain sizes have been examined by some researchers. They found that the bulk of REE reside in the silt and clay size fraction, although there is no direct correlation with clay mineralogy, perhaps suggesting that trivalent REE may be readily accommodated in most clay minerals. Silt fractions tend to have lower overall abundances in comparison to clay fractions although the shape of the REE pattern is similar, suggesting the major control is a dilution effect from quartz, a mineral with very low REE abundances. The heavy minerals such as sphene, zircon, allanite, monazite are usually enriched in REEs. Many of these minerals may be concentrated during sedimentary sorting processes; their presence may strongly influence the overall patterns of REEs in the given rock.

Thus, the pattern of trace and RE elements concentrations in the sediments will shed some light on identification and differentiation of the different litho-units since each could have variable grain size contrasts, general mineralogy and heavy mineral fractionation depending upon their diverse source materials and depositional environments. Then, juxtaposition of different litho-units and hence the different structures like thrusts could be identified and inferred structures could be confirmed. Consequently, petrography and ICP (MS) data are examined to be able to differentiate and distinguish the different litho-units, which may corroborate the field setting discussed in the chapter of Field Setting and Geological Profiles. For this purpose, sandstone samples from different locations of the belt across a section (Chumukedima - Piphema section) have been collected for petrographic and, Trace and REE patterns analysis. As the samples of believed to be Tipam sandstone are very fragile thin sections could not be prepared. Thus, petrography of such samples could not be carried out. Since petrography cannot be conveniently carried out for fined grained sediments, shale samples have been collected for Trace and REE patterns studies. Thus, ICP (MS) analysis is carried out for

both sandstone and shale samples. The station points from where the samples have been collected are shown in Figure 3.1. The ICP (MS) analysis was carried out at the Inter University Accelerator Centre (IUAC), New Delhi.

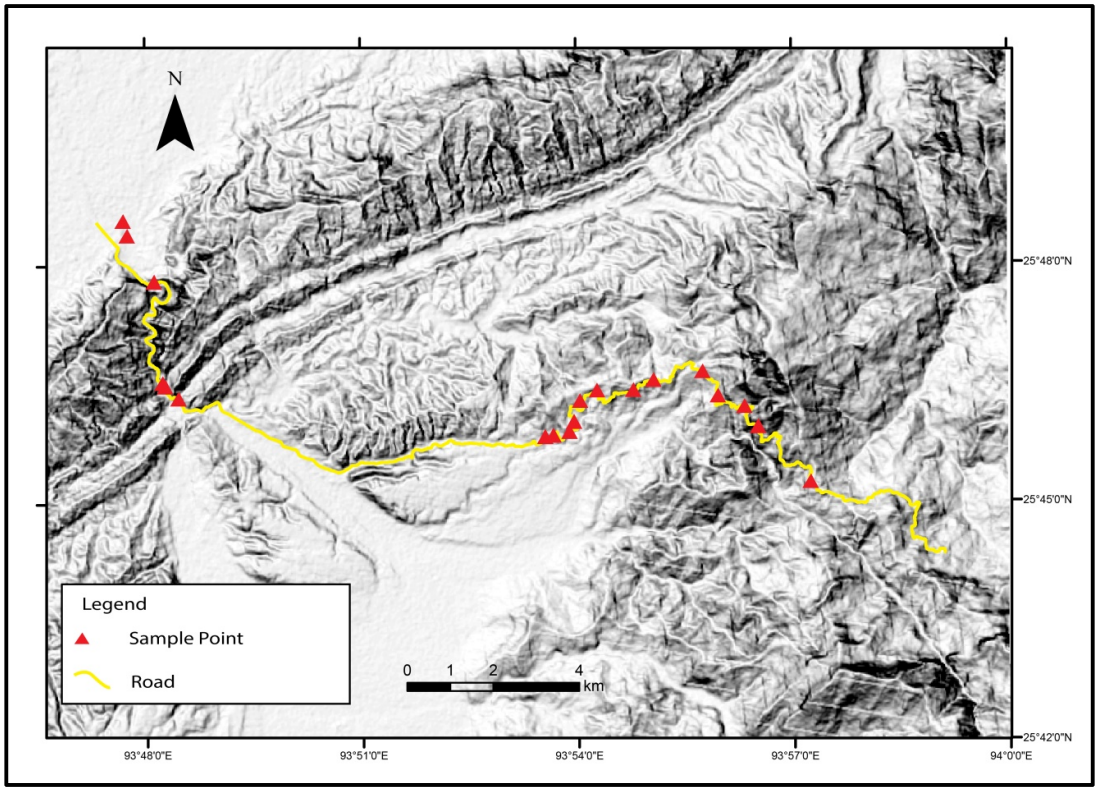

Fig. 3.1: Google terrain map showing the locations from where samples have been collected.

3.1 Petrography

The petrography of sandstone samples is specially carried out to know the modal proportions of the different mineral components particularly quartz and feldspar, as well as, those of rock- and lithic- fragments so that QFL (Dickinson, et al., 1983) and QFR (Folk, 1980) could be prepared. The QFR plot could reveal the types of sandstone out of the collected samples. The QFL plot tells us the tectonic environment of deposition and formation of the sandstones. Here Q, F, R and L stands respectively for Quartz, Feldspar, Rock fragments and Lithic fragments. As different litho-units are comprised of differential components and have been formed at variable times with changing environmental conditions will fall in different areas of these plots such that we can

classify and differentiate those litho-units from where the samples have been collected. The photomicrographs of the representative samples are shown in Figure 3.2.

The modal proportions of quartz and feldspar, as well as, those of rock- and lithic-fragments are as shown in Table 3.1. Form the modal proportions of these components QFR (Fig. 3.2) as well as QFL (Fig. 3.3) plots are prepared.

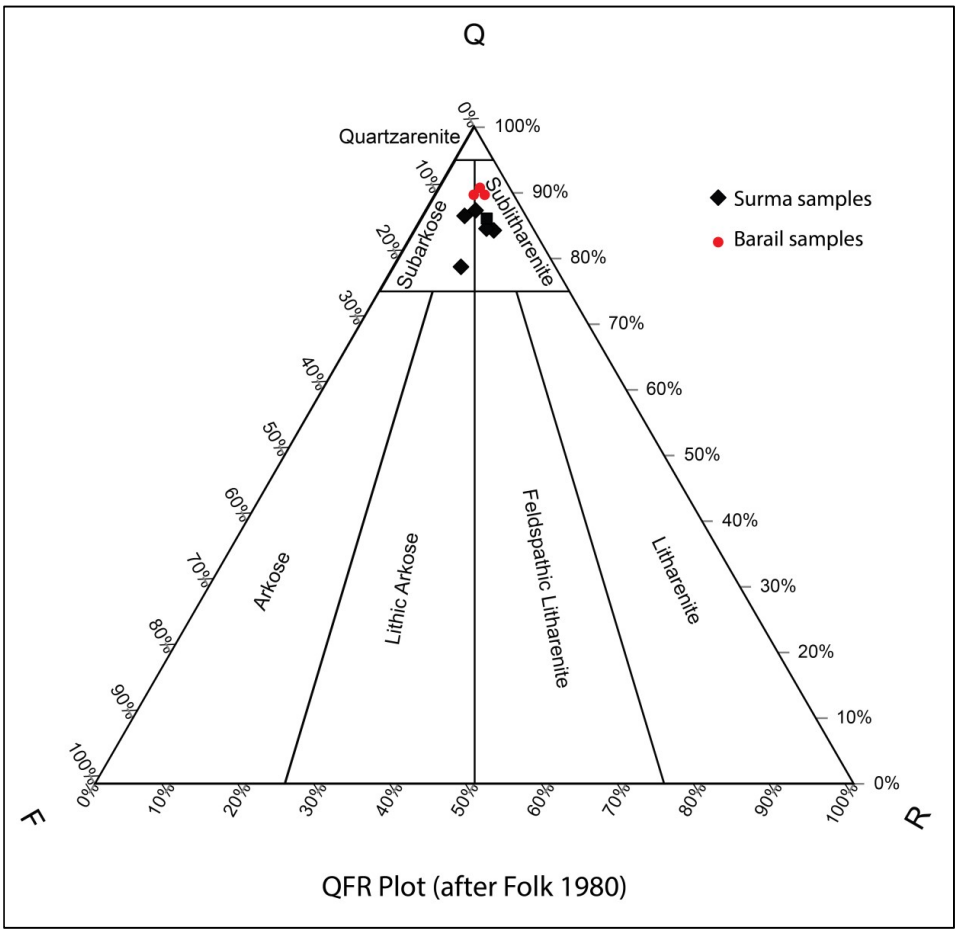

Fig. 3.2: QFR plot of sandstone samples from different points of Chumukedima - Piphema section. Only Barail and Surma Groups of rocks could be studied.

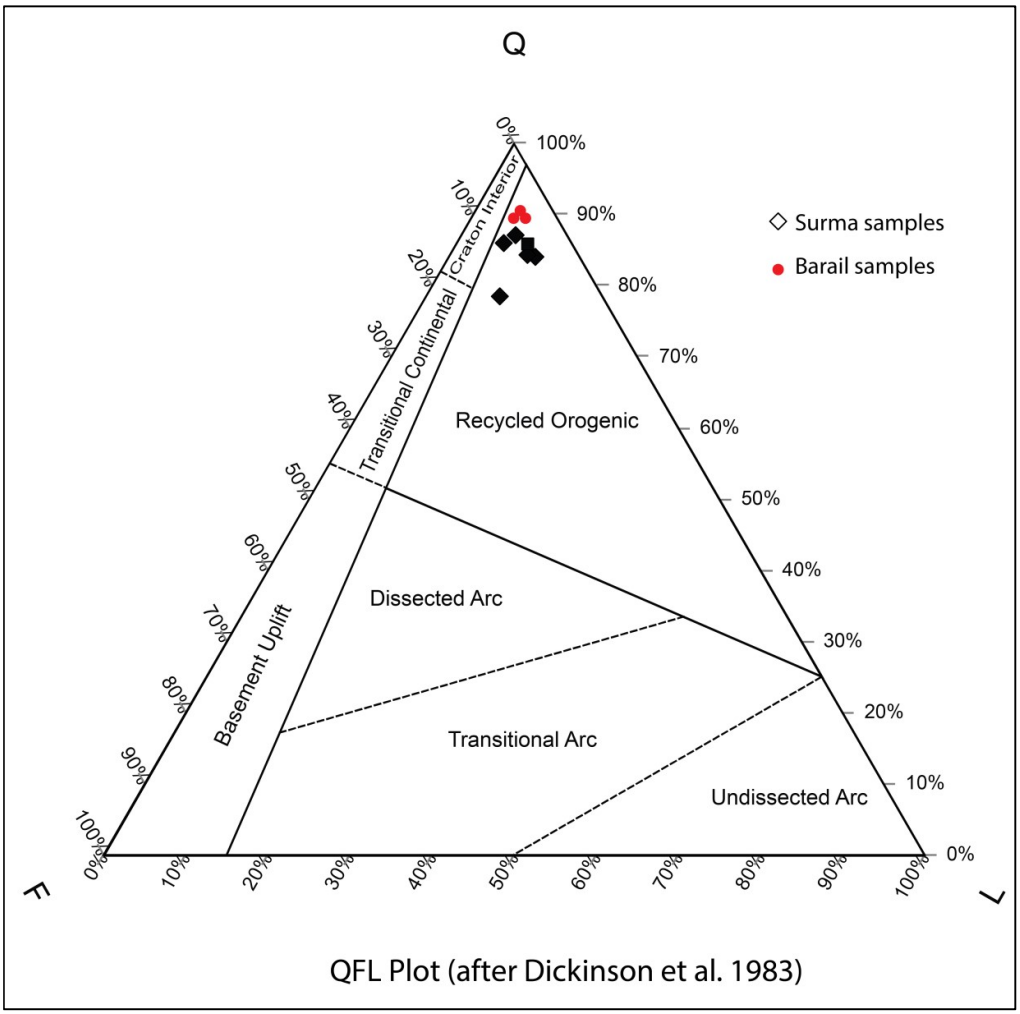

Fig. 3.3: QFL plot of sandstone samples from different points of Chumukedima – Piphema section. Only Barail and Surma Groups of rocks could be studied.

Table 3.1: Table showing the modal proportion of Quartz, Feldspar and Rock Fragments / Lithic Fragments

Sample No	Total framework grain				Framework Percentage			Cmt %	Mtrx %	Mica %	Heavy mineral %	Total %	Section Percentage				Recalculated for plotting		
	Q	F	RF/L	Total	Q%	F%	L%						Q%	F%	L%	Total	Q%	F%	L%
1	230	17	25	272	84.56	6.25	9.19	22	9	7	0.5	138.5	61.05	4.51	6.64	72.20	84.56	6.25	9.19
2	220	22	13	255	86.27	8.63	5.10	20	10	3	0.5	133.5	64.63	6.46	3.82	74.91	86.27	8.63	5.10
3	191	14	14	219	87.21	6.39	6.39	18	8	6	0.5	132.5	65.82	4.82	4.82	75.47	87.21	6.39	6.39
4	218	15	27	260	83.85	5.77	10.38	20	11	5	1	137	61.20	4.21	7.58	72.99	83.85	5.77	10.38
5	279	17	26	322	86.65	5.28	8.07	19	11	7	0.3	137.3	63.11	3.85	5.88	72.83	86.65	5.28	8.07
6	218	35	25	278	78.42	12.59	8.99	18	8	3	1	130	60.32	9.68	6.92	76.92	78.42	12.59	8.99
7	235	14	13	262	89.69	5.34	4.96	2	7	1.5	0.5	111	80.81	4.81	4.47	90.09	89.69	5.34	4.96
8	276	17	16	309	89.32	5.50	5.18	2.5	5	2	0.5	110	81.20	5.00	4.71	90.91	89.32	5.50	5.18
9	270	15	14	299	90.30	5.02	4.68	1.5	7	2	0.5	111	81.35	4.52	4.22	90.09	90.30	5.02	4.68

` It is observed from QFR and QFL plots that there are groups of rocks clustered in two separate areas. In QFR plot a group of samples pigeonholed near the dividing line of subarkose and sublitharenite fields with more enrichment in feldspar and lithic fragments. On the other hand a group of rocks fall in the field of sublitharenite with lesser proportion of feldspar and lithic fragments. At the same time in QFL plot all the samples are pigeonholed in the recycled orogenic field with considerably high quartz proportion. Here also there are two groups of rocks concentrated in different spots. These groups of rocks clustered in different spots are respectively the same with those segregated in two different areas QFR plot. From the field setting the samples segregated into two areas are found to belong respectively to Jenam Formation (Barail Group) and Surma Group. The samples inferred as Jenam formation of Barail Group are falling in sublitharenite field with about 90% quartz out of the three components of QFR, while those of Surma Group are clustered closely but falling both in subarkose and sublitharenite fields with quartz fraction lesser than 90% out of QFR. While in the QFL plot both the groups of rocks inferred to be of Jenam formation of Barail Group and Surma Group are pigeonholed in the recycled orogenic field. Samples of Jenam formation of Barail Group are having about 90% quartz out of the three components of QFL, while those of Surma Group are comprised of quartz fraction lesser than 90% out of QFL.

3.2 Trace and Rare Earth Elements Geochemistry

For understanding the trace and Rare Earth Elements geochemistry ICP (MS) analysis is carried out for representative samples of both sandstone and shale from all the areas of the Chumukedima - Piphema section, which may belong to the litho-units of Barail, Surma and Tipam Groups. The result of the ICP (MS) analysis of representative sample (both sandstone and shales) for REE Plots and UCC Plots respectively are enumerated in Table 3.2 and Table 3.3

Table 3.2: Table Showing REE in Sandstones and Shale samples

Label	La	Ce	Pr	Nd	Sm	Eu	Gd	Tb	Dy	Ho	Er	Tm	Yb	Lu
						Sandstone	samples							
WP-1583-S	36.57476	71.89175	8.68835	31.41942	6.278155	1.241748	4.83932	0.680583	3.66699	0.700971	1.928155	0.276214	1.970388	0.273786
WP-1625-S	31.73168	62.57228	7.617327	28.10495	5.964851	1.273762	4.921287	0.715842	3.845545	0.713366	1.929703	0.250495	1.727723	0.224257
WP-1630-S	37.72961	73.45049	8.281068	30.42718	5.953883	1.169417	5.083981	0.666019	3.187379	0.58932	1.574272	0.207767	1.586408	0.186893
WP-1596-S	31.70294	64.41422	7.890196	29.36225	6.051471	1.134314	4.293137	0.527941	2.433824	0.433333	1.202451	0.160294	1.118627	0.15098
WP-1608-S	30.99752	64.30495	7.94604	30.40594	6.311386	1.29901	4.872772	0.680693	3.294554	0.496535	1.277723	0.161881	1.1	0.153465
WP-1616-S	30.4905	63.008	7.6945	28.984	6.058	1.05	4.378	0.56	2.494	0.493	1.159	0.1515	0.97	0.139
WP-1638-S	17.14851	32.61931	4.243564	15.98465	3.30198	0.608416	2.499505	0.320792	1.168317	0.223267	0.541089	0.073267	0.437624	0.072277
						Shale	samples							
WP-1585-MS	61.19216	121.1304	13.97843	49.83382	10.02451	1.851471	7.466176	1.02549	5.636765	1.072549	3.937255	0.517647	3.251471	0.420098
WP-1590-M	51.21814	113.8814	12.49265	45.36863	9.231373	1.811275	7.108824	0.97549	6.522059	1.007353	2.777451	0.377451	3.343137	0.340686
WP-1590-MS	56.42745	116.4966	13.81127	51.05735	10.45882	2.214216	8.204902	1.136765	6.240196	1.161275	3.27402	0.439706	3.055882	0.404412
WP-1594-MS	42.33971	89.67598	11.25049	43.80637	9.729902	2.251471	8.262745	1.152451	6.211765	1.063235	2.808824	0.372059	2.415196	0.331863
WP-1598-MS	49.77129	106.1084	12.31832	45.11287	9.382673	1.975743	7.617327	1.031683	5.678218	1.039604	2.94901	0.388119	2.706436	0.366337
WP-1597-M	90.87233	191.5243	22.10243	83.05825	16.66019	3.444175	12.01796	1.453883	7.213592	1.26068	3.493204	0.475728	3.65	0.433981
WP-1619-M	70.47843	128.3049	18.22794	69.52892	14.98529	3.280882	11.94118	1.571078	8.221569	1.418627	3.889216	0.461275	3.239216	0.415686
WP-1621-M	48.21176	98.35539	11.57696	41.31765	8.111275	1.640686	5.852451	0.733333	3.523529	0.654902	1.869118	0.246078	1.802941	0.240196
WP-1635-M	50.78861	103.8723	12.02178	42.50149	8.312871	1.618812	6.064851	0.774752	3.916832	0.737624	2.178713	0.308911	2.248515	0.291584
WP-1637-MS	36.28218	74.46386	9.05	33.33218	6.706436	1.368317	5.194554	0.671782	3.146535	0.587624	1.59901	0.216832	1.619307	0.214851
WP-1638-MS	41.46942	83.77621	10.04612	36.56505	7.262136	1.415534	5.471845	0.697087	3.234951	0.566505	1.567476	0.204369	1.480097	0.196117
WP-1639-M	41.18932	84.33107	9.786408	35.41456	6.907767	1.406796	5.122816	0.647573	3.35534	0.666019	1.896117	0.227184	1.718932	0.228155

Table. 3.3: Table Showing UCC elements in Sandstones and Shale samples

Label	Cs	Rb	Ba	Th	U	La	Ce	Sr	Nd	Hf	Zr	Sm	Tb	Tm	Yb
Sandstone Samples															
WP-1595-S	2.252941	60.46029	212.6358	12.00686	1.998039	45.93578	94.26667	88.48775	40.62206	2.516667	112.4637	7.858333	0.683824	0.190196	1.27598
WP-1596-S	1.352941	38.86029	166.1284	7.867157	1.125	31.70294	64.41422	48.99363	29.36225	1.97451	81.12794	6.051471	0.527941	0.160294	1.118627
WP-1606-S	0.657282	16.5199	66.96117	7.072816	0.718932	31.19272	62.92282	37.08495	31.29029	1.474757	55.78447	6.571845	0.486893	0.108252	0.676214
WP-1608-S	1.408911	36.37228	143.8946	7.339604	1.691584	30.99752	64.30495	47.08069	30.40594	1.85297	73.46287	6.311386	0.680693	0.161881	1.1
WP-1616-S	1.2505	33.1815	131.17	9.8145	1.048	30.4905	63.008	38.2185	28.984	1.6995	79.2265	6.058	0.56	0.1515	0.97
WP-1618-S	1.44703	33.1	119.5589	9.042079	1.027723	43.27277	82.52376	38.98366	42.94604	1.725248	69.42178	8.99802	0.767822	0.160891	1.146535
WP-1638-S	0.674257	16.24356	51.15396	4.026238	0.737624	17.14851	32.61931	21.53119	15.98465	1.199505	40.76584	3.30198	0.320792	0.073267	0.437624
Shale samples															
WP-1583-MS	6.080198	131.3139	485.5104	21.63465	3.330693	75.03911	157.1322	188.0926	68.70644	5.027228	228.5421	14.54208	1.721782	0.593564	4.199505
WP-1585-MS	10.28676	169.3044	470.423	20.91814	3.07549	61.19216	121.1304	146.0039	49.83382	3.192157	196.8672	10.02451	1.02549	0.517647	3.251471
WP-1590-M	5.69951	102.5657	352.2093	16.91422	2.785784	51.21814	113.8814	103.8225	45.36863	2.386765	98.64902	9.231373	0.97549	0.377451	3.343137
WP-1590-MS	6.829412	104.9716	603.4627	18.47206	2.869608	56.42745	116.4966	217.648	51.05735	2.943137	133.773	10.45882	1.136765	0.439706	3.055882
WP-1595-MS	5.102913	102.067	364.935	18.35049	3.041748	64.89903	136.6684	179.7966	57.59466	4.323301	191.4646	11.31602	1.085922	0.392233	2.871359
WP-1597-M	8.681068	131.5403	347.8806	23.36845	3.366019	90.87233	191.5243	206.7345	83.05825	4.826699	223.9733	16.66019	1.453883	0.475728	3.65
WP-1598-MS	5.345545	87.51089	349.0267	15.78614	2.492574	49.77129	106.1084	178.9347	45.11287	2.565347	102.698	9.382673	1.031683	0.388119	2.706436
WP-1616-MS	5.667157	83.83824	291.1059	17.12402	2.380882	50.45049	99.63873	133.8373	41.97696	2.123039	86.25784	8.345098	0.858824	0.318137	2.256373
WP-1619-M	6.396569	97.02941	375.6397	15.36814	2.327451	70.47843	128.3049	124.0667	69.52892	3.762745	161.998	14.98529	1.571078	0.461275	3.239216
WP-1627-MS	6.69703	105.8535	314.8698	15.44505	2.444554	40.84307	80.95545	130.7025	34.82772	2.327723	86.88861	6.999505	0.737624	0.289604	2.024752
WP-1621-M	5.095098	85.78431	195.3887	13.96471	1.778922	48.21176	98.35539	138.4088	41.31765	2.885784	124.2716	8.111275	0.733333	0.246078	1.802941
WP-1635-M	6.118317	97.36287	203.8965	15.52574	2.084653	50.78861	103.8723	133.8624	42.50149	3.359406	145.1911	8.312871	0.774752	0.308911	2.248515
WP-1637-MS	3.227723	55.94851	233.4292	11.83168	1.569802	36.28218	74.46386	90.13713	33.33218	2.49703	102.2668	6.706436	0.671782	0.216832	1.619307
WP-1638-MS	2.884466	57.74612	172.5621	13.32087	1.624757	41.46942	83.77621	72.58835	36.56505	2.434466	92.83495	7.262136	0.697087	0.204369	1.480097
WP-1639-M	4.763592	72.72379	185.0291	12.23592	1.615049	41.18932	84.33107	99.36893	35.41456	2.730583	120.8714	6.907767	0.647573	0.227184	1.718932

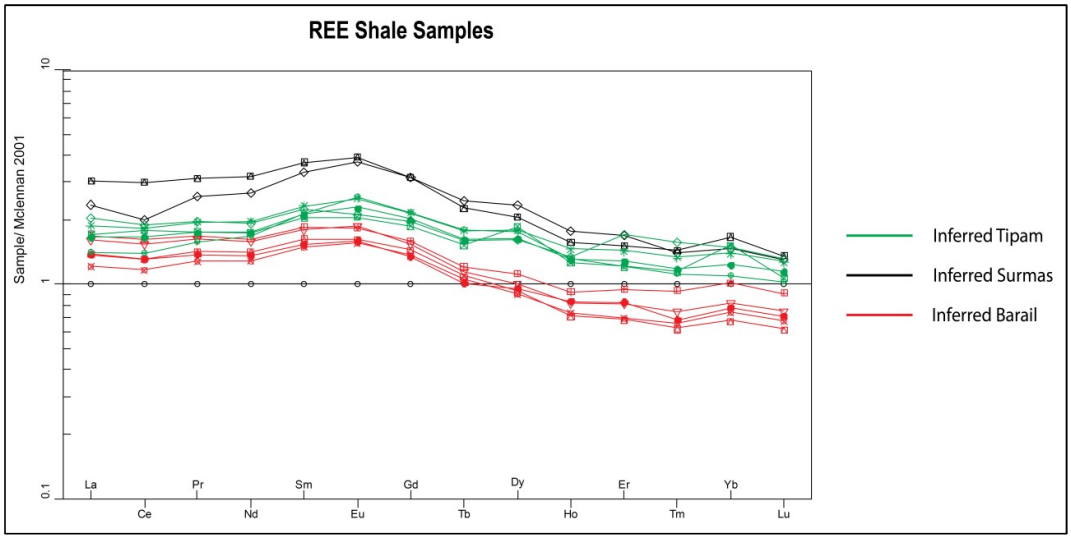

(a)

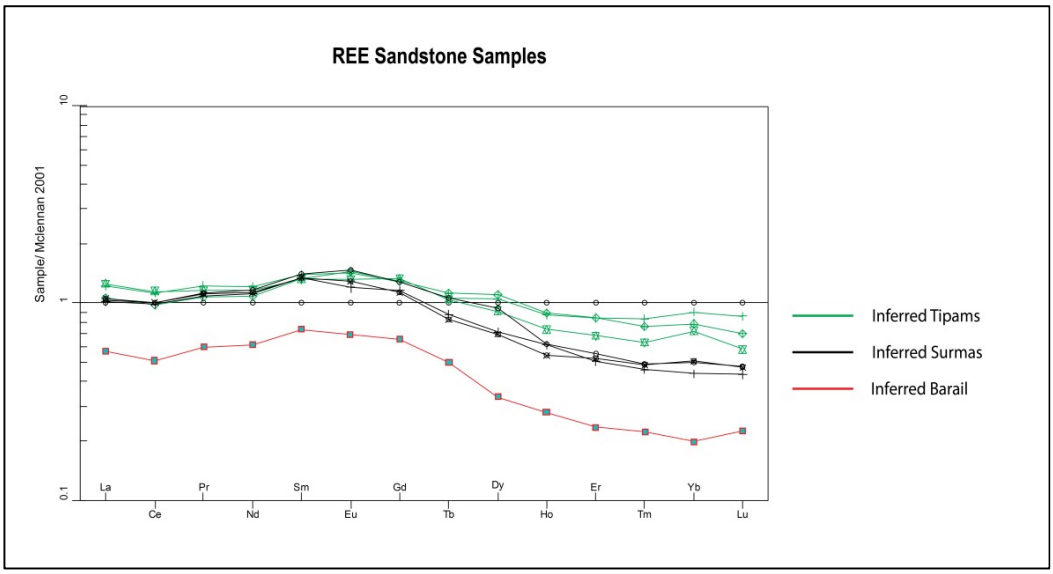

(b)

Fig. 3.4: Spider diagrams for REE standard normalisation, (a) representative samples of shale; (b) representative samples of sandstone.

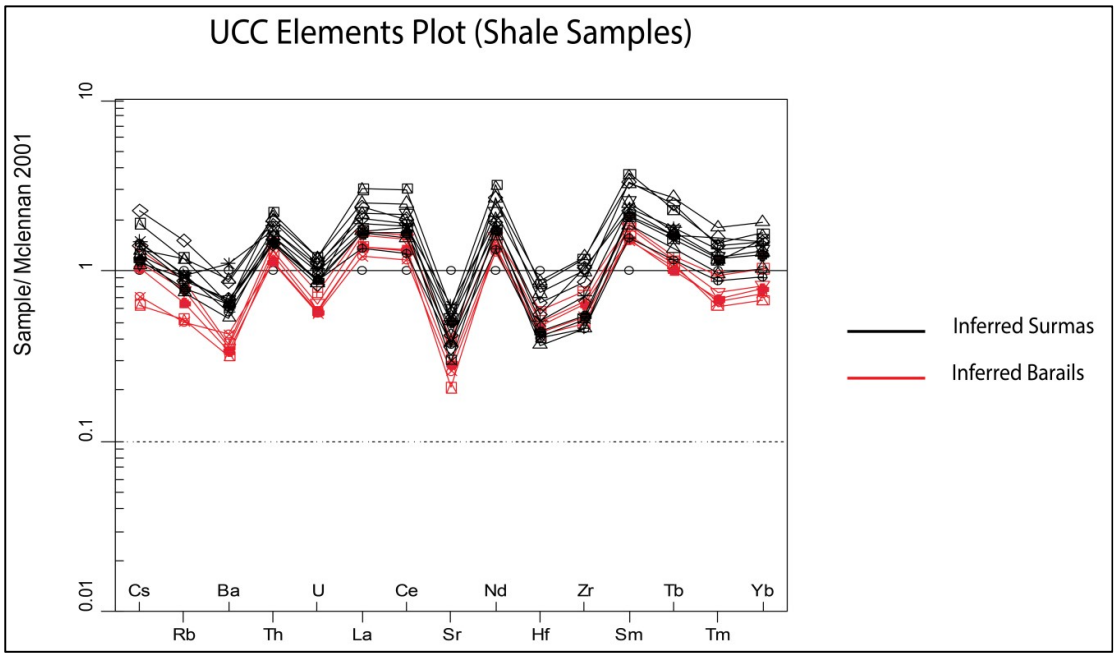

(a)

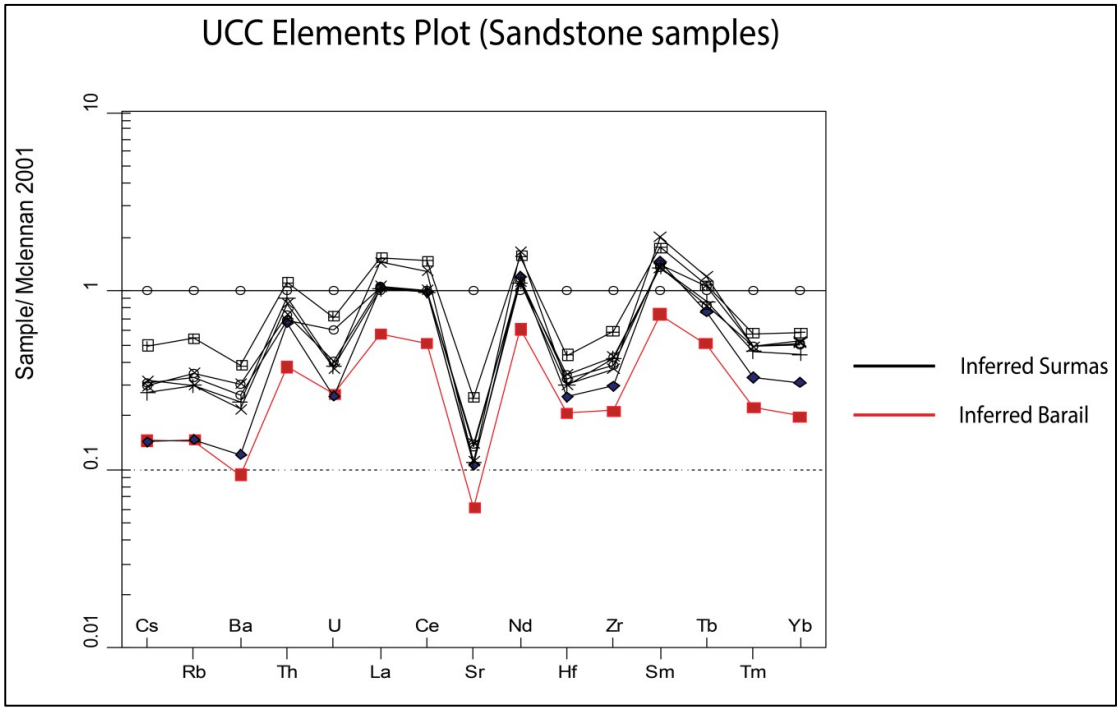

(b)

Fig. 3.5: Spider diagrams for UCC standard normalisation, (a) representative samples of shale; (b) representative samples of sandstone.

The data of Table 3.2 and Table 3.3 are plotted as spider diagrams for REE (Figs. 3.4 a and b) and UCC (Figs. 3.5 a and b) patterns both for shale and sandstone samples taking into consideration of the respective standards of normalisation. From Figures 3.4 a and b it is evident that there are three groups of samples segregated separately for shale and sandstone. Each of the groups both in the REE spider diagram patterns of shale and sandstone clustered separately are of the samples collected from the same litho-unit. Thus, samples of different litho-units segregate separately. Taking into consideration of the field setting the samples falling in the three separate clusters are inferred as of Barail, Surma and Tipam Groups. In Figures. 3.5 a and b also as in case of REE, the UCC spider diagram patterns of shale and sandstone clustered separately in shale sandstone analyses are of the samples collected from the same litho-unit. Here also taking into consideration of the field setting the samples falling in the three separate clusters are inferred as of Barail, Surma and Tipam Groups.

Thus, petrography and ICP (MS) data analysis could differentiate and distinguish the different litho-units, which corroborate and support the observations made while drawing inferences about the field setting and geological profiles in the three sections of the southern part of the Belt of Schuppen.

Chapter 4
Field Setting and Geological Profiles

The record of geological history and other phenomena of evolutionary changes are imprinted in the rocks but in the coded form. The geologists unveil the codes by carrying out certain studies so as to decrypt those encrypted imprints. Geological mapping is one of the techniques through which those imprinted codes found embedded in the exposed surface of outcrops of the rocks are translated into a geological language leading to arrive at a logical interpretation about the evolutionary history of the rocks as well as other geological phenomena. It also gives clues about the disposition and inter-relationship of the litho-units found exposed with respect to their original positions and structures developed later on them. Geological and structural mapping in effect is recording and plotting of the observations and other information obtained from the rock exposures on a base map and rationally interpret those towards unravelling how the litho-units are found exposed and related to each other in the present-day field setting. Thus, geological and structural mapping is helpful in the interpretation of how the litho-units are arranged and disposed giving rise to the present day field setting in due course of their evolution. Thus, geological and structural mapping is virtually inevitable for the understanding of the field setting of a region and how they have been generated. Consequently, to be able to portray the picture of generation of the Belt of Schuppen (BoS) of Nagaland in general and the southern part of the belt in particular geological and structural mapping is carried out in three sections in the southern part of the Belt of Schuppen of Nagaland. The sections are (i) Niuland - Zhadima section, (ii) Chumukedima - Piphema section and (iii) Pimla - Old Jalukie section; in the southern part of the BoS of Nagaland (Fig. 1.5).

The preparation of the geological and structural map has been made taking into consideration of the regional tectonic setting, most importantly at the time of judgement and inference of certain structures in some locations. As the mapping is carried out in limited points the boundaries of litho-contacts are sometimes drawn using intrapolation and extrapolation technique. Hence, there is a chance of having some variation in the boundaries of actual litho-contacts with those portrayed in the map. As the data points are limited and factors related with elevation has not been taken into account some litho-units lying exposed at higher altitudes above some of the underlying units at lower elevations could also have been missed in certain locations.

From the constructed geological and structural maps geological profiles across suitable sections are prepared along the three different sections of the BoS. The profile lines are so chosen to pass through the area almost perpendicular to the regional trend and that could exhibit maximum structural features in the section and also passes through the maximum number of data collection points. The geological profiles prepared should depict the best of topography, lithology and structural features across the study area.

For the purpose of interpretation of tectonic implications certain statistical analysis are inevitable. Consequently, few distinctive statistical analyses are carried out to understand the kinematics and tectonic significance of the constructed geological profiles across the three sections. For these particular statistical analyses GEOrient 9.4.0, Stereonet 11.6.0, is used. With the use of this software Rose Diagrams of the bedding planes are prepared to understand the general concentrations of the strikes, which is indicative about the tectonic forces responsible for the generation of the present day field setting. Cyclographic plot, pole and contour diagrams of the bedding attitudes are also prepared to shed light in the interpretation of the kinematics responsible for the generation of the BoS *Vis a Vis* the orogenesis and evolution of the Indo-Myanmar Ranges (IMR).

4.1 Niuland - Zhadima Section

Altogether 53 bedding data are collected from different locations along the studied section. The bedding data are then redefined so that pole along with pole direction of the beds could be evaluated for further construction of pole and contour diagrams. The bedding attitude data along with the respective locations as well as other related data derived from them are shown in Table. 4.1.

The dip-strike data of the beds along with their respective GPS locations are plotted in the base map using Arc GIS 10.7 software (Fig. 4.1). Using the orientation and pattern of the dip-strike data of the litho-units, and taking into consideration of other field data like the locations where evidences of geological structures like thrusts are observed, the types of rocks found in the different locations and areas of litho-contacts, etc., a geological and structural map is constructed (Fig. 4.2). For the preparation of geological profiles two best fitting sections along AB and BC are chosen as profile lines of the constructed geological and structural map. Accordingly, the data of bedding attitudes

falling within the areas of these sections are segregated into two groups in the data table (Table 4.1).

Table 4.1: Bedding attitudes at various stations of Niuland - Zhadima Section.

SL. NO	Latitude	Longitude	Dip Amount (◦)	Dip Direction (◦)	Poles (◦)	Poles Direction (◦)
Section A-B						
1	N25°56'26.6"	E94°00'39.2"	79	080	11	260
2	N25°56'26.7"	E94°00'40.6"	85	240	5	060
3	N25°56'26.6"	E94°00'43.4"	65	015	25	195
4	N25°56'53.6"	E94°00'52.5"	56	114	34	294
5	N25°56'44.5"	E94°00'54.4"	30	034	60	214
6	N25°56'48.2"	E94°00'57.9"	47	031	43	211
7	N25°57'10.2"	E94°01'16.7"	48	116	42	296
8	N25°57'16.4"	E94°01'21.3"	71	092	19	272
9	N25°57'05.8"	E94°01'22.9"	40	074	50	254
10	N25°57'58.3"	E94°01'29.9"	44	084	46	264
11	N25°56'40.5"	E94°01'23.4"	40	127	50	307
12	N25°56'36.4"	E94°01'39.8"	35	133	55	313
13	N25°56'32.3"	E94°01'48.8"	54	104	36	284
Section B-C						
14	N25°56'54.3"	E94°02'14.5"	50	084	40	264
15	N25°56'38.8"	E94°02'38.1"	34	044	56	224
16	N25°56'29.4"	E94°02'47.1"	28	041	62	221
17	N25°56'16.8"	E94°02'49.4"	47	080	43	260
18	N25°55'11.6"	E94°02'54.2"	37	135	53	315
19	N25°55'05.7"	E94°02'45.3"	46	138	44	318
20	N25°54'51.6"	E94°02'28.1"	20	139	70	319
21	N25°54'48.1"	E94°02'28.19"	18	097	72	277
22	N25°54'43.6"	E94°02'32.5"	39	098	51	278
23	N25°54'41.4"	E94°02'28.3"	26	076	64	256
24	N25°54'22.7"	E94°02'26.1"	44	105	46	285
25	N25°54'19.1"	E94°02'27.7"	42	124	48	304
26	N25°54'13.9"	E94°02'27.8"	36	116	54	296
27	N25°54'10.5"	E94°02'23.6"	31	110	59	290

SL. NO	Latitude	Longitude	Dip Amount (◦)	Dip Direction (◦)	Poles (◦)	Poles Direction (◦)
28	N25°53'55.8"	E94°02'27.7"	48	110	42	290
29	N25°53'59.6"	E94°02'40.5"	69	116	21	296
30	N25°53'57.7"	E94°02'40.9"	59	148	31	328
31	N25°53'29.2"	E94°02'26.7"	27	117	63	297
32	N25°53'00.1"	E94°02'17.1"	32	103	58	283
33	N25°54'15"	E94°02'28.0"	31	112	59	292
34	N25°53'56"	E94°02'27"	49	111	41	291
35	N25°53'0"	E94°02'18"	36	120	54	300
36	N25°52'59"	E94°2'16"	30	260	60	080
37	N25°52'58.6"	E094°02'11.4"	23	148	67	328
38	N25°52'58.5"	E094°02'10.3"	41	249	49	069
39	N25°52'45.7"	E094°02'07.1"	37	157	53	337
40	N25°52'35.4"	E094°02'14.1"	34	136	56	316
41	N25°52'32.8"	E094°02'16.3"	59	110	31	290
42	N25°52'30.8"	E094°02'17.4"	54	150	36	330
43	N25°52'30.8"	E094°02'19.8"	58	142	32	322
44	N25°52'28.4"	E094°02'35.4"	65	140	25	320
45	N25°52'25.5"	E094°02'37.4"	68	134	22	314
46	N25°52'17.4"	E094°02'39.6"	31	127	59	307
47	N25°52'13.7"	E094°02'40.0"	49	148	41	328
48	N25°51'55.7"	E094°02'58.8"	74	285	16	105
49	N25°51'54.8"	E094°03'04.7"	44	320	46	140
50	N25°51'48.9"	E094°03'15.4"	34	151	56	331
51	N25°50'38.4"	E094°03'12.3"	31	002	59	182
52	N25°50'07.8"	E094°03'50.8"	26	316	64	136
53	N25°49'52.6"	E094°02'45.4"	46	335	44	155

Two cross sectional geological profiles along AB and BC are constructed (Fig. 4.2) from the prepared geological and structural map. The study area is having numerous strike-slip faults and thrusts.

Cyclographic plot, Rose-, Pole- and Contour diagrams of the bedding attitudes of the segments along AB and BC as well as of the whole of Niuland - Zhadima Section are

prepared (Fig. 4.3) to be able to decrypt the kinematics responsible for the generation of the BoS as well as to understand the attitude of the controlling structural features of the belt. The summary of Rose and Pole diagrams of Figure 4.3 is enumerated in Table 4.2.

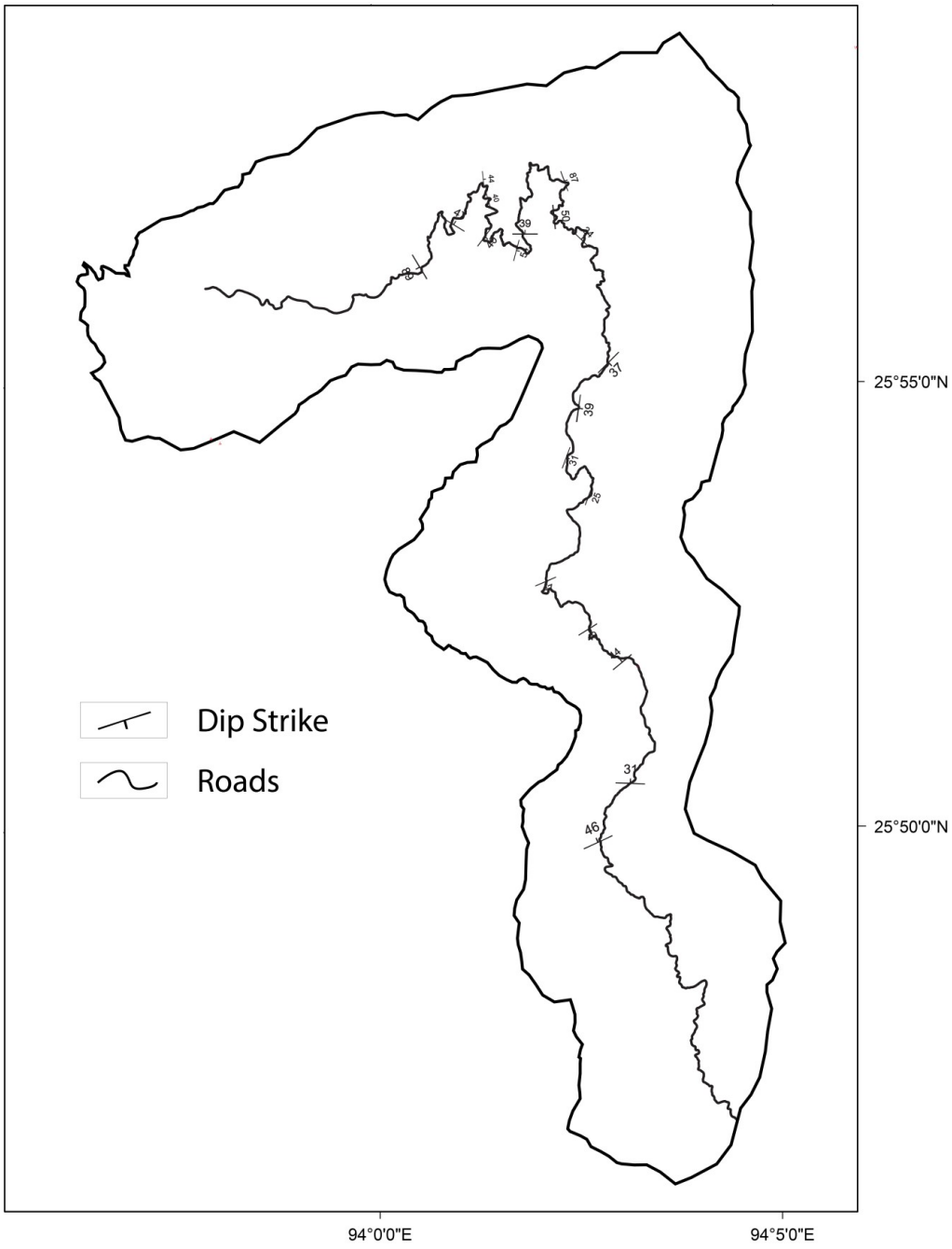

Fig. 4.1: The dip-strike plot of the beds at different locations of the Niuland - Zhadima Section.

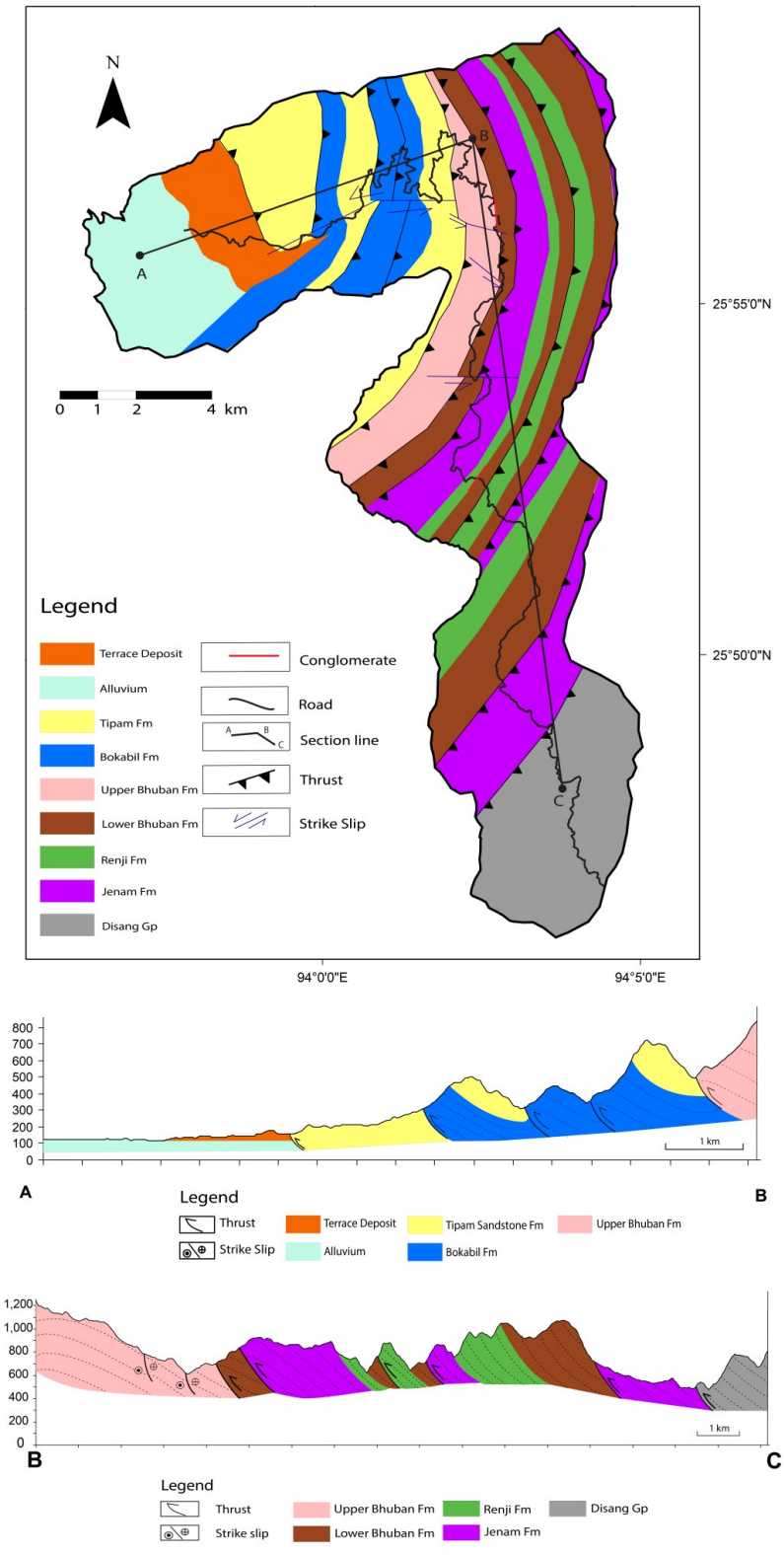

Fig. 4.2: Geological and Structural Map of Niuland - Zhadima Section and Geological Profiles along AB and BC.

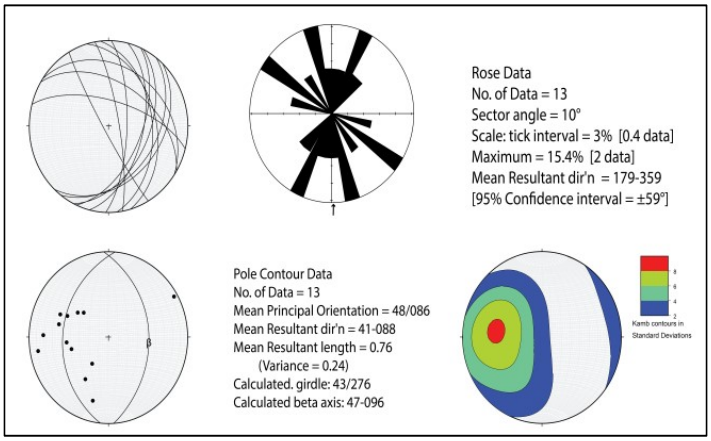

(a)

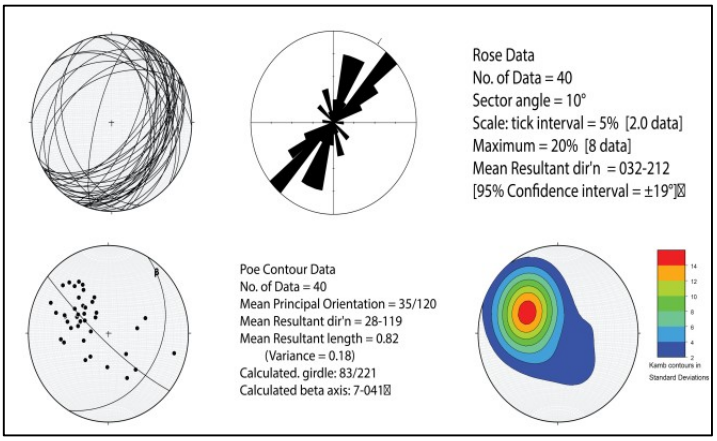

(b)

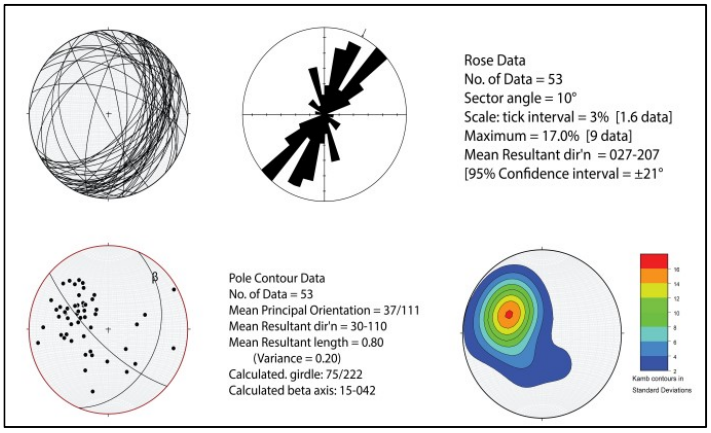

(c)

Fig. 4.3: Cyclographic plot, Rose-, Pole- and Contour diagrams of (a) AB segment; (b) BC segment and (c) whole of Niuland - Zhadima Section.

Table 4.2: Summary of Rose and Pole diagrams of Fig. 4.3.

Segments	(AB)	(BC)	Whole section
No. of Data	13	40	53
Mean Principal Direction	048°/086°	035°//120°	37°/111°
Mean Resultant Direction	041°-088°	028°-119°	030°/110°
Calculated β Axis	47°/096°	07°/041°	15°/042°
Calculated Girdle	43°/276°	83°/221°	75°/222°

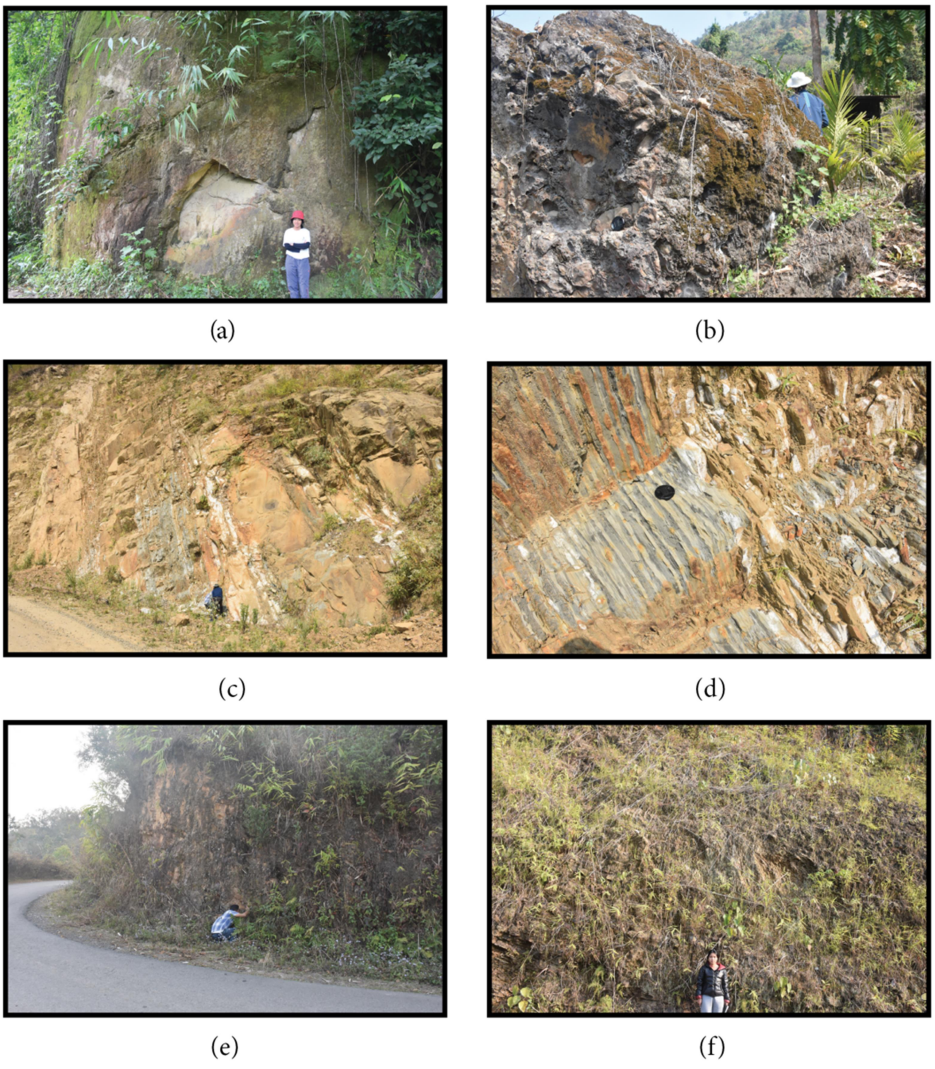

Fig. 4.4: Exposure of various lithology in Niuland – Zhadima Section (a) Exposure of Tipam sandstone (b) Exposure of Conglomerate bed (c) Exposure of Massive sandstone in Surma (d) Exposure of Sandstone – Shale alteration in Surma (e) Exposure of Renji Sandstone (f) Exposure of Jenam Shales.

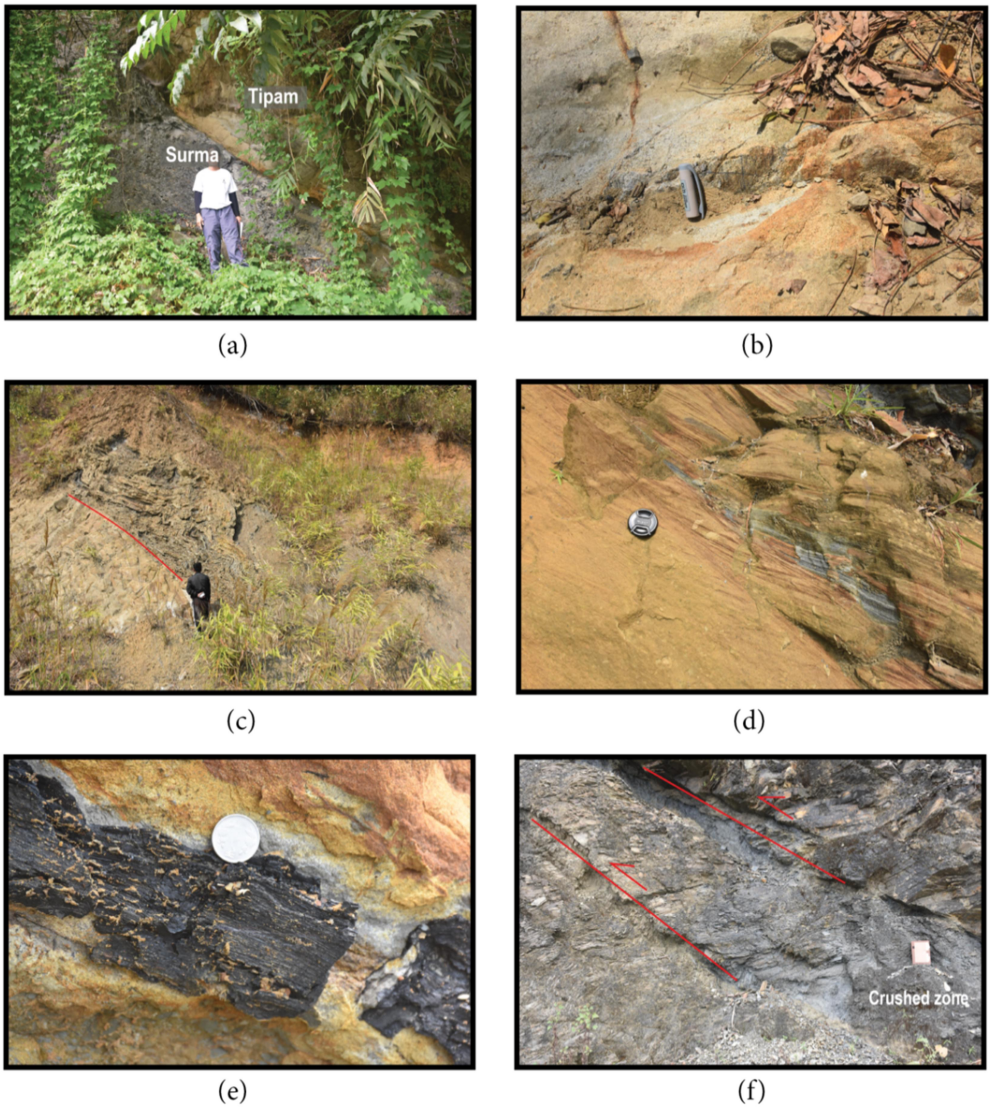

Fig. 4.5: Various structures observed in Niuland – Zhadima Section (a) Contact between Surma and Tipam (b) Slickenside in Surma sandstone (c) Shearing contact with drag folds on top of Renji sandstone (d) Cross bedding in Surma sandstone (e) Coal streak in Surma sandstone (f) Thrusting in Jenam formation crushing the materials in between the two thrust plane

The Niuland - Zhadima Section is found to have outcrops of various litho-units of the different Formations of the Barail, Surma and Tipam Groups, which are mostly juxtaposed against each other along different geological structure (Fig. 4.2). The field photographs of the different litho-units and their various features as well as the important geological structures depicting the field setting of the section are shown in Figures 4.4 and 4.5

4.2 Chumukedima - Piphema Section

Altogether 159 bedding data are collected from different locations along Chumukedima - Piphema Section. The entire section is divided into 3 segments (Fig. 4.6) in which Segment I (Chumukedima – Medziphema Segment) has 43 data, Segment II (Medziphema – Pherima Segment) has 47 data, Segment III (Pherima – Piphema Segment) has 69 data. The bedding data are then redefined so that pole along with pole direction of the beds could be evaluated for further construction of pole and contour diagrams of the three segments. The bedding attitude data along with the respective locations as well as other related data derived from them are shown in Table 4.3.

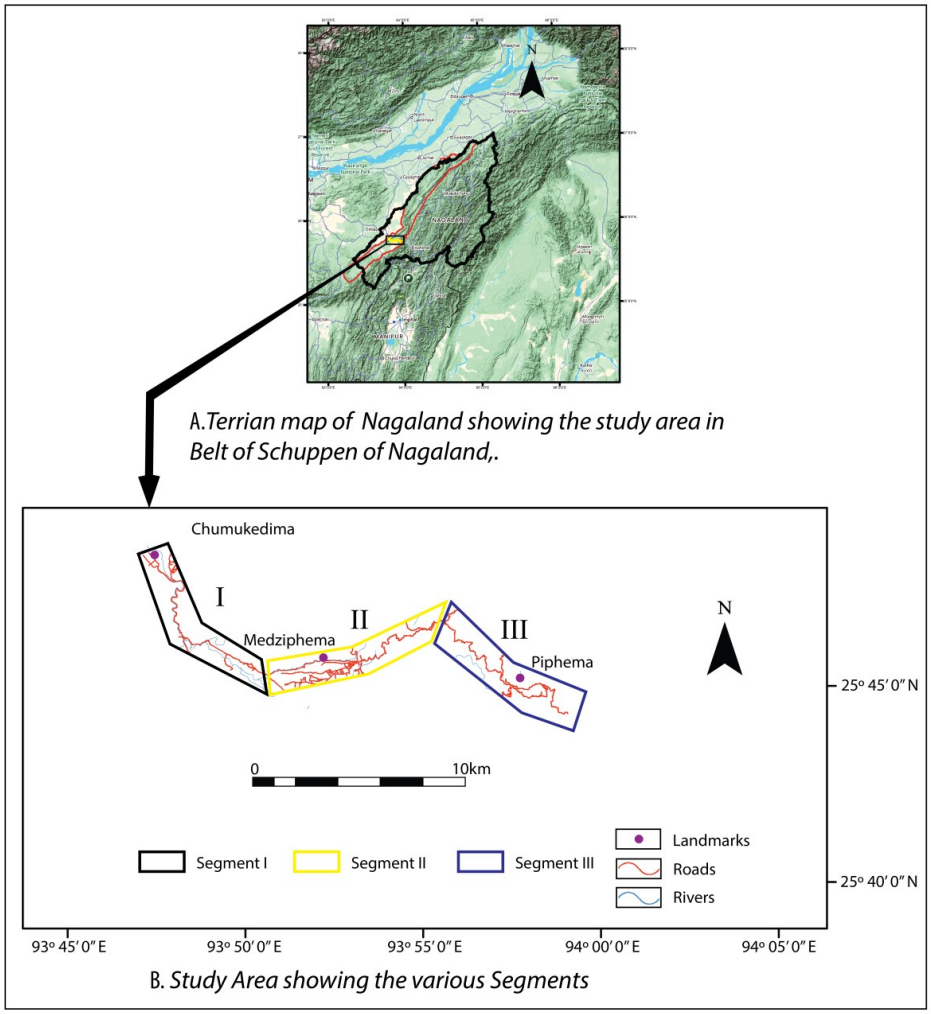

Fig. 4.6: Terrain map of Nagaland showing the Chumukedima - Piphema Section and the three subdivisions of the section.

The dip-strike data of the beds along with their respective GPS locations are plotted in the base maps of the three segments using Arc GIS 10.7 software (Fig. 4.7). Using the orientation and pattern of the dip-strike data of the litho-units, and taking into consideration of other field data like the locations where evidences of geological structures like thrusts are observed, the types of rocks found in the different locations and areas of litho-contacts, etc., geological and structural maps of the three segments are constructed (Figs 4.8, 4.9 and 4.10).

Table 4.3: Bedding attitudes at various stations of Chumukedima - Piphema Section.

Sl. No	Latitude	Longitude	Dip Amount (◦)	Dip Direction (◦)	Pole Value (◦)	Pole Direction (◦)
Segment I						
1	25°48'33.10"N	93°47'40.00"E	77	124	13	304
2	25°48'21.90"N	93°47'41.60"E	80	138	10	318
3	25°47'52.80"N	93°47'54.80"E	32	138	58	318
4	25°47'47.40"N	93°48'08.60"E	60	130	30	310
5	25°47'42.30"N	93°48'18.60"E	45	140	45	320
6	25°47'39.50"N	93°48'21.20"E	40	150	50	330
7	25°47'33.80"N	93°48'19.00"E	45	128	45	308
8	25°47'32.10"N	93°48'11.10"E	30	150	60	330
9	25°47'31.50"N	93°48'06.90"E	47	135	43	315
10	25°47'25.50"N	93°48'08.40"E	43	133	47	313
11	25°47'19.90"N	93°47'58.90"E	47	130	43	310
12	25°47'08.70"N	93°48'08.80"E	50	130	48	310
13	25°46'59.70"N	93°48'06.40"E	44	119	46	299
14	25°46'25.20"N	93°48'16.20"E	55	120	35	300
15	25°46'0.40"N	93°49'23.30"E	46	113	44	293
16	25º48'23.53"N	93º47'43.01"E	56	126	34	054
17	25º48'07.50"N	93º47'34.67"E	50	327	40	213
18	25º47'49.70"N	93º47'56.46"E	40	135	50	045
19	25º47'31.26"N	93º48'13.37"E	40	137	50	043
20	25º47'33.52"N	93º48'06.81"E	35	127	55	053
21	25º46'46.50"N	93º48'04.71"E	45	135	45	045
22	25º46'20.48"N	93º48'26.00"E	60	133	30	047
23	25º45'56.63"N	93º49'30.86"E	75	300	15	240
24	25º45'46.55"N	93º49'55.45"E	50	137	40	043
25	25º47'48.04"N	93º47'43.54"E	30	120	60	060

Sl. No	Latitude	Longitude	Dip Amount (◦)	Dip Direction (◦)	Pole Value (◦)	Pole Direction (◦)
26	25º47'52.02"N	93º47'55.64"E	30	141	60	039
27	25º48'09.29"N	93º47'45.93"E	70	325	20	215
28	25º48'02.06"N	93º47'48.17"E	25	120	65	060
29	25º48'06.58"N	93º47'46.52"E	30	315	60	225
30	25º46'21.82"N	93º48'21.23"E	35	135	55	045
31	25º46'11.70"N	93º48'40.70"E	45	115	45	065
32	25º48'09.80"N	93º47'34.50"E	49	337	41	203
33	25º47'53.20"N	93º47'32.10"E	46	107	44	073
34	25º47'42.80"N	93º47'29.60"E	30	123	60	057
35	25º47'44.60"N	93º47'37.70"E	37	134	53	046
36	25º47'27.30"N	93º47'31.30"E	25	134	65	046
37	25º47'19.50"N	93º47'29.90"E	36	134	54	046
38	25º47'02.50"N	93º47'13.10"E	24	140	66	040
39	25º46'50.50"N	93º47'03.60"E	26	140	64	040
40	25º46'30.80"N	93º47'12.00"E	37	142	53	038
41	25º46'25.20"N	93º47'12.50"E	33	145	57	035
42	25º46'22.60"N	93º47'19.20"E	35	163	55	017
43	25º46'06.70"N	93º47'41.80"E	45	143	45	037
Segment II						
1	25°45'50.20"N	93°53'31.90"E	70	055	20	235
2	25°45'53.70"N	93°53'42.00"E	45	040	45	220
3	25°45'54.10"N	93°53'54.80"E	45	333	45	153
4	25°46'05.70"N	93°53'52.10"E	44	100	46	280
5	25°46'09.40"N	93°53'53.10"E	36	360	54	180
6	25°46'12.60"N	93°53'54.30"E	45	094	45	274
7	25°46'12.10"N	93°53'59.50"E	37	140	53	320
8	25°46'15.80"N	93°54'02.10"E	32	138	58	318
9	25°46'19.50"N	93°54'04.90"E	60	121	30	301
10	25°46'20.50"N	93°54'05.80"E	56	116	34	296
11	25°46'21.30"N	93°54'07.60"E	32	160	58	340
12	25°46'21.80"N	93°54'10.40"E	35	185	55	005
13	25°46'23.20"N	93°54'12.20"E	35	205	55	025
14	25°46'23.70"N	93°54'14.10"E	29	180	61	360
15	25°46'23.70"N	93°54'14.10"E	41	150	49	330
16	25°46'17.00"N	93°54'23.10"E	40	164	50	344
17	25°46'18.70"N	93°54'27.00"E	30	170	60	350
18	25°46'23.10"N	93°54'42.20"E	30	203	60	023

Sl. No	Latitude	Longitude	Dip Amount (◦)	Dip Direction (◦)	Pole Value (◦)	Pole Direction (◦)
19	25°46'27.90"N	93°54'51.10"E	31	165	59	345
20	25°46'27.90"N	93°54'51.10"E	36	136	54	316
21	25°46'31.70"N	93°55'04.10"E	38	182	52	002
22	25°46'32.40"N	93°55'04.70"E	25	165	65	345
23	25°46'43.70"N	93°55'29.30"E	55	114	35	294
24	25º45'48.85"N	93º53'38.88"E	45	005	45	175
25	25º45'48.03"N	93º53'47.56"E	60	310	30	230
26	25º45'48.67"N	93º53'46.03"E	45	080	45	100
27	25º45'50.19"N	93º53'39.90"E	30	037	60	143
28	25º45'54.79"N	93º53'55.40"E	35	360	55	180
29	25º46'12.31"N	93º54'03.46"E	55	136	35	044
30	25º46'27.66"N	93º54'53.43"E	40	145	50	035
31	25º46'20.49"N	93º54'07.76"E	35	170	55	010
32	25º45'46.57"N	93º53'22.43"E	45	060	45	120
33	25º45'48.78"N	93º53'32.84"E	55	081	35	099
34	25º45'50.03"N	93º53'39.55"E	25	042	65	138
35	25º45'52.90"N	93º53'42.49"E	50	080	40	100
36	25º45'52.38"N	93º53'51.38"E	45	345	45	195
37	25º45'54.91"N	93º53'55.39"E	30	358	60	182
38	25º46'12.40"N	93º54'03.72"E	50	121	40	059
39	25º46'23.60"N	93º54'19.03"E	35	176	55	004
40	25º46'39.10"N	93º55'04.20"E	22	090	68	090
41	25º46'28.10"N	93º54'55.50"E	40	156	50	024
42	25º46'24.00"N	93º54'17.10"E	45	155	45	025
43	25º46'24.10"N	93º54'16.90"E	45	135	45	045
44	25º46'31.40"N	93º55'08.80"E	37	235	53	305
45	25º46'22.40"N	93º54'18.70"E	32	169	58	011
46	25º46'24.40"N	93º54'17.00"E	36	147	54	033
47	25º45'56.90"N	93º53'57.30"E	31	032	59	148
Segment III						
1	25°46'14.70"N	93°56'07.30"E	38	120	52	300
2	25°46'14.20"N	93°56'08.40"E	45	130	45	310
3	25°45'44.50"N	93°56'34.20"E	35	120	55	300
4	25°45'32.10"N	93°56'50.10"E	53	145	37	325
5	25°45'26.90"N	93°56'52.70"E	46	150	44	330
6	25°45'20.90"N	93°57'15.50"E	40	160	50	340
7	25°44'59.10"N	93°57'46.60"E	30	090	60	270

Sl. No	Latitude	Longitude	Dip Amount (◦)	Dip Direction (◦)	Pole Value (◦)	Pole Direction (◦)
8	25°45'04.20"N	93°58'09.20"N	29	072	61	252
9	25°45'05.20"N	93°58'12.30"E	35	155	55	335
10	25°45'05.80"N	93°58'15.40"E	35	105	55	285
11	25°45'02.10"N	93°58'31.50"E	47	149	43	329
12	25°45'01.90"N	93°58'31.70"E	88	118	02	298
13	25°45'01.90"N	93°58'32.10"E	40	290	50	110
14	25°45'01.70"N	93°58'32.30"E	35	293	55	113
15	25°45'01.50"N	93°58'32.70"E	49	075	51	255
16	25°45'00.60"N	93°58'33.80"E	45	303	45	123
17	25°44'59.50"N	93°58'35.60"E	46	122	44	302
18	25°44'59.40"N	93°58'35.40"E	82	288	08	108
19	25°44'56.30"N	93°58'36.80"E	63	294	27	114
20	25°44'54.00"N	93°58'41.70"E	44	099	46	279
21	25º45'15.21"N	93º57'14.12"E	40	143	50	037
22	25º45'34.81"N	93º56'50.40"E	45	143	45	037
23	25º45'58.78"N	93º56'25.42"E	75	145	15	035
24	25º45'47.93"N	93º56'39.00"E	15	099	75	081
25	25º45'48.78"N	93º56'48.70"E	55	155	35	025
26	25º45'45.39"N	93º56'47.95"E	30	130	60	050
27	25º46'12.47"N	93º56'19.34"E	40	122	50	058
28	25º46'15.54"N	93º55'57.10"E	25	144	65	036
29	25º46'32.21"N	93º55'52.40"E	20	110	70	070
30	25º46'39.21"N	93º55'43.74"E	25	094	65	086
31	25º46'38.22"N	93º55'45.33"E	30	098	60	082
32	25º46'13.60"N	93º56'10.17"E	42	125	48	055
33	25º45'51.22"N	93º56'47.36"E	54	150	36	030
34	25º45'35.22"N	93º56'49.97"E	40	150	50	030
35	25º44'57.62"N	93º57'57.35"E	43	052	47	128
36	25º45'00.55"N	93º58'35.04"E	53	132	37	048
37	25º44'53.97"N	93º58'41.98"E	35	108	55	072
38	25º46'14.28"N	93º56'08.83"E	44	148	46	032
39	25º46'11.78"N	93º56'25.38"E	32	135	58	045
40	25º45'57.57"N	93º56'29.05"E	77	158	13	022
41	25º45'47.93"N	93º56'34.89"E	69	343	21	197
42	25º45'50.45"N	93º56'47.39"E	60	154	30	026
43	25º45'45.29"N	93º56'48.01"E	39	131	51	049
44	25º45'28.48"N	93º56'52.79"E	58	153	32	027

Sl. No	Latitude	Longitude	Dip Amount (◦)	Dip Direction (◦)	Pole Value (◦)	Pole Direction (◦)
45	25º45'21.38"N	93º57'14.87"E	44	100	46	080
46	25º45'03.10"N	93º57'39.13"E	47	119	43	061
47	25º44'58.46"N	93º57'57.16"E	61	272	29	268
48	25º45'00.31"N	93º58'24.06"E	49	292	41	248
49	25º44'53.78"N	93º58'41.93"E	36	130	54	050
50	25º45'05.81"N	93º58'12.64"E	20	120	70	060
51	25º45'06.94"N	93º58'18.10"E	30	145	60	035
52	25º44'59.60"N	93º57'44.50"E	40	060	50	120
53	25º45'04.70"N	93º58'09.00"E	50	075	40	105
54	25º45'05.90"N	93º58'14.80"E	30	048	60	132
55	25º44'50.90"N	93º58'41.70"E	45	112	45	068
56	25º44'10.80"N	93º59'19.60"E	55	130	35	050
57	25º44'02.00"N	93º59'47.70"E	25	160	65	020
58	25º44'01.20"N	93º59'57.20"E	25	185	65	355
59	25º44'02.50"N	94º00'05.80"E	29	225	61	315
60	25º44'05.00"N	94º00'09.90"E	44	120	46	060
61	25º45'44.80"N	93º56'33.20"E	35	110	55	070
62	25º45'57.70"N	93º56'28.10"E	76	150	14	030
63	25º44'04.40"N	94º00'09.90"E	36	110	54	070
64	25º44'02.10"N	94º00'07.20"E	33	195	57	345
65	25º44'28.00"N	93º58'36.99"E	19	273	71	267
66	25º44'57.70"N	93º58'41.90"E	31	135	59	045
67	25º45'46.00"N	93º57'13.00"E	42	167	48	013
68	25º45'51.20"N	93º56'47.00"E	61	158	29	022
69	25º45'51.20"N	93º56'47.00"E	27	109	63	071

For the preparation of geological profiles best fitting sections along AB, BC and CD are chosen as profile lines of the constructed respective geological and structural maps of the three segments. Three cross sectional geological profiles along AB, BC and CD are constructed (Figs 4.8, 4.9 and 4.10) from the prepared geological and structural maps of the three segments. The study areas are having numerous strike-slip faults and thrusts, and some normal folds and anticlinal folds are also observed.

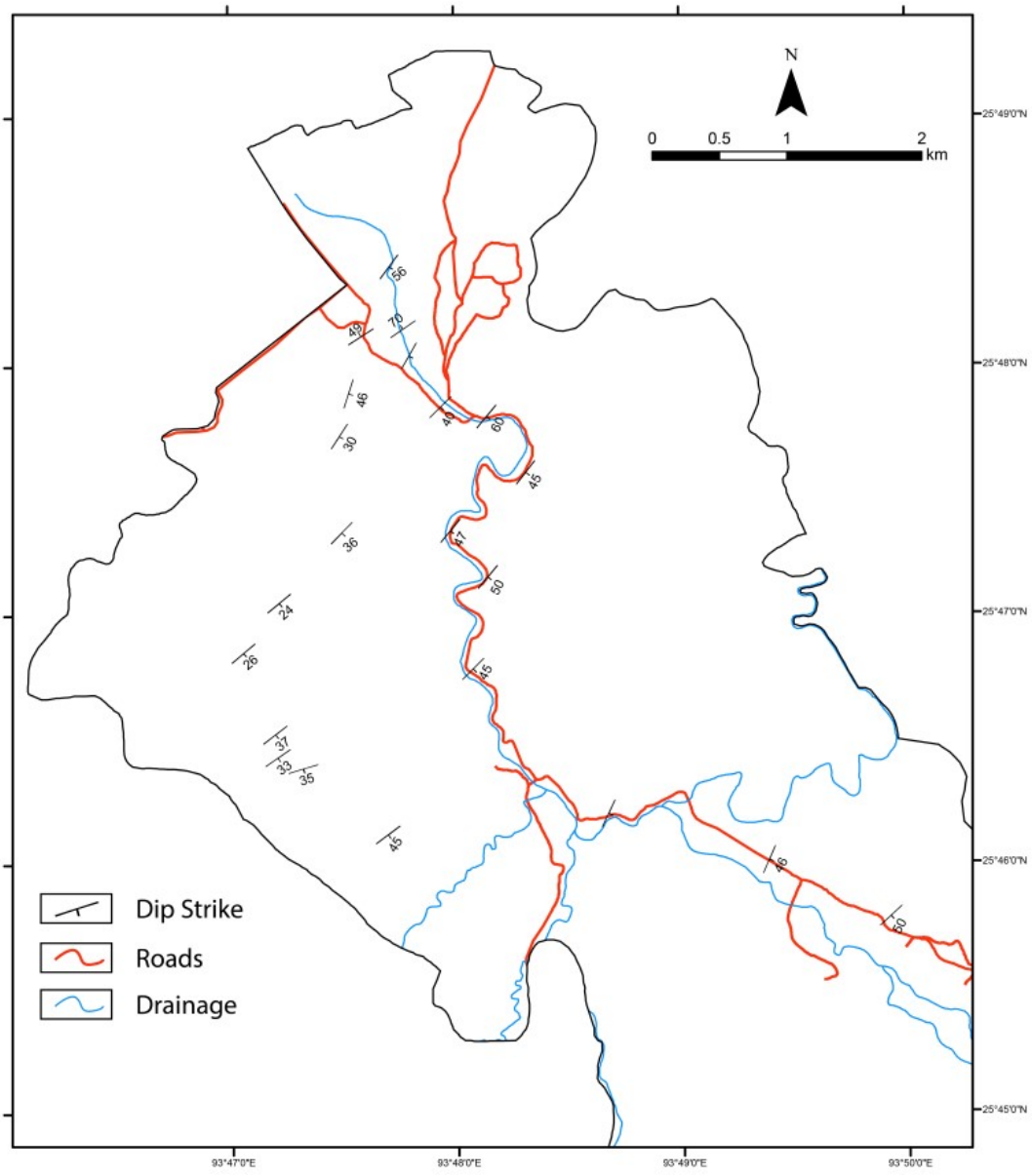
N
0 0.5 1 2
km
25°49'0"N
25°48'0"N
25°47'0"N
25°46'0"N
25°45'0"N
93°47'0"E
93°48'0"E
93°49'0"E
93°50'0"E
Dip Strike
Roads
Drainage

(a)

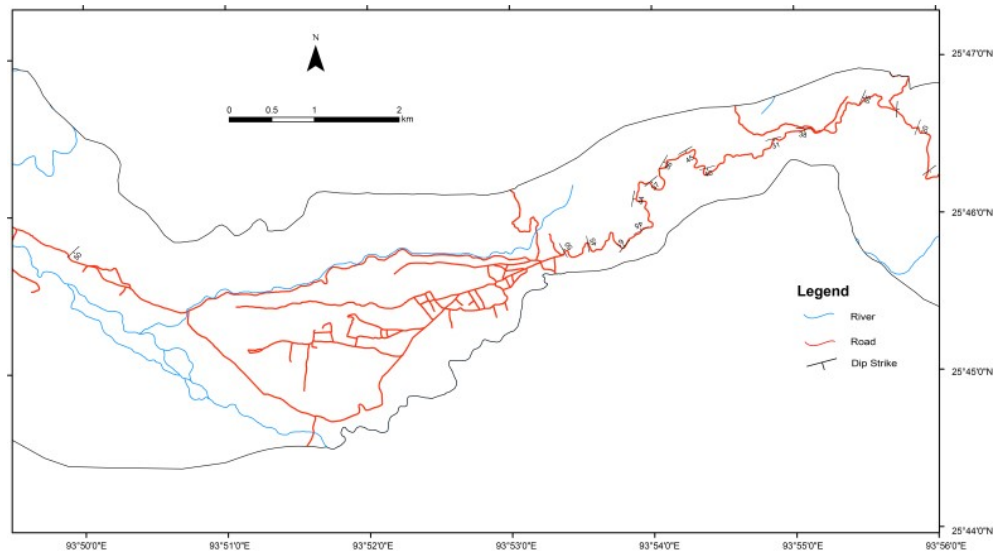

(b)

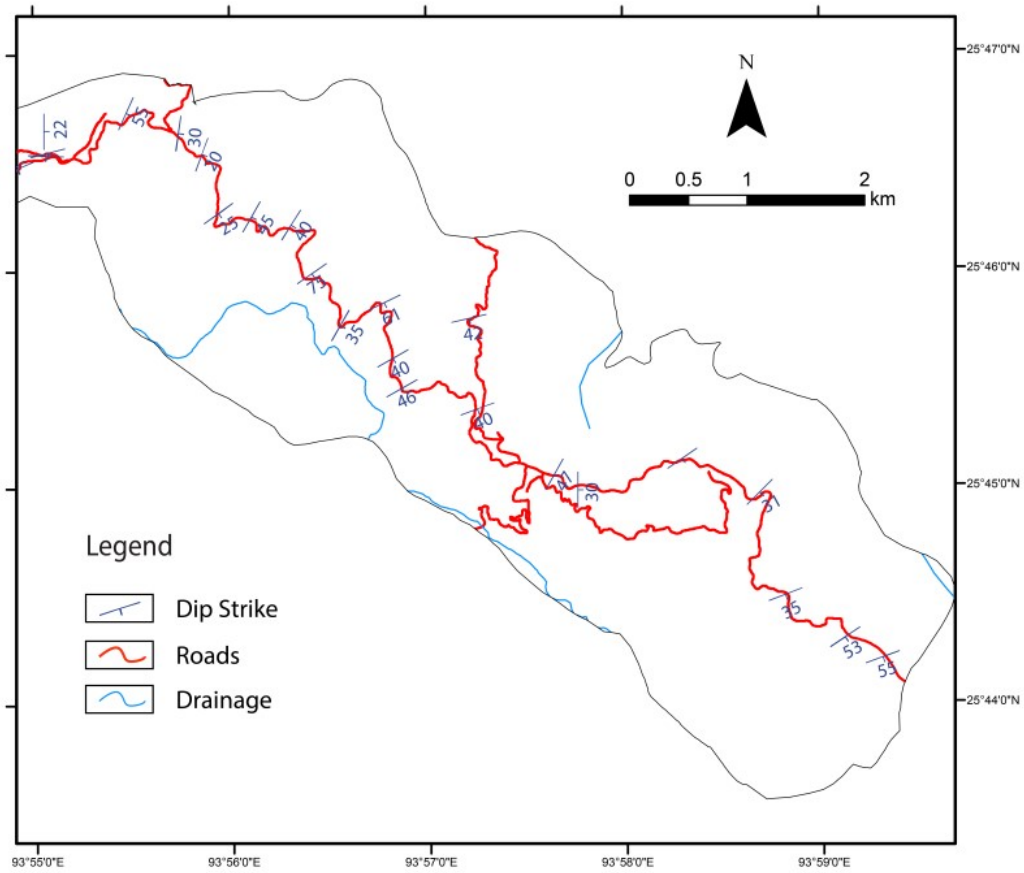

(c)

Fig. 4.7: The dip-strike plot of the beds at different locations of the Chumukedima - Piphema Section**;** (a) Segment I, (b) Segment II and (c) Segment III.

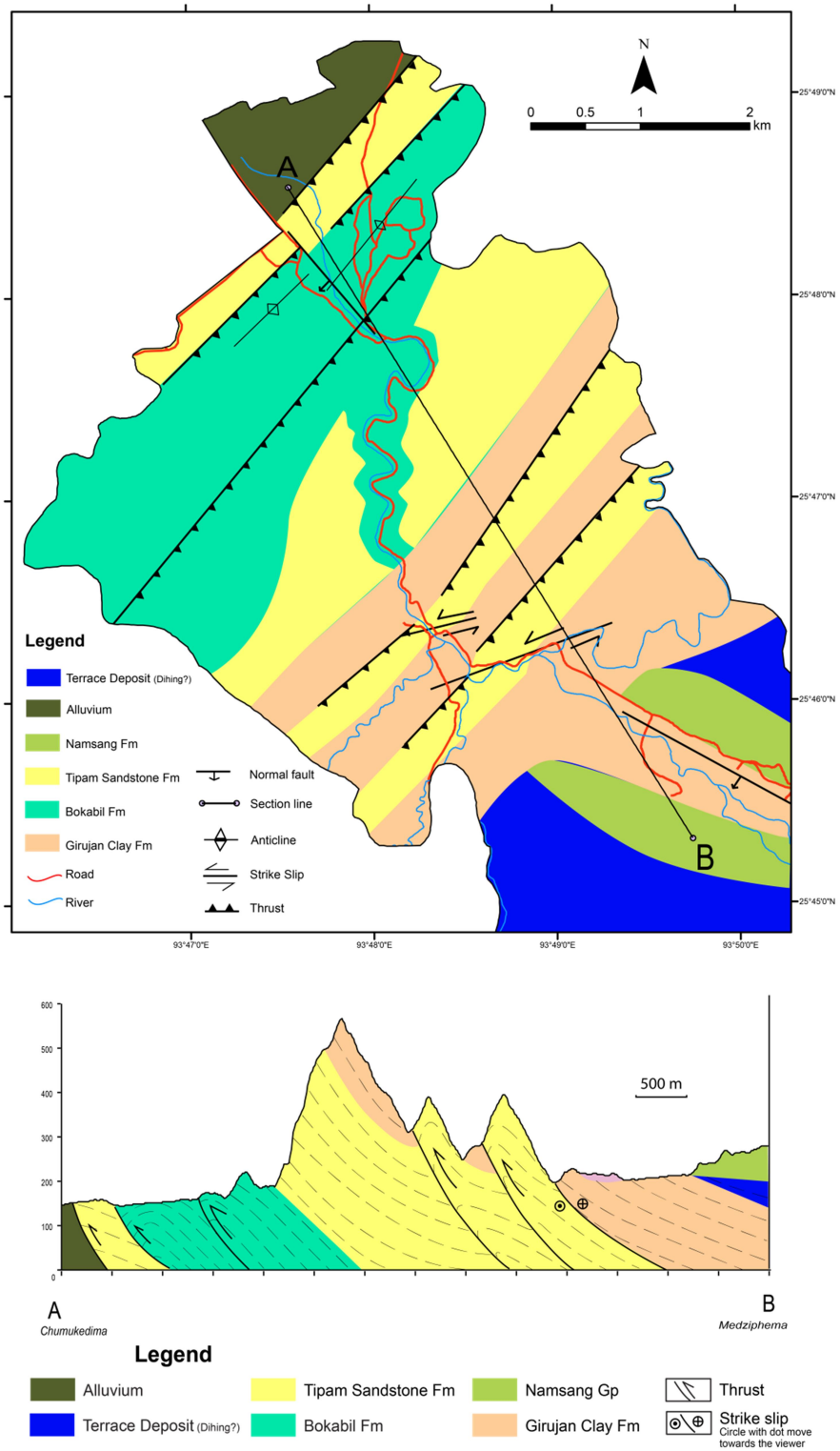

Fig. 4.8: Geological and Structural Map of Chumukedima - Medziphema Segment (segment I) and Geological Profile along sectional line AB.

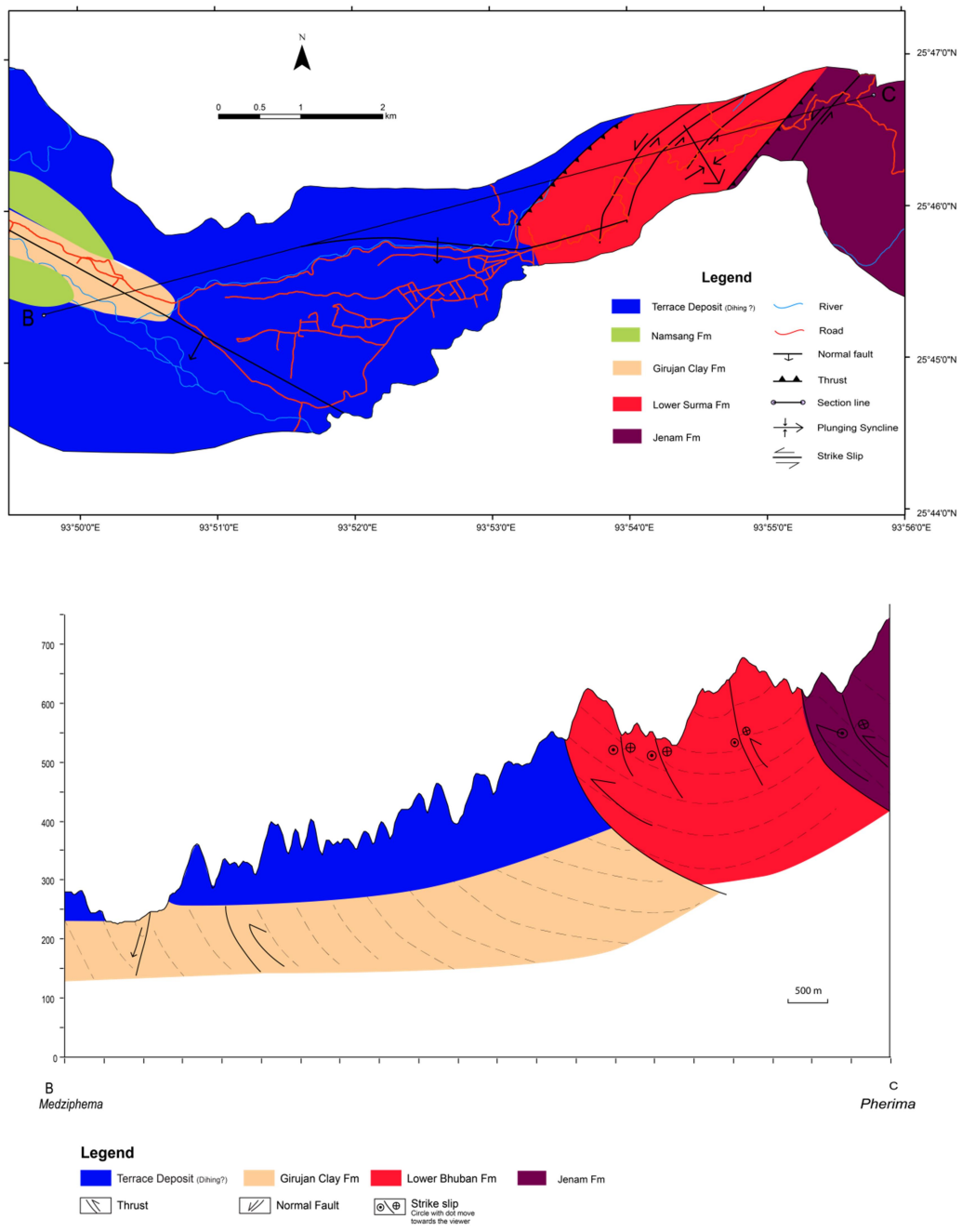

Fig. 4.9: Geological and Structural Map of Medziphema – Pherima Segment (segment II) and Geological Profile along sectional line BC.

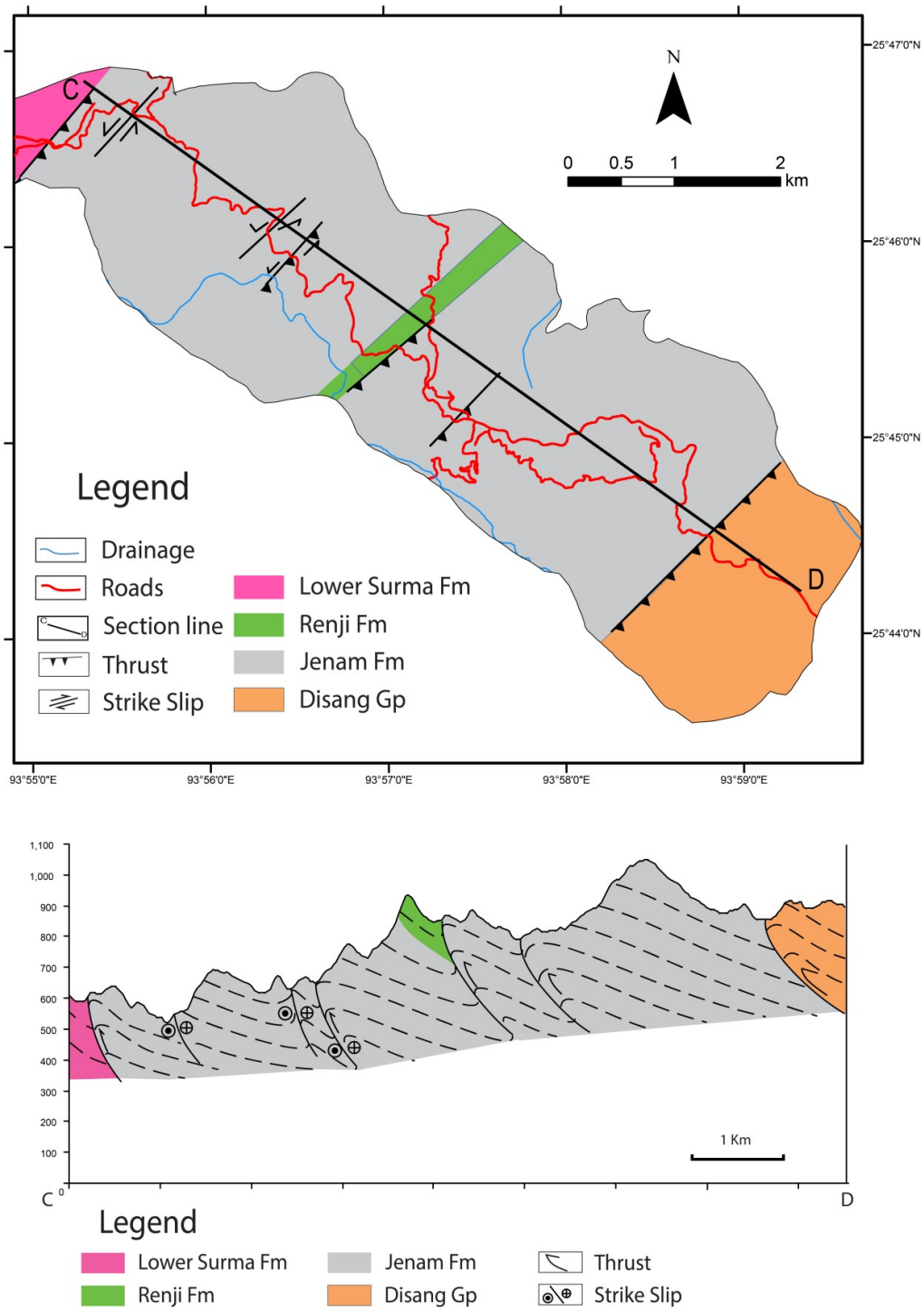

Fig. 4.10: Geological and Structural Map of Pherima – Piphema Segment (segment III)
And Geological Profile along sectional line CD.

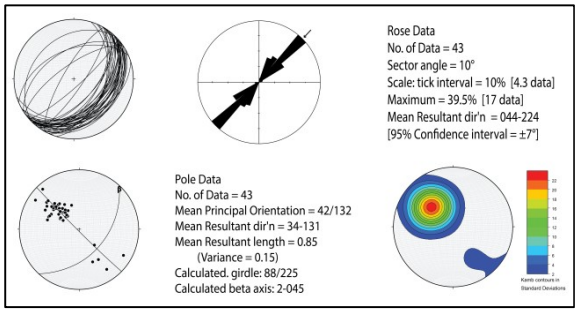

(a)

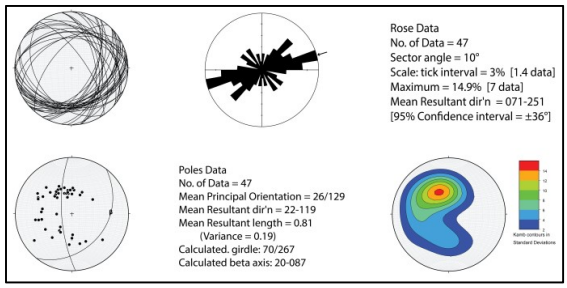

(b)

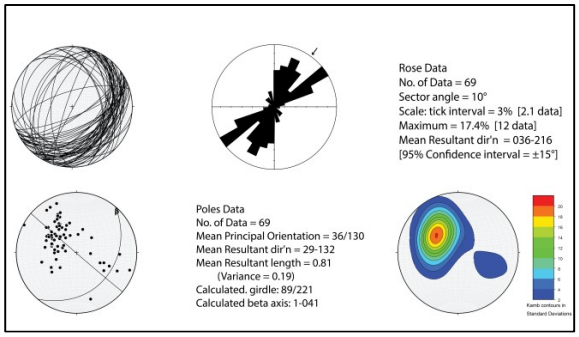

(c)

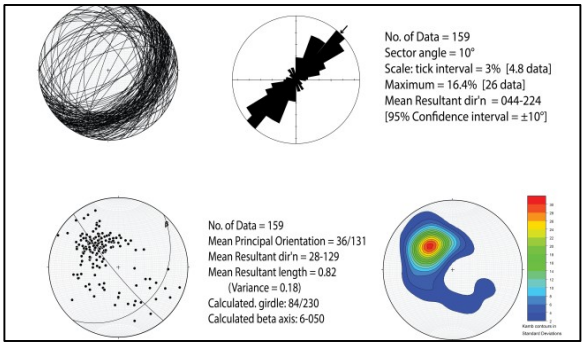

(d)

Fig. 4.11: Cyclographic plot, Rose-, Pole- and Contour diagrams of (a) Chumukedima – Medziphema Segment (AB); (b) Medziphema – Pherima Segment (BC); (c) Pherima – Piphema Segment (CD) and (d) whole of Chumukedima - Piphema Section.

Table 4.4: Summary of Rose and Pole diagrams of Fig. 4.11

Segments	I (AB)	II (BC)	III (CD)	I-III (Whole)
No. of Data	43	47	69	159
Mean Principal Direction	042°/132°	026°/129°	029°/130°	036°/131°
Mean Resultant Direction	034°-131°	022°-119°	029°-132°	028°-129°
Calculated β Axis	02°/045°	20°/087°	01°/041°	06°/050°
Calculated Girdle	88°/225°	70°/267°	89°/221°	84°/050°

Cyclographic plot, Rose-, Pole- and Contour diagrams of the bedding attitudes of the segments along AB (Chumukedima - Medziphema Segment), BC (Medziphema – Pherima Segment) and CD (Pherima – Piphema Segment) as well as of the whole of Chumukedima - Piphema Section are prepared (Fig. 4.11) to be able to decrypt the kinematics responsible for the generation of the BoS as well as to understand the attitude of the controlling structural bad tectonic features of the belt. The summary of Rose and Pole diagrams of Figure 4.11 is enumerated in Table 4.4.

The Chumukedima - Piphema Section is found to have outcrops of various litho-units of the different Formations of the Barail, Surma, Tipam and Dupitila Groups, which are mostly juxtaposed against each other along different geological structure (Figs. 4.8, 4.9 and 4.10). The field photographs of the different litho-units and their various features as well as the important geological structures depicting the field setting of the section are shown in Figures 4.12 and 4.13.

The valley of Medziphema area is found to have been exposed by younger group of litho-units. The Quaternary Terrace Deposit (Dihing?) comprising predominantly of mixtures of water borne clasts of variable sizes ranging from rounded boulders to cobbles embedded in the groundmass of fine grained sand is found to float over Girujan Clay and Namsang Formation. The Quaternary terrace deposit is very hard and almost compacted and hence could have been very old and deposited at the time of uplift of the litho-units at the time of orogenesis of the hill ranges. In the valley area this terrace deposit is very thick sometimes few hundreds of meters and found buried below the surface in some areas. In some areas on the western margin of the belt of this particular section, thin layers of this terrace deposit is found to float over Tipam sandstone as well. In the valley area

this deposit is quite thick because of the subsidence of the litho-units consequent to the generation of the intermontane basin (valley) thereby making less erosion therein than other elevated areas.

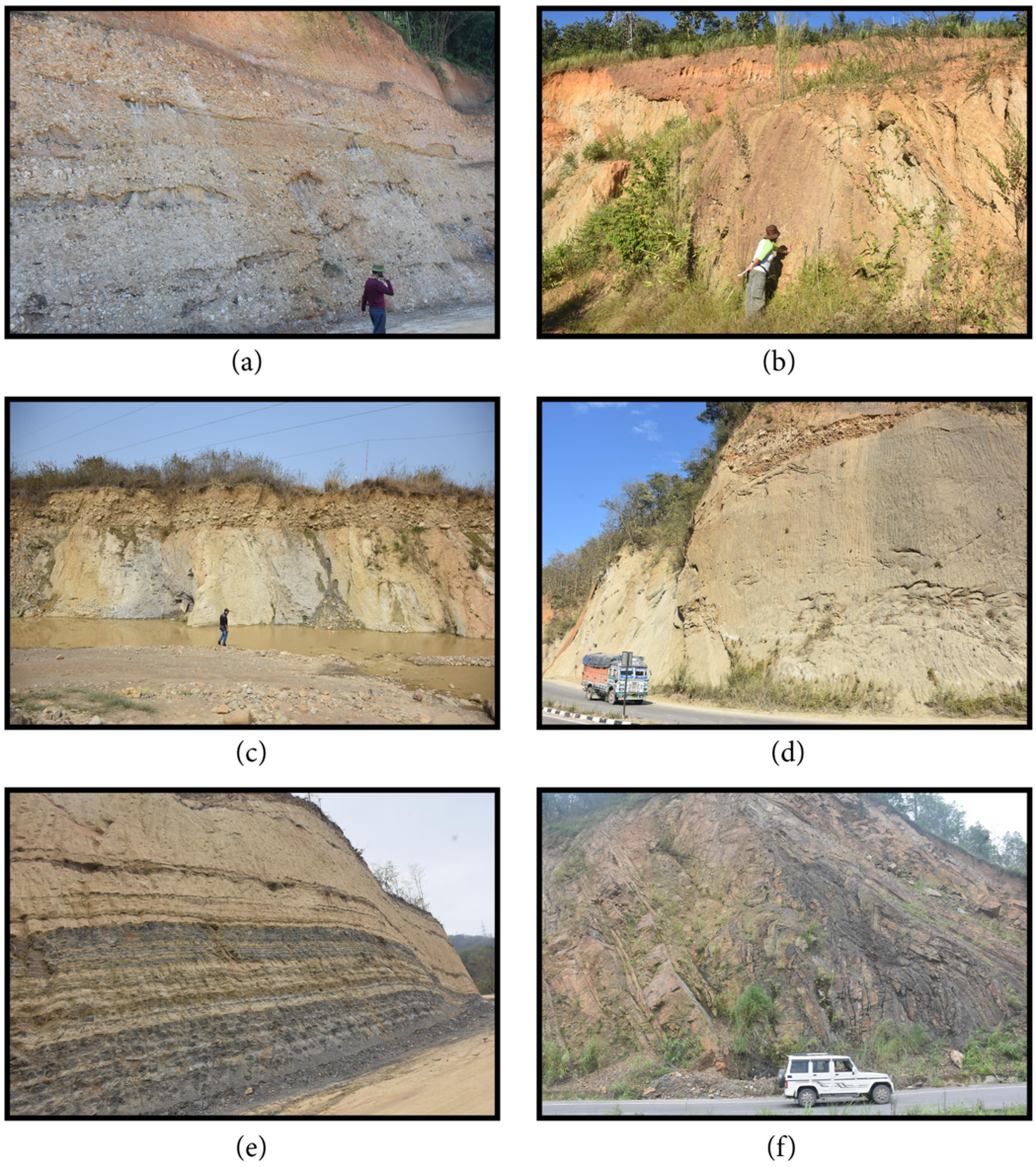

Fig. 4.12: (a) Exposure of Dihing formation (b) Exposure of Namsang Formation (c) Exposure of Girujan Clay (d) Exposure of Tipam Sandstone (e) Exposure of Surma Group. (f) Exposure of Renji formation.

Fig. 4.13: (a) Ripple marks in siltstone bed (b) Thrusting in Jenam formation (c) Fold in Shale beds (d) Thrusting between Renji sandstone and Jenam shales (e) Rip up clast in Surma Sandstone (f) Normal Faulting in Jenam formation

4.3 Pimla - Old Jalukie Section

Altogether 131 bedding data are collected from different locations along Pimla - Old Jalukie Section. The bedding data are then redefined so that pole along with pole direction of the beds could be evaluated for further construction of pole and contour

diagrams. The bedding attitude data along with the respective locations as well as other related data derived from them are shown in Table 4.5.

Table 4.5: Bedding attitudes at various stations of Pimla - Old Jalukie Section.

Sl. No	Latitude	Longitude	Dip Amount (º)	Dip Direction (º)	Poles (º)	Pole Direction (º)
1	25º40'21.42"N	94º03'36.00"E	40	315	50	135
2	25º40'10.68"N	94º03'34.50"E	64	243	26	063
3	25º37'13.80"N	93º55'59.40"E	40	327	50	147
4	25º36'43.80"N	93º54'44.60"E	25	215	65	035
5	25º36'00.20"N	93º53'36.40"E	25	194	65	014
6	25º35'41.40"N	93º53'37.40"E	15	175	75	355
7	25º34'59.91"N	93º51'56.29"E	50	117	40	297
8	25º34'44.20"N	93º52'10.00"E	55	118	35	298
9	25º34'48.20"N	93º51'15.40"E	75	121	15	301
10	25º36'16.70"N	93º50'16.10"E	40	265	50	085
11	25º39'06.20"N	93º36'02.00"E	40	164	50	344
12	25º36'19.10"N	93º40'57.90"E	30	090	60	270
13	25º36'18.10"N	93º40'57.50"E	25	240	65	060
14	25º34'15.90"N	93º38'46.40"E	50	167	40	347
15	25º34'00.30"N	93º38'39.30"E	60	178	30	358
16	25º33'43.40"N	93º38'39.40"E	55	189	35	009
17	25º33'16.40"N	93º38'16.10"E	40	333	50	153
18	25º33'16.40"N	93º38'16.10"E	60	337	30	157
19	25º32'27.30"N	93º37'41.10"E	40	145	50	325
20	25º32'26.30"N	93º37'41.70"E	40	231	50	051
21	25º33'03.50"N	93º37'24.60"E	45	197	45	017
22	25º33'03.70"N	93º37'26.10"E	70	023	20	203
23	25º33'01.20"N	93º37'23.50"E	40	200	50	020
24	25º33'00.50"N	93º36'58.40"E	70	200	20	020
25	25º33'01.10"N	93º35'39.50"E	10	055	80	235
26	25º33'05.00"N	93º35'45.60"E	75	067	15	247
27	25º33'04.40"N	93º35'58.60"E	55	352	35	172
28	25º33'07.90"N	93º36'51.60"E	35	315	55	135
29	25º33'09.00"N	93º36'55.60"E	30	015	60	195
30	25º33'09.30"N	93º36'57.40"E	60	147	30	327
31	25º33'06.40"N	93º36'57.80"E	35	089	55	269
32	25º41'43.20"N	93º52'48.30"E	75	343	15	163

Sl. No	Latitude	Longitude	Dip Amount (º)	Dip Direction (º)	Poles (º)	Pole Direction (º)
33	25º41'43.60"N	93º52'53.50"E	65	036	25	216
34	25º41'43.40"N	93º52'56.90"E	85	079	05	259
35	25º41'43.90"N	93º53'02.10"E	75	089	15	269
36	25º42'26.20"N	93º52'36.20"E	40	116	50	296
37	25º42'31.90"N	93º52'40.30"E	35	053	55	233
38	25º42'30.60"N	93º52'39.80"E	20	335	70	155
39	25º42'28.90"N	93º52'36.40"E	30	046	60	226
40	25º42'29.10"N	93º52'32.30"E	30	085	60	265
41	25º42'27.00"N	93º52'32.80"E	65	092	25	272
42	25º36'27.90"N	93º40'55.60"E	39	020	51	200
43	25º36'28.00"N	93º40'54.00"E	50	173	40	353
44	25º36'29.10"N	93º40'52.60"E	80	014	10	194
45	25º36'01.40"N	93º41'11.40"E	25	308	65	128
46	25º36'00.70"N	93º41'11.00"E	75	173	15	353
47	25º35'59.20"N	93º41'08.10"E	25	201	65	021
48	25º35'59.70"N	93º41'10.00"E	70	158	20	338
49	25º35'52.80"N	93º41'21.70"E	30	280	60	100
50	25º35'49.90"N	93º41'22.10"E	60	290	30	110
51	25º35'47.80"N	93º41'23.10"E	65	283	25	103
52	25º35'42.60"N	93º41'29.10"E	85	283	05	103
53	25º35'41.80"N	93º41'27.69"E	70	285	20	105
54	25º35'33.70"N	93º41'29.70"E	35	135	55	315
55	25º35'33.70"N	93º41'29.70"E	55	285	35	105
56	25º35'33.70"N	93º41'29.70"E	85	097	05	277
57	25º42'12.60"N	93º40'45.00"E	20	150	70	330
58	25º42'43.60"N	93º40'48.93"E	25	157	65	337
59	25º43'04.40"N	93º41'03.70"E	20	175	70	355
60	25º43'26.40"N	93º40'58.50"E	15	220	75	040
61	25º43'42.80"N	93º41'00.60"E	75	141	15	321
62	25º43'54.90"N	93º41'05.20"E	75	151	15	331
63	25º43'55.90"N	93º41'08.30"E	10	213	80	033
64	25º43'55.00"N	93º41'08.20"E	50	110	40	290
65	25º43'59.70"N	93º41'07.10"E	50	144	40	324
66	25º44'00.80"N	93º41'06.10"E	55	130	35	310
67	25º43'06.20"N	93º39'47.00"E	50	163	40	343
68	25º43'11.50"N	93º39'40.80"E	55	160	35	340
69	25º46'49.40"N	93º43'37.90"E	65	243	25	063

Sl. No	Latitude	Longitude	Dip Amount (º)	Dip Direction (º)	Poles (º)	Pole Direction (º)
70	25º36'11.68"N	93º41'17.21"E	61	185	29	005
71	25º36'05.41"N	93º41'14.78"E	84	313	06	133
72	25º35'59.15"N	93º41'19.31"E	27	217	63	037
73	25º35'59.15"N	93º41'19.31"E	20	254	70	074
74	25º35'52.54"N	93º41'21.62"E	21	282	69	102
75	25º35'52.54"N	93º41'21.62"E	31	284	59	104
76	25º35'51.18"N	93º41'21.53"E	55	263	35	083
77	25º39'12.02"N	93º35'46.55"E	46	161	44	341
78	25º40'11.74"N	93º35'12.87"E	14	138	76	318
79	25º40'32.12"N	93º34'47.05"E	59	305	31	125
80	25º43'11.97"N	93º39'47.53"E	51	158	39	338
81	25º44'06.31"N	93º41'12.01"E	53	140	37	320
82	25º44'04.09"N	93º41'06.40"E	35	127	55	307
83	25º43'43.19"N	93º41'00.13"E	51	152	39	332
84	25º43'42.21"N	93º41'03.73"E	55	317	35	137
85	25º43'26.62"N	93º40'58.54"E	17	201	73	021
86	25º43'11.05"N	93º41'02.49"E	21	189	69	009
87	25º43'08.04"N	93º41'03.06"E	52	245	38	065
88	25º42'12.47"N	93º40'45.07"E	30	140	60	320
89	25º36'42.35"N	93º42'08.58"E	54	022	36	202
90	25º36'38.89"N	93º42'11.10"E	51	166	39	346
91	25º36'20.54"N	93º42'23.14"E	44	144	46	324
92	25º36'17.68"N	93º42'24.18"E	11	244	79	064
93	25º35'53.40"N	93º42'26.09"E	33	026	57	206
94	25º35'27.82"N	93º42'20.40"E	14	154	76	334
95	25º35'27.82"N	93º42'20.40"E	42	132	48	312
96	25º35'27.82"N	93º42'20.40"E	16	122	74	302
97	25º34'44.95"N	93º42'44.33"E	47	092	43	272
98	25º34'39.02"N	93º42'57.49"E	24	071	66	251
99	25º34'31.71"N	93º43'19.38"E	31	248	59	068
100	25º34'06.90"N	93º43'49.72"E	13	198	77	018
101	25º34'06.90"N	93º43'49.72"E	72	003	18	183
102	25º34'11.87"N	93º43'59.33"E	42	021	48	201
103	25º34'11.87"N	93º43'59.33"E	35	028	55	208
104	25º34'11.87"N	93º43'59.33"E	31	056	59	236
105	25º33'34.76"N	93º44'11.89"E	32	082	58	262
106	25º33'06.25"N	93º43'54.05"E	48	119	42	299

Sl. No	Latitude	Longitude	Dip Amount (º)	Dip Direction (º)	Poles (º)	Pole Direction (º)
107	25º32'26.82"N	93º43'53.41"E	28	108	62	288
108	25º32'08.76"N	93º44'03.42"E	44	137	46	317
109	25º32'44.82"N	93º44'06.48"E	22	101	68	281
110	25º32'51.14"N	93º43'58.58"E	67	333	23	153
111	25º32'51.14"N	93º43'58.58"E	46	134	44	314
112	25º33'03.22"N	93º43'56.00"E	42	124	48	304
113	25º33'03.22"N	93º43'56.00"E	81	313	09	133
114	25º33'34.10"N	93º44'05.35"E	80	241	10	061
115	25º33'34.10"N	93º44'05.35"E	56	209	34	029
116	25º33'34.10"N	93º44'05.35"E	38	078	52	258
117	25º33'47.30"N	93º44'18.05"E	28	117	62	297
118	25º43'59.57"N	93º41'07.65"E	98	132	08	312
119	25º43'54.97"N	93º41'04.86"E	57	121	33	301
120	25º42'35.42"N	93º40'51.67"E	53	254	37	074
121	25º41'58.48"N	93º40'56.23"E	40	127	50	307
122	25º41'43.33"N	93º40'56.58"E	48	143	42	323
123	25º41'02.06"N	93º41'30.54"E	35	150	55	330
124	25º40'57.85"N	93º41'36.88"E	44	164	46	344
125	25º39'43.97"N	93º50'15.97"E	29	076	61	256
126	25º42'27.14"N	93º52'33.13"E	56	082	34	262
127	25º42'27.07"N	93º52'33.31"E	54	108	36	288
128	25º42'27.07"N	93º52'33.31"E	89	055	01	235
129	25º42'25.60"N	93º52'36.57"E	34	069	56	249
130	25º42'31.72"N	93º52'40.28"E	30	040	60	220
131	25º46'00.03"N	93º48'26.28"E	58	131	32	311

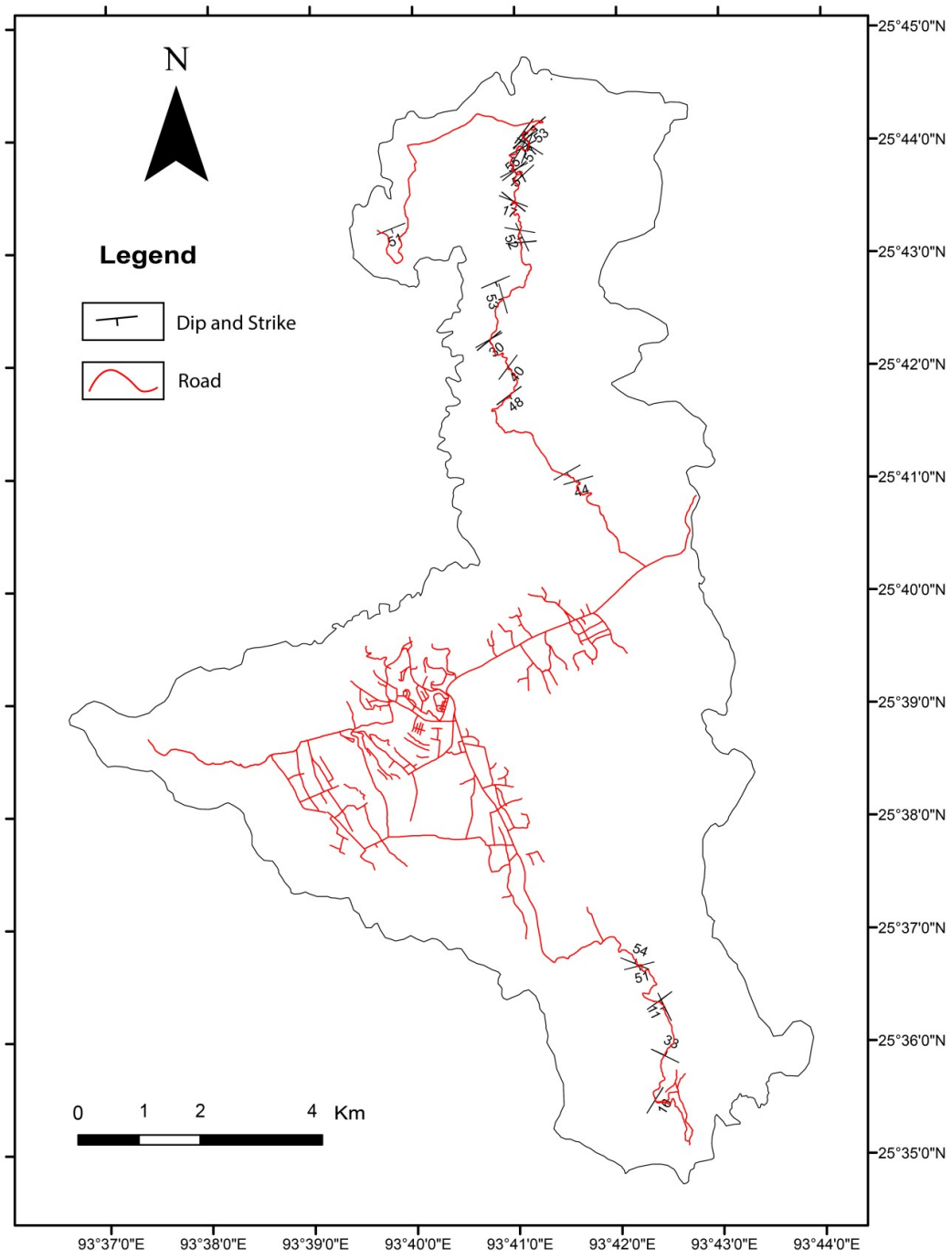

Fig. 4.14: The dip-strike plot of the beds at different locations of the Pimla - Old Jalukie Section.

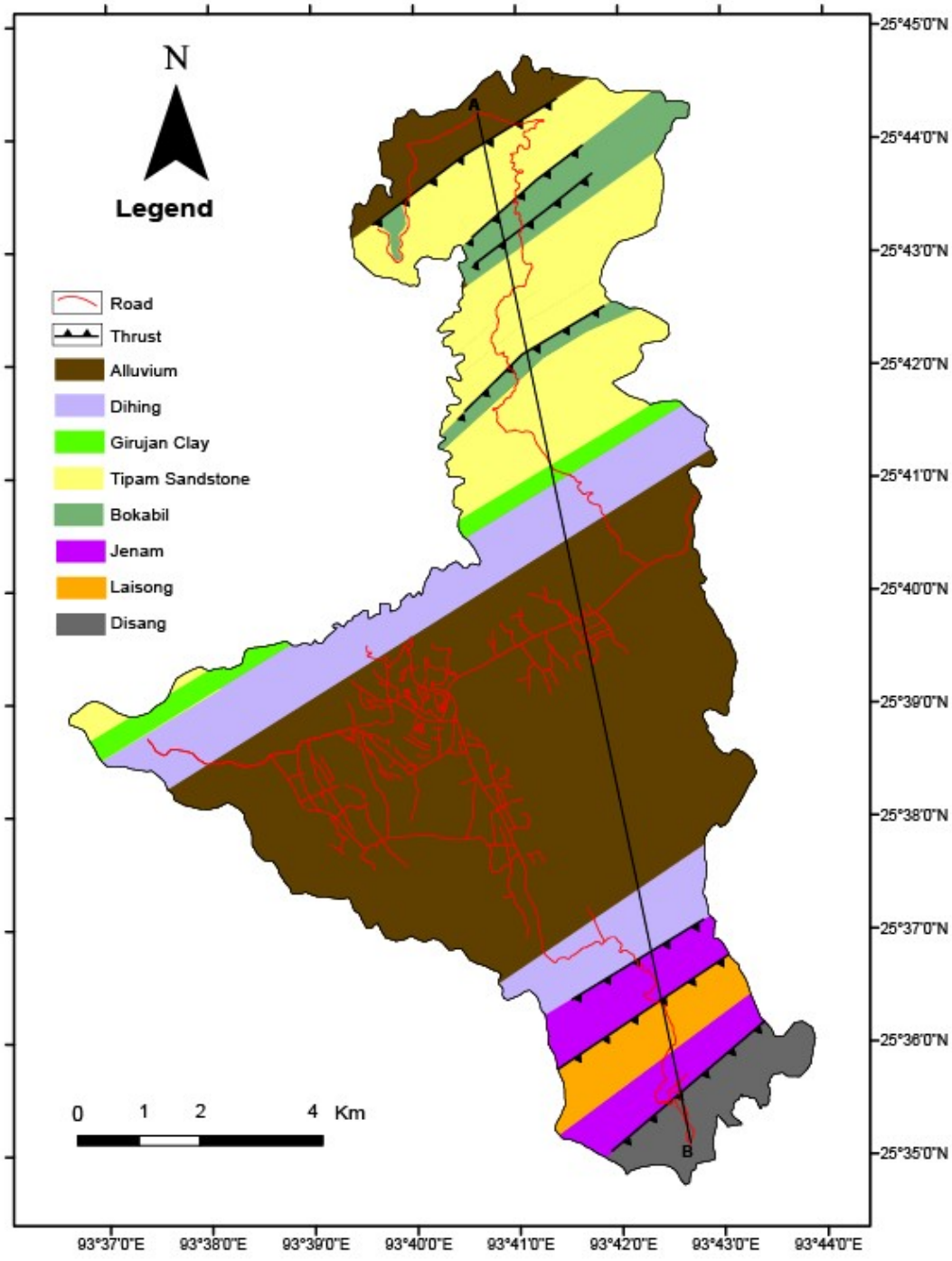

Fig. 4.15: Geological and Structural Map of the Pimla - Old Jalukie Section.

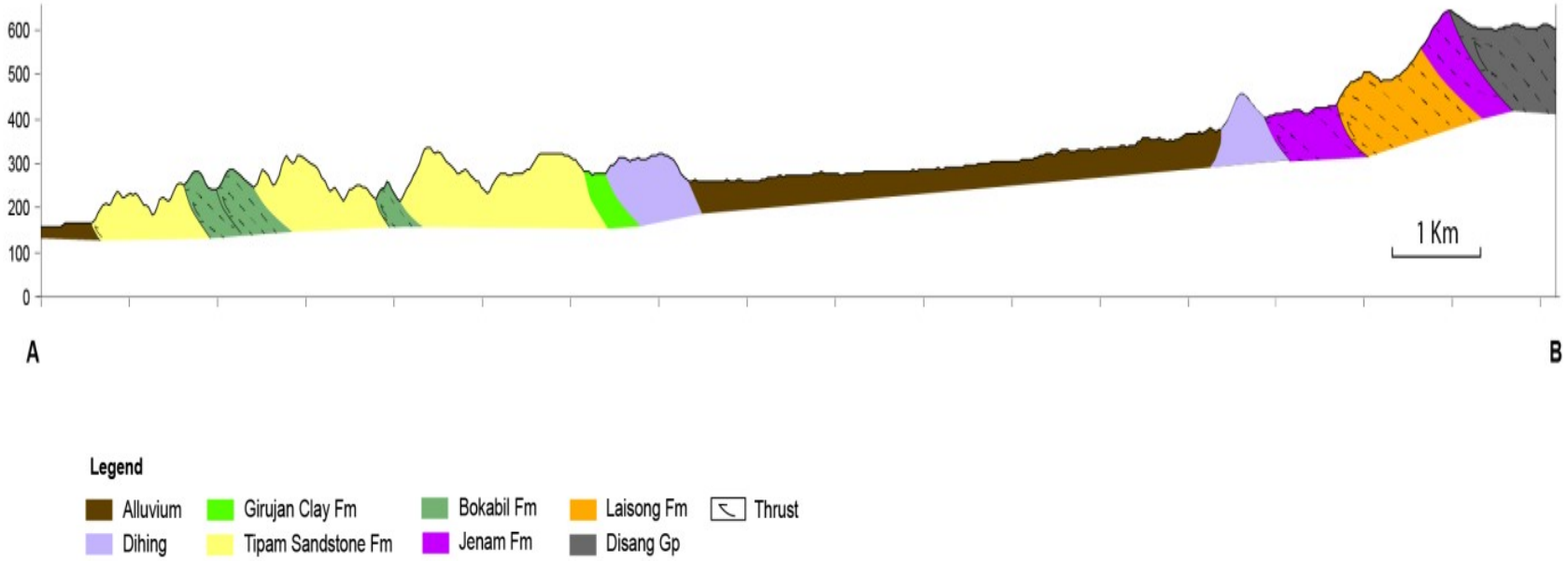

Fig. 4.16: Geological Profile along the sectional line AB of the Pimla - Old Jalukie Section.

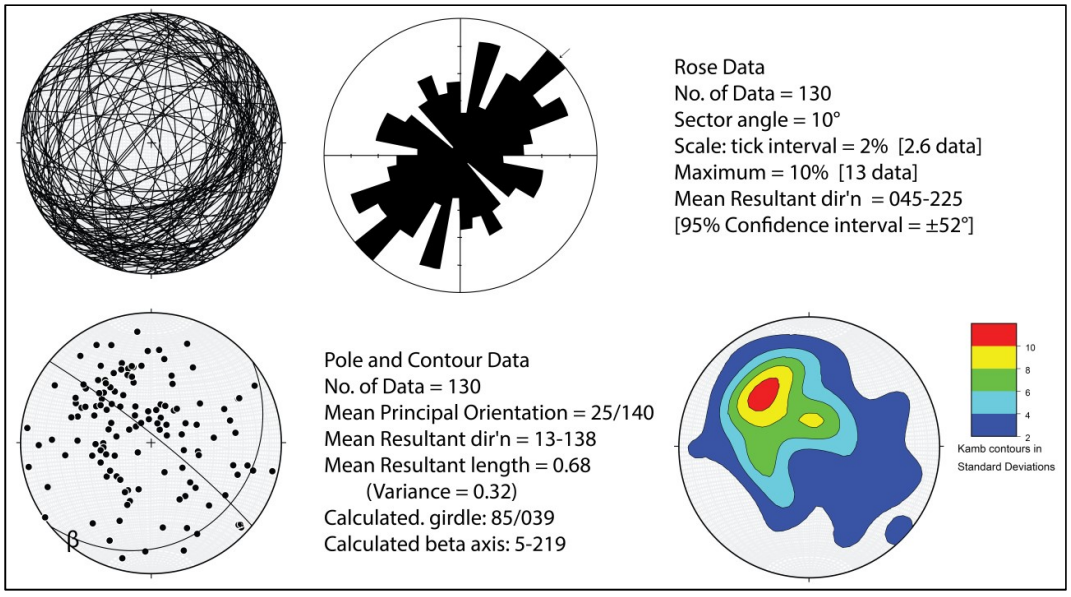

Fig. 4.17: Cyclographic plot, Rose, Pole and Contour diagrams of the Pimla - Old Jalukie Section.

Table 4.6: Summary of Rose and Pole diagrams of Fig. 4.17.

Section	**AB**
No. of Data	130
Mean Principal Direction	025°/140°
Mean Resultant Direction	013°-138°
Calculated β Axis	05°/219°
Calculated Girdle	85°/039°

The dip-strike data of the beds along with their respective GPS locations are plotted in the base map using Arc GIS 10.7 software (Fig. 4.14). Using the orientation and pattern of the dip-strike data of the litho-units, and taking into consideration of other field data like the locations where evidences of geological structures like thrusts are observed, the types of rocks found in the different locations and areas of litho-contacts, etc., a geological and structural map is constructed (Fig. 4.15). For the preparation of geological profiles the best fitting section along AB is chosen as profile lines of the constructed

geological and structural map. A cross sectional geological profiles along AB is constructed (Fig. 4.16) from the prepared geological and structural map. The study area is having numerous strike-slip faults and thrusts.

Cyclographic plot, Rose-, Pole- and Contour diagrams of the bedding attitudes of the whole of Pimla - Old Jalukie Section are prepared (Fig. 4.17) to be able to decrypt the kinematics responsible for the generation of the BoS as well as to understand the attitude of the controlling structural and tectonic features of the belt. The summary of Rose and Pole diagrams of Figure 4.17 is enumerated in Table 4.6.

Fig. 4.18: (a) Exposure of Dihing? Formation (b) Exposure terrace deposit over Girujan clay (c) Terrace deposit over Tipam sandstone (d) Exposure of Tipam sandstone (e) Exposure of Surma Sandstones in a river bed (f) Exposure of Jenam Formation

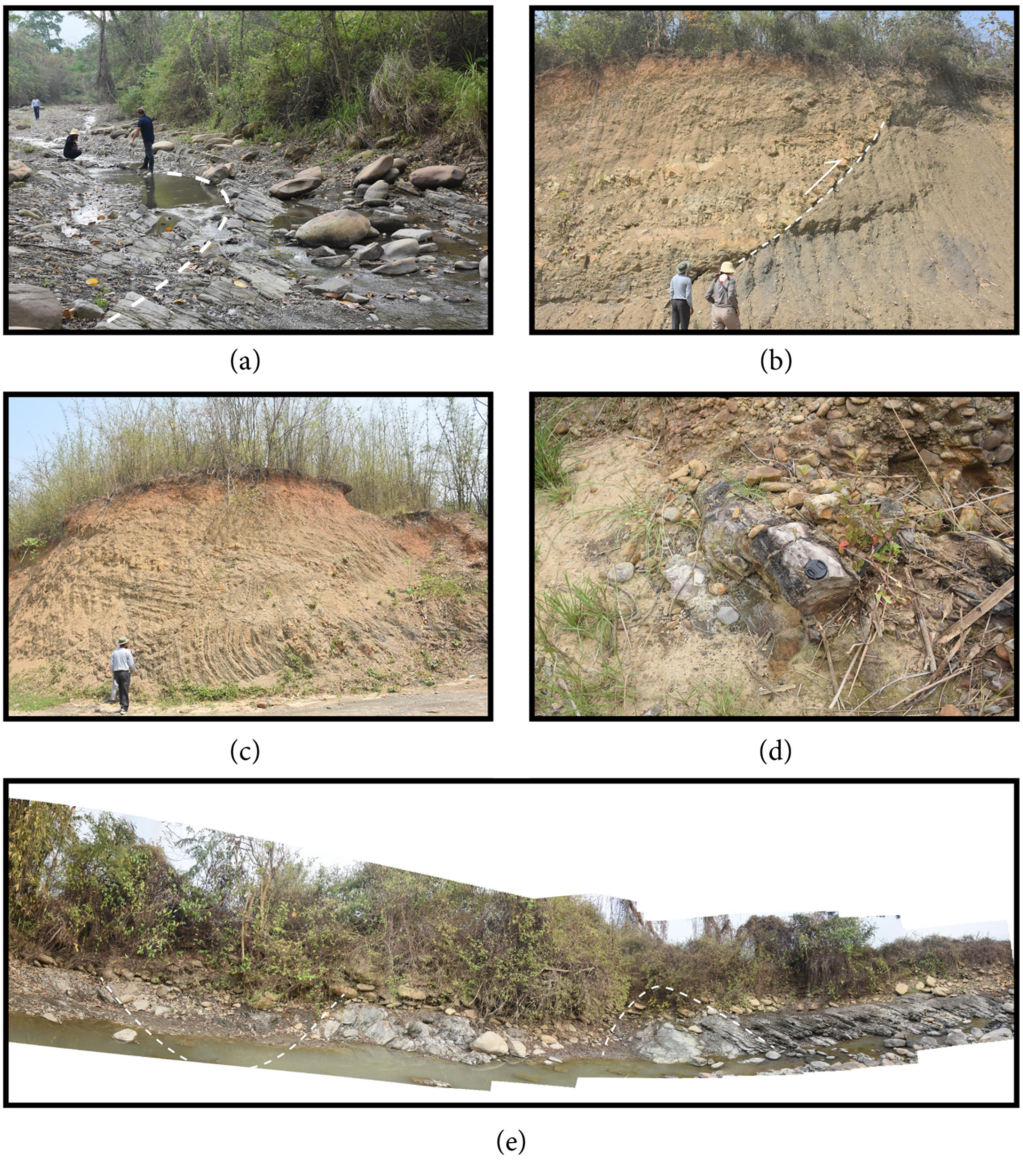

Fig. 4.19: (a) Closure of a fold (b) Thrust contact between Laisong and Jenam formation (c) Drag fold developed in Jenam shales (d) Petrified wood (e) closure of a pair of Syncline and Anticline

The Pimla - Old Jalukie section is found to have outcrops of various litho-units of the different Formations of the Barail, Surma and Tipam Groups, which are mostly juxtaposed against each other along different geological structure (Figs 4.15 and 4.16) . The field photographs of the different litho-units and their various features as well as the important geological structures depicting the field setting of the section are shown in Figures 4.18 and 4.19.

Just at the western margin of the Jalukie valley in this section the Jenam Formation is found to overthrusts the Girujan Clay Formation. The Benioff zone of this thrust is considerably wide and found to be the exposure of the mixture of huge blocks to boulder sized broken pieces of sandstone embedded in crushed materials. In the valley area the Girujan Clay is found cover by sporadic deposits of Quaternary Terrace Deposit (Dihing?), which is comprised predominantly of mixtures of water borne clasts of variable sizes ranging from rounded boulders to cobbles embedded in the groundmass of fine grained sand. This terrace deposit is very hard and almost compacted and hence could have been comparatively old. Considerably thick pile of such terrace deposit is found on tops of some exposures of Tipam sandstone and Girujan clay in the extreme western margin of the BoS. Just below the extensive thrust occupying on the eastern side, in a river bed just at the immediate west at a lower elevation, shale of Upper Disang Formation overlain by sandstone of Laisong Formation is exposed (lat 25º 36'05.4" N and 93º 41' 14.78" E long). In the immediate west of this river bed there is exposure of Girujan clay just above the exposure of shale of Disang Group overlain by sandstone of Laisong Formation. The shale and sandstone formations are found folded. In shale of Upper Disang Formation closures of a pair of adjacent anticline and syncline are found preserved (Fig. 4.19e). The two adjoining anticline and syncline axes are found to plunge by 27° towards 250°. There is also an exposure of plunging anticline developed in sandstone (Laisong Formation) at the same river bed (Fig. 4.19a). When the plunge and direction are measured at the closure of the anticline the values are the same with those of the anticline and syncline developed in shale.

Chapter 5

Joint, Conjugate Fracture and Slickenside Analyses

Rocks are books of history in which all of the different episodes of geologic events of the earth are recorded. These events are implanted in them in coded form as various microscopic, mesoscopic and megascopic features. When rocks near or within the surface of the earth are subjected to a system of forces particularly at the time of orogenesis, they deform according to the nature, direction and nature of amplitude of the forces. The system of forces acting on the rocks is responsible for a variety of features developed in the rocks. Joint is one of these features from which, the tectonic events of deformation of the surviving exposure in relation to the present geologic setting can be decoded. Again, the stress conditions, the rocks suffered at the moment they were deformed or fractured have been encrypted in the form of various geological structures. Consequently, paleo-stress conditions in rocks could be evaluated from certain geological structures. The evaluation of the paleo-stress conditions could shed some light on the deformation mechanism, kinematic and tectonic environment of a part or the whole of an orogen. The structures which are conveniently used for the evaluation of the stress field of a region of an orogen include conjugate fractures (fault/joint) and slickensides. Among the different deformation structures, the conjugate fractures are considered as the most significant and the easiest means of evaluation of the principal stress orientations of the stress field that led to the development of such failure structures. Slickensides also are structures from which principal stress orientations can be conveniently evaluated.

The litho-units of the Belt of Schuppen (BoS) in Nagaland are found to have been characterized by various joint systems, which are developed as closely spaced systematic joint sets in a number of horizons in the sequence of the various formations. Conjugate joint (fracture) pairs and slickensides are also developed in various locations of the belt. An attempt is made in this chapter to analyse the array and geometry of the joints, conjugate fractures and slickensides.

With an aim to make portray a clearer picture about the tectonic conditions of the generation of the whole section in particular and for the different tectono-morpho landforms in general, the section of the BoS from Chumukedima to Piphema along the National Highway No. 2 is divided into four different segments (Fig. 5.1). The segment I

is on the westernmost part of the section, which lies on the western side of the extreme northern margin of the Jalukie-Medziphema intermontane valley. The segment II is the part the studied section that just touches the extreme northern margin of the valley. The segment III is on the eastern side of the extreme northern margin of the valley, which touches the segment II. The area of the most depressed portion of the valley doesn't reach this segment but lies toward the southeast of segment III. Bedrocks are still standing instead of valley filling alluvium deposits. The segment IV is just beyond the belt, which falls within the adjacent geotectonic unit of the inner fold belt. Joints of segment IV is studied to correlate with the data of other segments as well as to examine whether the BoS is having related additional tectonism other than that of the rest of the orogen.

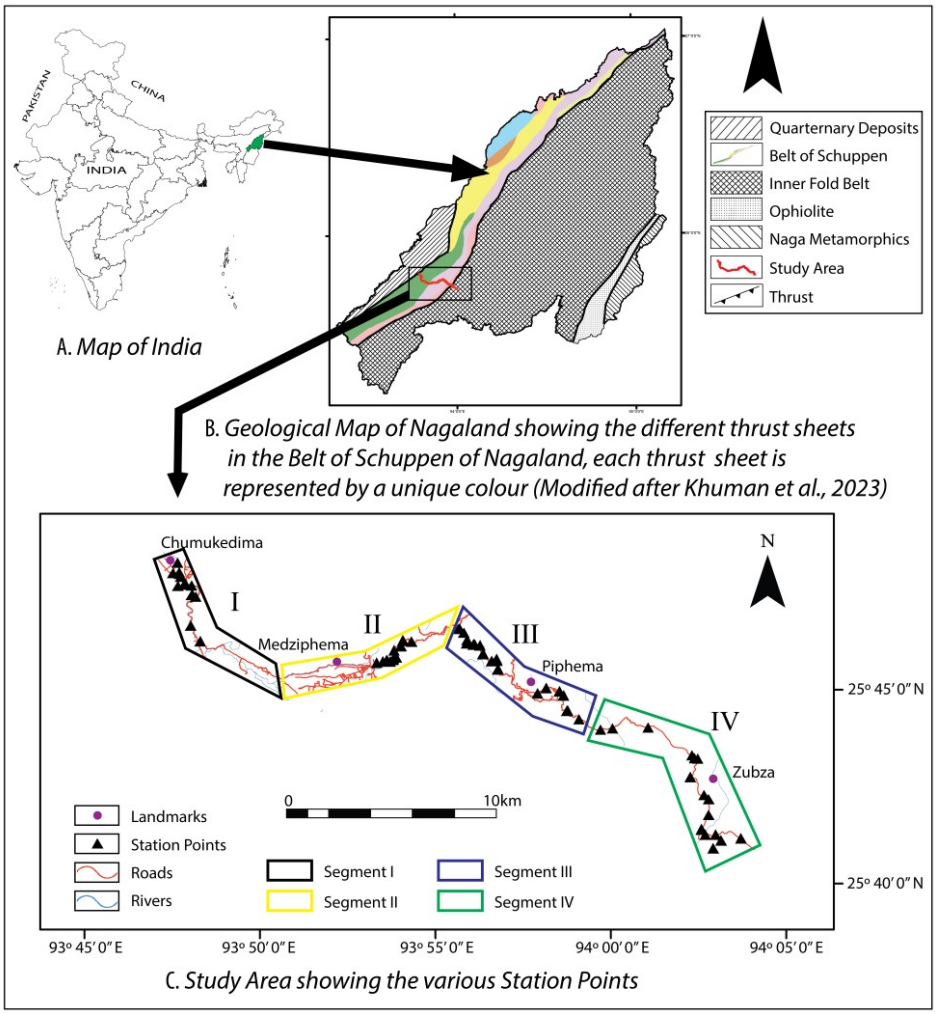

Fig. 5.1: Geological map of Nagaland showing the different geotectonic units and the location of the study area.

5.1 Joint Analysis

Joints are breaks or fractures found on a body of rock (across which cohesion is more or less completely lost) that have resulted due to the action of stress. Joints show very little (microscopic), to no displacement along the fracture planes (Ghosh, 1993). Generally, there has been no visible movement parallel to the surface of the joint, if not; it would be classified as a fault (Park, 1997). A group of parallel or sub-parallel joints constitute a joint set. Short and local irregular joints that are not part of a set are called non-systematic joints (Hodgson, 1961). Joints generally occur in parallel or sub-parallel sets, and where differently oriented sets cross, the resulting geometric pattern is known as a joint system (Ramsay and Huber, 2006).

Joints are more commonly of tectonic origin. Many joint types, especially those associated with folded and faulted rocks are clearly related to the processes of crustal deformations or tectonics. Joints are mostly developed in response to the nature and orientation of the stress systems. They are most commonly developed in the upper crust in response to its brittle conditions. They show different types of joints (Fig. 5.2): (i) Tensile joints (Mode-I, tensile-fracturing), (ii) Shear joints (Mode-II, shear fracturing) and Hybrid joints (Mode-III, hybrid fracturing). With strong compressive force, a tensile force may be developed at 90º to the compressive direction, which causes the longitudinal jointing or splitting) thereby producing Mode-I fractures giving rise to tensile joints. Thus, tensile joints are aligned nearly parallel to the regional compression direction of an orogen. Shear joints are generally developed at low to moderate confining pressure and they are commonly observed in the vicinity of fault plane or shear zone. In both tri-axial extension and tri-axial compression tests the shear joints develop at the angle of 25-35º to the maximum principle compressive stress. They are generally developed about 30º away on both sides of the regional compression direction. The hybrid joints are those failed on a mixed mode and grow due to tensile as well as shear fracturing. These joints are not necessarily parallel to the maximum principle compressive stress but orient at low angles (about 15-20º).

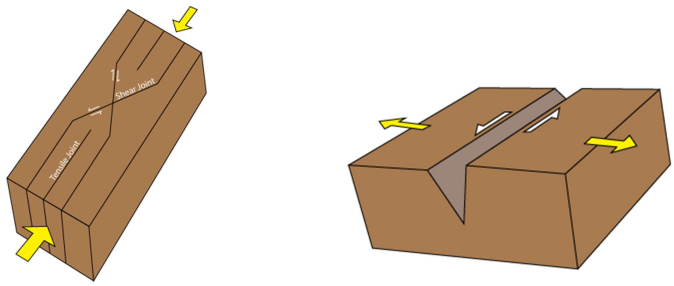

(a) (b)

Fig. 5.2: Schematic representation of different types of joints with respect to compression direction. (a) Tensile fracture (Mode-I) and Shear fracture (Mode-II); (b) Mixed mode or Hybrid fracture (Mode-III).

An understanding of the geometry and orientation of joints could reveal the nature of brittle deformation in relation with the structural and tectonic setting of the rocks of a region. Furthermore, systematic joints also reflect the regional tectonic stress trajectories at the time of fracturing, whereas the non-systematic joints indicate the local heterogeneities of the stress field (Pollard and Aydin, 1988). Information on fracture arrays in a region helps to define the stress and strain history of a region and thus is important for regional tectonic analysis.

The joints developed in various horizons of the formations along the studied section have a wide range of orientations. This may be partly due to the presence of several sets of joints or partly by the dispersion within each set as well as rotational displacement of blocks of rocks in due course of later tectonic evolution or may be because of some additional stress fields of other related tectonic phenomena. In order to be able to get an idea about the tectonic conditions of the nature of brittle failure, and the generation of the BoS and the later evolutionary changes, attitudes of 562 joints were collected from different parts of the section (Table 5.1). The joint data are analyzed in the form of rosettes, stereo-net plots of planes, pi and contour diagrams.

The rose diagrams of the joints of the different segments are shown side by side with those of the bedding attitudes of the respective segments (Fig. 5.3). The major concentration of the orientations of bedding may give clues about the controlling deformation mechanisms of the respective areas and their relations to the orientations of the joints in the different segments. The β diagrams of the bedding planes of the four

segments (Fig. 5.4) are prepared to make portrayed their distribution in space with an aim to understand their relation with the orientations of the principal stresses that are responsible for the generation of the joints. The stereo-plot, pi and contour diagrams of the joint planes of the four different segments are shown in (Fig. 5.5). From these diagrams, the distribution and major concentrations of the joint planes as well as the mode of dip of the joints in the different segments are understood.

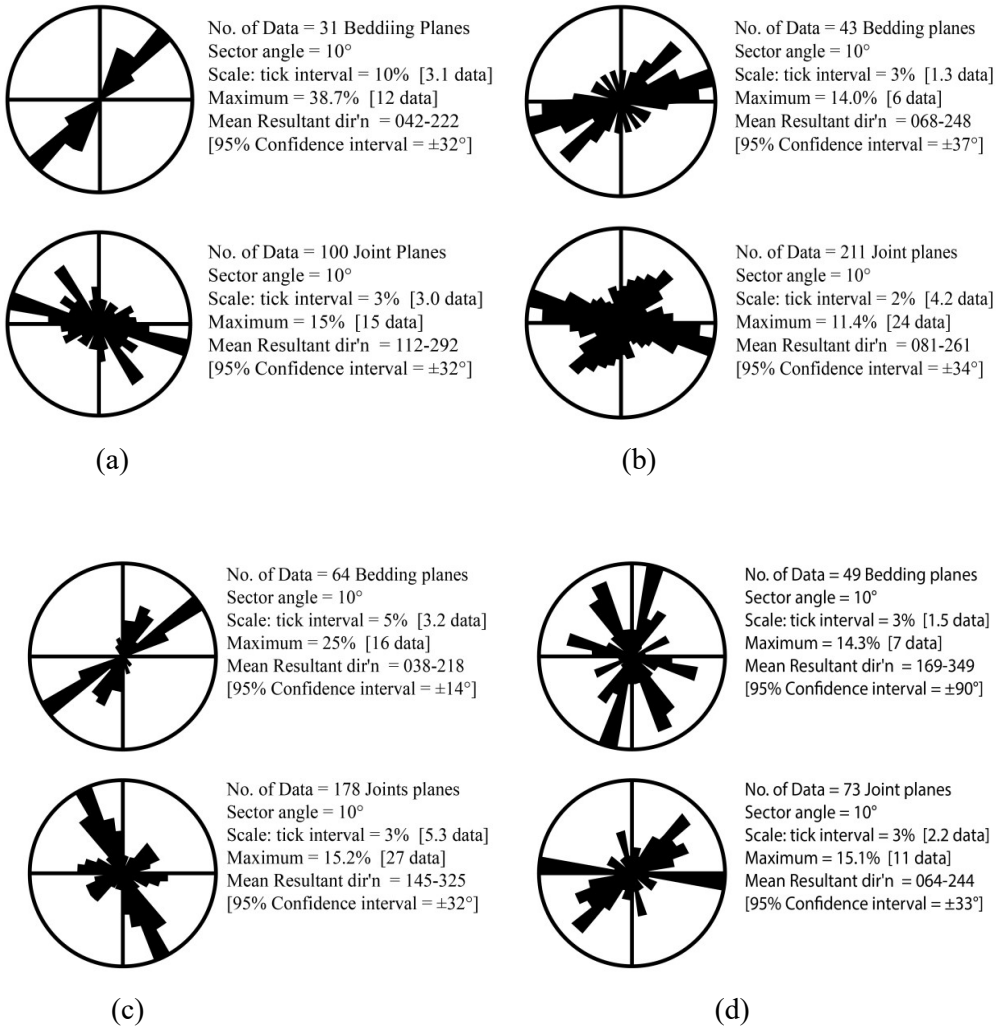

Fig. 5.3: Rose diagrams of beddings and joints. (a) Segment I, (b) Segment II, (c) Segment III, (d) Segment IV.

Table 5.1: Attitudes of joints from different locations of Chumukedima – Piphema Section.

SL. No.	Latitude Longitude	dip amount (°)	dip direction (°)
1	25°45'48.8"N	55	183
2	93°53'48.8" E	80	069
3		70	111
4		55	149
5		70	135
6		55	124
7		55	136
8		55	214
9		65	136
10		75	274
11	25°45'48.7"N	60	261
12	93°53'46.0" E	75	196
13		85	354
14		15	294
15		50	272
16		70	175
17		60	204
18		80	335
19	25°45'50.2"N	75	158
20	93°53'39.9" E	55	230
21		85	128
22		55	192
23		60	259
24		65	189
25		85	189
26		55	223
27		50	199
28	25°45'54.8"N	65	195
29	93°53'55.4" E	70	121
30		60	131
31		85	255
32		60	177
33		60	194
34		70	260
35		70	120
36		60	210
37		70	147
38		60	120
39		65	189
40		60	110
41		65	200
42	25°46'12.3" N	50	009
43	93°54'03.5" E	65	210
44		50	354
45		75	205
46		85	203
47		50	226
48		55	295
49		70	210
50		45	010
51	25°45'34.8" N	40	321
52	93°56'50.4" E	75	233
53		70	249
54		85	242
55		75	246
56		45	305

SL. No.	Latitude Longitude	dip amount (°)	dip direction (°)
57		75	070
58		45	266
59		45	330
60	25°46'14.1" N	70	250
61	93°56'08.5" E	40	315
62		60	335
63		65	261
64		80	200
65	25°45'58.8" N	60	231
66	93°56'25.3" E	30	070
67		60	071
68		60	235
69		85	063
70	25°45'47.9" N	80	194
71	93°56'39.0" E	80	338
72		70	244
73		80	092
74		75	016
75		70	331
76		70	195
77		80	245
78		80	160
79	25°45'48.8" N	55	010
80	93°56'48.7" E	80	257
81		85	180
82	25°46'12.5" N	80	209
83	93°56'19.3" E	45	225
84		85	169
85		75	019

SL. No.	Latitude Longitude	dip amount (°)	dip direction (°)
86		85	024
87		65	249
88		75	350
89		70	019
90		55	257
91		80	004
92		55	284
93	25°46'15.5" N	75	264
94	93°55'57.1" E	70	021
95		65	299
96		60	330
97		80	264
98	25°46'32.2" N	80	214
99	93°55'52.4" E	65	272
100		75	356
101	25°46'39.2" N	70	336
102	93°55'43.7" E	80	215
103	25°46'20.5" N	65	025
104	93°54'07.8" E	80	155
105		65	165
106		85	050
107		75	331
108		75	287
109		75	030
110		55	310
111	25°48'02.0" N	80	212
112	93°47'48.2" E	75	287
113		80	340
114		60	350

SL. No.	Latitude Longitude	dip amount (°)	dip direction (°)
115		80	218
116		85	060
117		80	163
118	25°48'06.6" N	80	150
119	93°47'46.5"E	45	106
120		70	200
121	25°46'21.8" N 93°48'21.2"E	45	015
122	25°40'55.5"N	65	166
123	94°02'55.3' E	75	087
124		60	052
125		70	077
126		85	010
127	25°41'07.9" N	80	075
128	94°03'09.1" E	55	320
129	25°45'05.8" N	85	205
130	93°58'12.6" E	55	305
131		70	003
132	25°44'30.2"N	65	015
133	93°58'47.7" E	55	072
134		60	109
135		75	089
136		40	345
137		75	245
138		65	030
139	25°43'15.3" N	50	034
140	94°02'24.6" E	50	309
141	25°42'46.6"N	75	160
142	94°02'17.1" E	50	139

SL. No.	Latitude Longitude	dip amount (°)	dip direction (°)
143		70	038
144		55	060
145	25°42'18.7" N	60	325
146	94°02'40.7" E	60	014
147		70	075
148		80	065
149		60	005
150		75	120
151	25°41'47.5" N	85	320
152	94°02'48.1" E	85	354
153		65	320
154		40	347
155		75	303
156	25°41'25.2" N	75	164
157	94°02'35.8" E	25	115
158		50	090
159		70	338
160		80	031
161		50	160
162		70	105
163		80	124
164		60	335
165		50	160
166		45	155
167	25°47'48.1" N	63	253
168	93°48'06.9" E	70	210
169		55	236
170		66	331
171		50	236

SL. No.	Latitude Longitude	dip amount (°)	dip direction (°)
172		80	021
173		81	015
174		60	270
175		87	190
176		65	260
177		43	257
178		68	005
179		51	213
180		67	004
181	25°47'47.6" N	88	193
182	93°48'16.8" E	61	243
183		34	012
184		72	351
185		83	312
186		42	013
187	25° 47'34.0"N	81	060
188	93°48'08.2" E	62	020
189		48	310
190		60	012
191		83	332
192		83	028
193		83	033
194		53	319
195		56	340
196		79	048
197		89	300
198		66	051
199		70	042
200		40	092

SL. No.	Latitude Longitude	dip amount (°)	dip direction (°)
201		71	289
202		42	357
203		85	018
204		47	325
205		45	302
206		74	035
207	25°45'50.4" N	82	171
208	93°53'39.8" E	89	180
209		64	194
210		85	253
211		61	286
212		53	202
213		78	154
214		48	212
215		66	191
216		77	297
217		77	328
218		63	199
219		77	180
220		88	164
221		87	355
222		53	196
223		73	168
224		63	258
225		63	287
226		68	176
227	25°45'51.2" N	41	184
228	93°53'49.7' E	86	140
229		35	182

SL. No.	Latitude Longitude	dip amount (°)	dip direction (°)
230		75	139
231		47	190
232		70	127
233		85	093
234		56	136
235		69	132
236		51	178
237		82	258
238		45	199
239		48	169
240		79	270
241		29	181
242		65	097
243		48	165
244		73	123
245		56	166
246		80	117
247		73	270
248		43	179
249	25°45'55.0" N	73	131
250	93°53'55.3" E	66	204
251		69	125
252		70	187
253		70	059
254		70	187
255		52	190
256		72	097
257		56	150
258		43	218

SL. No.	Latitude Longitude	dip amount (°)	dip direction (°)
259		58	210
260		88	060
261		50	144
262		45	202
263		58	260
264		61	202
265		50	192
266		66	129
267		82	112
268		54	188
269		69	139
270		61	193
271		58	189
272		85	126
273	25°46'21.1" N	88	050
274	93°53'07.5" E	69	307
275		76	298
276		72	020
277		66	288
278		71	081
279		31	343
280		77	055
281		52	012
282		77	072
283		68	067
284		31	020
285		23	330
286		60	060
287		65	060

SL. No.	Latitude Longitude	dip amount (°)	dip direction (°)
288		54	345
289	25°46'19.1" N	68	321
290	93°54'22.0" E	42	010
291		68	328
292		85	260
293		80	282
294		66	332
295		35	317
296		70	031
297		72	038
298		58	262
299		50	056
300		82	222
301		74	309
302		57	023
303		85	271
304		60	315
305		78	295
306		57	018
307		77	040
308		65	248
309	25°46'20.6" N	77	239
310	93°55'57.5" E	80	331
311		64	275
312		79	336
313		74	242
314		75	290
315		76	244
316		57	325

SL. No.	Latitude Longitude	dip amount (°)	dip direction (°)
317		57	314
318		81	236
319		75	308
320		84	054
321		68	294
322		87	068
323		81	241
324		83	006
325		89	190
326		72	305
327	25°46'13.7" N	66	249
328	93°56'08.7" E	46	358
329		47	341
330		67	242
331		60	254
332		60	333
333		54	005
334		70	247
335		72	011
336		61	247
337		71	243
338		72	005
339		60	330
340		81	237
341		51	320
342		73	236
343		60	256
344		46	348
345	25.766455° N	60	030

SL. No.	Latitude Longitude	dip amount (°)	dip direction (°)
346	93.940078° E	70	256
347		65	042
348		57	262
349		67	259
350		30	343
351		52	254
352		87	231
353		57	267
354		84	233
355		84	198
356		54	269
357		68	247
358		53	313
359		60	254
360		82	044
361	25°45'35.3" N	90	243
362	93°56'50.2" E	48	327
363		43	332
364		84	240
365		69	284
366		55	320
367		78	251
368		60	320
369		84	253
370		64	273
371		54	279
372		81	234
373		87	254
374		49	315

SL. No.	Latitude Longitude	dip amount (°)	dip direction (°)
375		88	234
376		58	357
377		89	225
378		51	319
379		55	261
380		55	260
381		43	319
382		85	252
383		33	305
384		61	008
385		81	245
386	25°46'05.7" N	77	105
387	93°53'52.4" E	73	135
388		64	303
389		39	105
390		77	330
391	25°48'23.5" N	40	233
392	93°47'43.0" E	45	262
393		65	023
394		45	323
395		55	015
396		30	347
397	25°48'07.5" N	65	095
398	93°47'54.7" E	45	170
399		55	122
400		70	085
401		50	135
402	25°47'49.7" N	85	020
403	9°47'56.5" E	80	220

SL. No.	Latitude Longitude	dip amount (°)	dip direction (°)
404		55	355
405		75	007
406		75	240
407		45	270
408		60	003
409	25°47'36.4" N	85	045
410	93°48'20.6" E	55	340
411		45	350
412		80	040
413	25°47'33.5" N	55	290
414	93°48'06.8" E	65	010
415		75	305
416		55	007
417		50	353
418		50	280
419		75	015
420	25°46'46.5" N	65	245
421	93°48'04.7" E	70	223
422		50	257
423		55	313
424		50	270
425	25°45'46.6" N	60	140
426	93°53'22.4" E	75	064
427		70	200
428		80	276
429		65	215
430		75	273
431		55	091
432		35	190

SL. No.	Latitude Longitude	dip amount (°)	dip direction (°)
433		70	162
434	25°47'48.0" N	75	240
435	93°47'43.5"E	75	020
436		70	340
437	25°47'52.0" N	70	277
438	93°47'55.6" E	50	051
439		80	355
440		80	053
441		65	024
442		35	352
443		75	051
444		75	018
445		70	004
446	25°48'09.3" N	80	227
447	93°47'45.9" E	70	266
448	25°45'48.8" N	78	191
449	93°53'32.8" E	35	305
450		70	165
451		60	108
452		80	353
453		40	261
454		80	164
455		65	284
456	25°45'50.0" N	55	199
457	93°53'39.5" E	60	270
458		80	143
459		80	132
460		65	190
461		85	266

SL. No.	Latitude Longitude	dip amount (°)	dip direction (°)
462	25°45'52.4" N	55	106
463	93°53'51.4" E	50	186
464		60	117
465		65	230
466		55	188
467	25°45'54.9" N	65	197
468	93°53'55.4" E	70	112
469		80	175
470		75	242
471		45	130
472		45	196
473		60	155
474		85	199
475	25°46'12.4" N	55	317
476	93°54'03.7" E	85	203
477		70	225
478		60	323
479		70	020
480		80	033
481		60	325
482		60	317
483		60	036
484	25°46'3802"N	84	010
485	93°55'45.3"E	53	253
486		75	216
487		35	223
488		80	010
489	25°46'13.6" N	60	005
490	93°56'10.2" E	68	247

SL. No.	Latitude Longitude	dip amount (°)	dip direction (°)
491		72	241
492		55	332
493	25°45'51.2" N	70	245
494	93°56'47.4" E	55	025
495		20	325
496		40	350
497	25°45'50.0" N	80	240
498	93°56'50.0" E	40	325
499		53	265
500		70	230
501		50	330
502		85	240
503	25°44'57.6" N	70	321
504	93°57'57.3" E	85	002
505		78	064
506		85	145
507		65	055
508	25°45'00.0" N	30	051
509	93°58'35.0" E	32	344
510	25°44'54.0" N	60	332
511	93°58'42.0" E	60	263
512		83	240
513		80	201
514	25°44'30.1" N	70	015
515	93°58'49.0" E	60	290
516		60	015
517		70	270
518		50	001
519	25°44'17.2" N	35	313

SL. No.	Latitude Longitude	dip amount (°)	dip direction (°)
520	93°59'07.5" E	68	316
521		30	355
522		85	054
523	25°44'01.0" N 93°59'44.7" E	58	340
524	25°44'02.6" N	50	352
525	94°00'05.0"E	68	069
526		82	285
527		60	329
528		65	007
529		82	087
530		55	004
531	25°44'03.8" N	39	028
532	94°01'05.6" E	55	273
533		70	330
534	25°43'20.1" N	46	006
535	94°02'20.3" E	85	350
536		68	009
537	25°43'15.0" N	65	252
538	94°02'30.7" E	60	003
539		76	206
540	25°42'46.2" N	81	140
541	94°02'17.5" E	60	186
542		50	124
543		53	023
544		53	015
545	25°42'11.9" N	60	080
546	94°02'48.1" E	63	130
547	25°41'24.6" N	77	001

SL. No.	Latitude Longitude	dip amount (°)	dip direction (°)
548	94°02'48.1" E	29	094
549		75	144
550		41	100
551		78	168
552	25°41'17.0" N	45	330
553	94°02'42.0" E	85	325
554		64	319
555		70	135
556	25°41'16.7" N	80	006
557	94°02'59.8" E	63	316
558		61	314
559	25°41'10.5" N	70	102
560	94°03'42.7" E	75	005

In segment I the joints are mostly concentrated along two major directions. The maximum of the joints are oriented around 100-110° and quite a good proportion are also found to concentrate along 150-160°. The beddings in this segment are almost entirely concentrated within 030-040°. The β diagram shows that the beds in an average dip at 46° along 131° direction. The number of oppositely dipping beds is negligible (Fig. 5.5a). The calculated β axis is 02°/043°. The trend of the margin of the BoS on the west as a whole (from SW end to roughly up to 26° latitude) is found to strike roughly along 045° (Fig. 5.4). But in the area of the studied section, the western margin of the belt is a bit rotated (twisted) anticlockwise, which of course again resumes the normal trend as continued further southwest and northeastward. Hence, the beddings in this area are found to strike at an average along 040° as against the 045° general trend. From the stereo-net plot of the

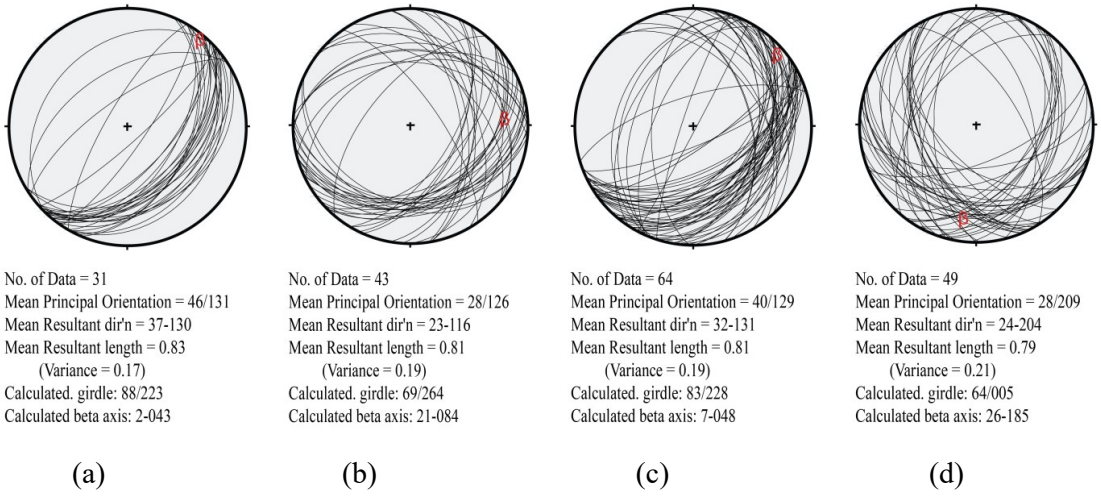

Fig 5.4: Beta diagrams of the bedding planes of the four segments of the studied section. (a) Segment I, (b) Segment II, (c) Segment III, (d) Segment IV.

planes and pi (pole) diagram (Fig. 5.5a), it is learnt that majority of the joints have high angle of dip. The calculated π girdle is 37° along 131° direction. The girdle orientation exactly coincides with that of the mean principal orientation of 131° of the beds of in this segment. The calculated β axis of the joints is 53°/331°. The poles of joints of segment I (Fig. 5.5a) show maximum concentration at a point little away towards west of the southern end to the periphery of the net indicating that majority of the E-W trending joints are nearly vertical.

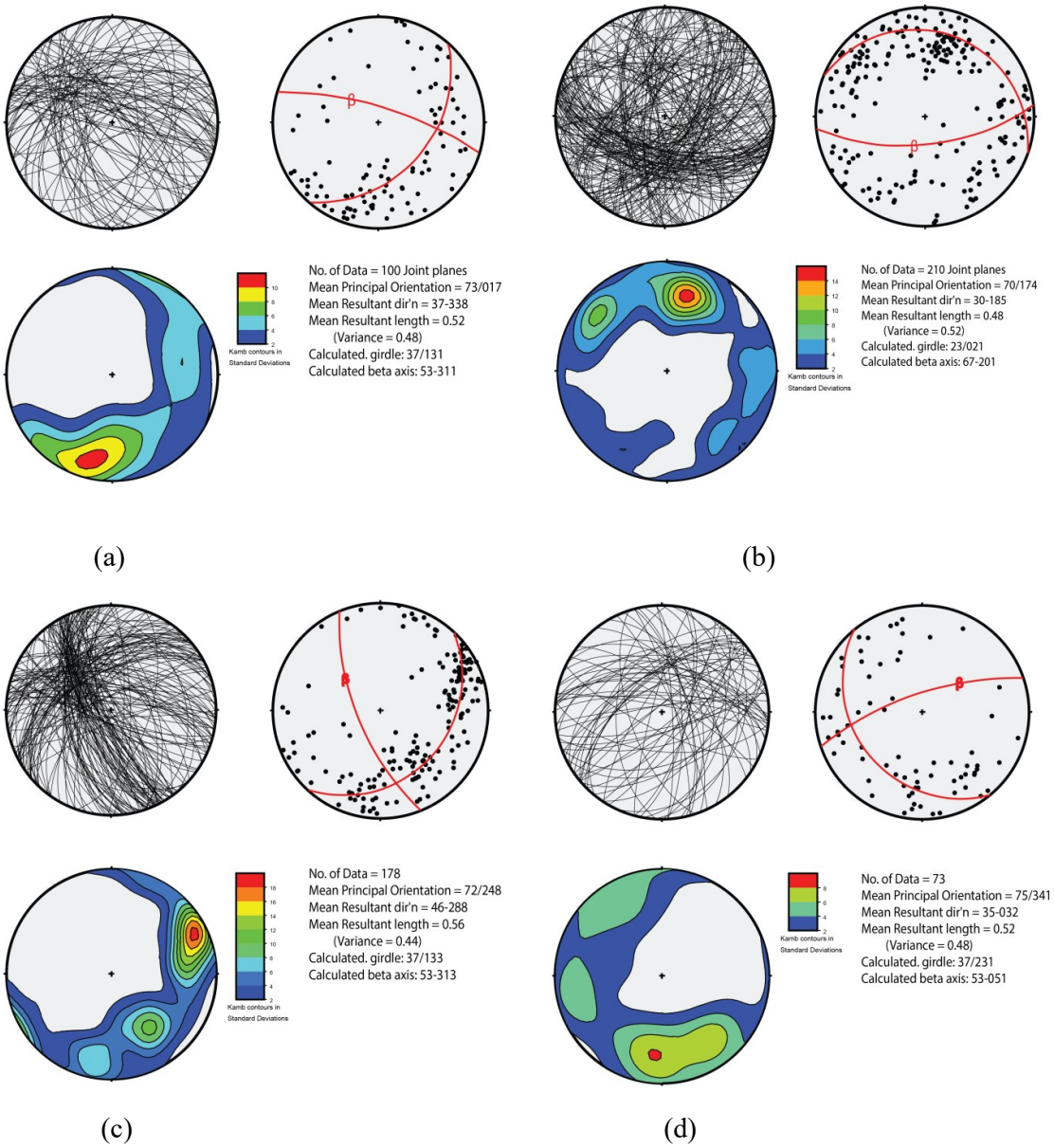

Fig. 5.5: Projected planes, Pi and Contour diagrams of joints. (a) Segment I, (b) Segment II, (c) Segment III, (d) Segment IV.

In segment II, the majority of the joints are oriented along 100-110°. It is also found that another group is concentrated at around 040-050°. The rose diagram of bedding of this segment shows that beds mostly strike in two directions, where the majority of them are concentrated along 070-080°. But many are also found clustered at around 040-050°, which is the general trend of the BoS. But there are some beds whose trends are swinging on both the sides but tend to adhere to these two major concentration

directions. The β diagram (Fig. 5.4b) shows mean principal orientation as 28°/126° while that of the calculated β axis is 21°/084°. From the β diagram it is learnt that a good proportion of the beds are dispersed both anticlockwise and clockwise around the mean principal orientation; but the majority of them are found being rotated clockwise. The stereo-net plot of the planes and pole diagram (Fig. 5.5b) show that the maximum proportion of the joints are concentrated at around 70°/174° (mean principal orientation). It is also observed that a considerably good proportion of joints dipping almost in the opposite direction with nearly similar dips (high angles) but striking similar to those having the maximum concentration, are also present. The calculated π girdle is dipping 23° along 021° direction. The calculated β axis of the joints is 67°/201°. In this segment, it is observed that the poles of the majority of the joints concentrate in the NNE direction with a considerably high angle.

In segment III the joints are found to cluster at around three distinct directions (Fig. 5.3c). But the maximum number of the joints is found to strike along 150-170°. The orientation along which the next higher proportions concentrate is within 050-070°. A good number of joints are also found to orient around 090-110° with some swinging clockwise but tending to adhere to it. The beddings of the litho-units in segment III are mostly concentrated around 070-080°. The next more concentrated direction is 030-050° with a few closely adhering to this direction but swinging roughly about 10° each on both sides; the beds swinging clockwise being more than those swinging anticlockwise. But, the β diagram (Fig. 5.4c) shows that the general (average) orientation direction of the beds of this segment is 40°/129°, which is almost similar with that of segment I (46°/131°). It appears that there is only one concentration direction of the beds in the β diagram. In this segment also the number of oppositely dipping beds is negligible. The calculated β axis of 07°/048° is almost similar with 02°/043° of segment I. It is observed from the β diagram that few of the beds are dispersed (rotated) towards the anticlockwise direction around the mean principal orientation. From the stereo-net plot of the planes (Fig. 5.5c) it is observed that the pattern of concentration and orientation of groups of joints of this segment (140-170°, 060-080° and 090-110°) are very similar with those of segment I; but the degree of clustering of the respective groups is very conspicuous in segment III. The proportion of joints striking NNW-SSE and dipping SW (with high angle) unlike that of segment I is the maximum, which is also evident from the clustering of maximum number of poles in

the NE quadrant (pi and contour diagrams) near the periphery of the net. The calculated π girdle is dipping 37° along 133° direction. The calculated β axis of the joints is 53°/313°.

In segment IV the joints are found to orient mostly along three main directions (Fig. 5.3d). The majority of them are clustered at around 090-100°. A good number of joints are also concentrated at around 040-070°. There are some other joints concentrated at around 160-170°. The rose diagram of the beddings of this segment (Fig. 5.3d) shows three major concentration directions. The majority of the beds are along 010-020° with some dispersed more clockwise. The next prominent orientation in which the beds are striking is along 150-170°. Considerable amount of the beddings are also found to cluster at around 090-110°. The β diagram shows that the majority of the bedding planes are found to strike roughly along NNE-SSW and NNW-SSE in almost equal proportions; these groups dip oppositely. The calculated β axis is 26°/185°. Few other planes are found dispersed more towards E-W and dipping southerly (Fig. 5.4d). The stereo-net plot (Fig. 5.5d) shows three main concentration directions of the joints along 090-110°, 060-080° and 140-170°. Out of the three main orientation directions two are similar with those of segment III in terms of strike and dip, except the one striking NNW-SSE. In segment III the NNW-SSE striking planes dip towards SW while in segment IV the similarly striking planes dip towards NE. The calculated π girdle is dipping 37° along 231° direction. The calculated β axis of the joints is 53°/051°. Maximum number of poles concentrates along SSW with about 25° towards the center of projection.

5.2 Conjugate Fracture Analysis

The paleo-stress analysis using conjugate fractures is based on the brittle failure theory, which states that rocks generally fail either of tensile or shear stress fields (Murrell, 1958; 1963). In tensile failure (also known as Griffith theory of failure) theory rocks are failed by tensile stress i.e., by opening up of microscopic fractures/flaws called the Griffith cracks. The fractures are developed perpendicular to the tensile stress component, which is usually the orientation of the least (minimum) principal stress (σ_3). The direction parallel to the fractures is that of the maximum principal stress (σ_1). Determination of orientations of the principal stresses σ_1 (maximum), σ_2 (intermediate) and σ_3 (minimum) with the help of tensile fractures is not as simple as in the case of the

sheared conjugate fractures. As a result, we consider fractures produced by shear brittle failure.

Shear brittle failure (first proposed by Coulomb, 1773 and later substantiated by Mohr, 1882) states that rocks owing to shear stress, fail in such a way that fractures are developed at some angle (θ) with respect to the maximum principal stress ($\sigma_{1)}$, which is given by

$$\theta = 45° - \phi/2$$

where ϕ is the internal friction angle. Under geological conditions where $\sigma_1 > \sigma_2 > \sigma_3$, two shear fractures may be developed in a conjugate manner intersecting at some angle since there are two possible directions about σ_1 along which shear stress is either maximum or has some optimum value to cause shear fracturing. The maximum principal stress (σ_1) bisects the acute angle (2θ) between the fractures, while the minimum principal stress (σ_3) bisects the obtuse angle ($180° - 2\theta$). The σ_1 is contained in the plane of the acute bisectrix, while the σ_3 is in the obtuse bisectrix plane. The acute and obtuse bisectrixes are perpendicular to each other and thus σ_3 is present in a plane perpendicular to σ_1. The intermediate principal stress (σ_2) runs parallel to the intersection line of the two fractures. Hence, σ_2 is common to both the planes of acute and obtuse bisectrixes (Fig. 5.6). It is assumed that one principal stress is always vertical and explains the occurrence of three classes of fractures (Fig. 5.7): normal faults (σ_1 vertical), strike-slip faults (σ_2 vertical), and thrust faults (σ_3 vertical). This assumption also allows us to reconstruct the orientation of the stress ellipsoid responsible for a given population of fractures.

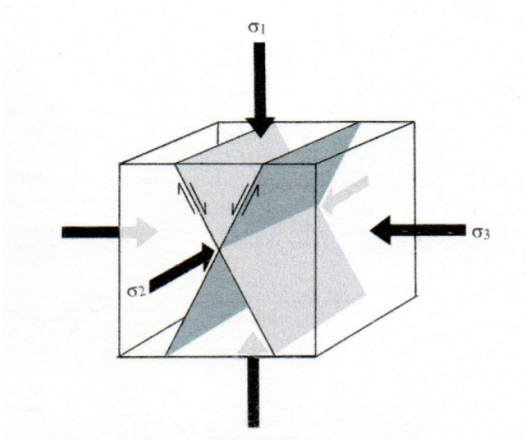

Fig. 5.6: Relationship between the three principal stresses and conjugate shear surfaces.

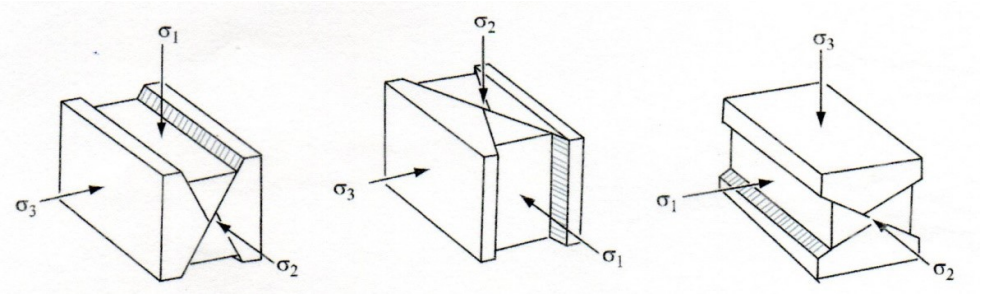

Fig. 5.7: Block diagrams of three classes of faults predicted by E. M. Anderson.

To investigate the palaeo-stress conditions of the rocks of the BoS, as many as 75 pairs of conjugate fractures/joints are collected from different parts of the study area (Table 5.2). These data sets are then plotted on equal area projections for segments I, II, III, IV and section as a whole (I-IV), in order to get the orientations of the three principal stresses from the conjugate fractures, as detailed in Table 5.3. The orientations of the principal stresses obtained are plotted in the form of Pi (pole) and Contour diagrams as shown in Figure 5.8 (a-e).

Table 5.2: Data of 75 conjugate fracture pairs collected from different locations of Chumukedima – Piphema section

Sl. No.	Latitude	Longitude	Conjugate				θ	σ_1		σ_2		σ_3	
			Joint 1		Joint 2								
			DA(º)	DD(º)	DA(º)	DDº(º)		Plunge (º)	Trend (º)	Plunge (º)	Trend (º)	Plunge (º)	Trend (º)
	SEGMENT I												
1	25°47'49.37" N	93°47'56.5" E	80	220	55	355	31	47	095	40	301	14	200
2	25°47'49.37" N	93°47'56.5" E	75	007	75	240	30	31	124	59	304	0	034
3	25°47'31.3" N	93°48'13.4" E	85	045	55	340	33	26	094	54	322	23	196
4	25°47'31.3" N	93°48'13.4" E	45	350	80	040	28	35	086	41	319	30	199
5	25°46'46.5" N	93°48'04.7" E	85	195	65	245	26	23	136	62	276	17	039
6	25°48'02" N	93°47'48.2" E	60	350	80	212	28	45	092	43	293	11	192
7	25°47'48.1"N	93°48'06.9" E	50	236	80	021	30	55	150	30	296	16	036
8	25°47'48.1"N	93°48'06.9" E	87	190	65	258	34	19	138	64	273	17	042
9	25°47'48.1"N	93°48'06.9" E	51	213	67	004	34	66	126	22	284	17	008
10	25°47'47.6"N	93°48'16.8" E	88	193	61	243	27	30	136	55	280	17	036
11	25°47'47.6"N	93°48'16.8" E	83	312	42	013	33	35	270	40	036	31	156
12	25°47'34"N	93°48'8.2" E	48	310	60	012	25	11	064	48	321	40	163
13	25°47'34"N	93°48'8.2" E	83	332	83	028	28	00	090	82	360	8	180
14	25°47'34"N	93°48'8.2" E	56	340	79	048	33	20	097	56	335	27	197
15	25°47'34"N	93°48'8.2" E	85	018	47	325	30	36	064	42	292	26	175

Sl. No.	Latitude	Longitude	Conjugate				θ	σ_1		σ_2		σ_3	
			Joint 1		Joint 2								
			DA(º)	DD(º)	DA(º)	DDº(º)		Plunge (º)	Trend (º)	Plunge (º)	Trend (º)	Plunge (º)	Trend (º)
SEGMENT II													
1	25°45'48.8"N	93°53'48.8" E	55	136	55	214	31	00	265	48	175	42	355
2	25°45'48.7"N	93°53'46.0" E	60	261	75	196	30	14	143	60	258	26	047
3	25°45'54.8"N	93°53'55.4" E	65	195	70	121	34	04	069	62	167	27	337
4	25°45'54.8"N	93°53'55.4" E	60	194	70	260	30	09	313	59	208	29	049
5	25°45'54.8"N	93°53'55.4" E	65	189	60	110	34	04	238	56	142	34	331
6	25°45'50.4"N	93°53'39.8" E	64	192	85	253	30	21	308	62	173	18	045
7	25°45'50.4"N	93°53'39.8" E	78	154	48	212	29	28	106	46	231	30	359
8	25°45'50.4"N	93°53'39.8" E	77	328	63	199	32	40	089	49	253	07	352
9	25°45'51.2"N	93°53'49.7"E	41	184	86	140	29	45	099	32	228	28	337
10	25°45'51.2"N	93°53'49.7"E	35	182	75	139	26	40	103	29	221	37	334
11	25°45'51.2"N	93°53'49.7"E	47	190	70	127	29	21	080	47	194	36	334
12	25°45'51.2"N	93°53'49.7"E	82	258	45	199	31	33	302	43	175	30	054
13	25°45'51.2"N	93°53'49.7"E	29	181	65	097	33	25	068	29	172	50	303
14	25°45'51.2"N	93°53'49.7"E	56	166	80	117	25	27	062	53	193	24	319
15	25°45'55.0"N	93°53'55.3"E	73	131	66	204	34	06	079	64	181	25	347
16	25°45'55.0"N	93°53'55.3"E	69	125	70	187	29	01	246	66	153	24	336

Sl. No.	Latitude	Longitude	Conjugate				θ	σ_1		σ_2		σ_3	
			Joint 1		Joint 2								
			DA(º)	DD(º)	DA(º)	DDº(º)		Plunge (º)	Trend (º)	Plunge (º)	Trend (º)	Plunge (º)	Trend (º)
17	25°45'55.0"N	93°53'55.3"E	70	059	70	187	32	40	303	50	123	00	033
18	25°45'55.0"N	93°53'55.3"E	56	150	43	218	26	11	102	42	202	45	360
19	25°45'55.0"N	93°53'55.3"E	50	192	66	129	27	15	079	50	187	36	337
20	25°45'55.0"N	93°53'55.3"E	58	189	85	126	32	25	075	57	208	21	334
21	25°46'21.1"N	93°53'07.5"E	52	012	77	072	29	24	122	51	059	29	226
22	25°46'21.1"N	93°53'07.5"E	23	330	60	060	31	24	084	22	344	56	216
23	25°46'21.1"N	93°53'07.5"E	65	060	54	345	32	09	108	52	006	37	205
24	25°46'19.1"N	93°54'22.0"E	35	317	70	031	32	25	068	37	317	42	183
25	25°46'19.1"N	93°54'22.0"E	74	309	57	023	34	14	261	57	013	30	163
26	25°45'50.0" N	93°53'39.5" E	55	199	60	270	29	04	322	51	227	38	056
27	25°45'52.4" N	93°53'51.4" E	55	106	50	186	31	04	058	45	152	45	324
28	25°45'54.9" N	93°53'55.4" E	80	175	75	242	33	05	119	74	226	15	028
29	25°46'12.4" N	93°54'03.7" E	60	323	70	020	26	10	077	60	329	28	173
30	25°46'12.4" N	93°54'03.7" E	80	033	60	325	33	17	84	60	320	24	182
SEGMENT III													
1	25°46'12.5"N	93°56'19.3" E	85	024	65	249	27	34	143	53	301	11	045
2	25°46'32.2"N	93°55'52.4" E	80	214	65	272	32	18	212	60	336	23	115

Sl. No.	Latitude	Longitude	Conjugate				θ	σ_1		σ_2		σ_3	
			Joint 1		Joint 2								
			DA(º)	DD(º)	DA(º)	DDº(º)		Plunge (º)	Trend (º)	Plunge (º)	Trend (º)	Plunge (º)	Trend (º)
3	25°45'51.2" N	93°56'47.4" E	70	245	55	025	33	56	124	33	321	08	226
4	25°44'57.6" N	93°57'57.3" E	85	002	78	064	31	07	304	78	68	10	213
5	25°44'30.2"N	93°58'47.7" E	75	245	65	030	26	50	132	39	322	05	228
6	25°46'20.6"N	93°55'57.5"N	81	241	83	006	29	17	124	73	300	01	033
7	25°46'20.6"N	93°55'57.5"N	89	190	72	305	33	17	065	70	277	10	158
8	25°45'35.3"N	93°56'50.2"N	88	234	58	357	32	32	107	53	321	17	208
9	25°45'35.3"N	93°56'50.2"N	58	357	89	225	28	36	101	49	313	17	203
10	25°45'35.3"N	93°56'50.2"N	61	008	81	245	33	36	120	52	323	11	218
SEGMENT IV													
1	25°44'3.58"N	93°56'50.2"N	46	352	54	284	26	07	233	44	330	45	135
2	25°44'1.73"N	93°56'4.80"N	63	334	85	039	32	20	92	62	318	63	244
3	25°44'1.74"N	93°56'58.62"N	85	034	78	340	27	08	96	78	328	10	187
4	25°44'1.71"N	93°56'58.60"N	68	050	76	343	32	07	289	67	036	21	196
5	25°44'1.99"N	93°56'58.60"N	71	315	63	021	30	07	261	62	005	27	167
6	25°44'0.86"N	93°56'58.68"N	75	316	58	026	33	15	266	58	021	28	168
7	25°44'0.89"N	93°56'57.24"N	53	011	80	068	29	26	119	51	351	26	223
8	25°44'1.24"N	93°56'57.24"N	50	349	72	053	29	20	101	50	346	33	205

Sl. No.	Latitude	Longitude	Conjugate				θ	σ_1		σ_2		σ_3	
			Joint 1		Joint 2								
			DA(º)	DD(º)	DA(º)	DDº(º)		Plunge (º)	Trend (º)	Plunge (º)	Trend (º)	Plunge (º)	Trend (º)
9	25°44'1.33"N	93°56'45.97"N	64	009	70	315	25	07	255	64	358	26	161
10	25°44'1.32"N	93°56'45.99"N	71	313	74	006	25	03	069	70	329	19	160
11	25°44'20.99"N	93°56'55.52"N	63	012	44	296	31	15	055	43	311	43	160
12	25°44'29.68"N	93°56'48.43"N	58	279	44	353	29	11	234	42	334	45	132
13	25°44'29.94"N	93°56'49.02"N	88	255	66	006	36	22	127	64	341	13	222
14	25°44'2.16"N	93°56'5.51"N	71	050	79	348	30	08	291	71	044	17	198
15	25°44'2.35"N	93°56'5.67"N	83	301	69	351	25	16	240	67	014	15	145
16	25°44'7.84"N	93°56'16.22"N	72	005	72	288	38	00	057	68	327	23	147
17	25°44'7.97"N	93°56'15.56"N	71	288	69	355	31	02	232	66	326	24	141
18	25°44'7.63"N	93°56'10.63"N	60	357	89	311	26	33	254	52	040	17	152
19	25°44'2.07"N	93°56'15.40"N	81	352	77	237	34	20	115	70	288	02	024
20	25°44'1.71"N	93°56'11.15"N	74	237	63	346	40	34	109	55	303	07	203

Table 5.3: Values of the three principal stresses of the segments- I, II, III, IV and I-IV.

Segment		**I**	**II**	**III**	**IV**	**I-IV**
No. of Data		**15**	**30**	**10**	**20**	**75**
σ1	Mean Principal Direction (degree)	33/105	13/090	33/118	02/083	16/094
	Mean Resultant Direction (degree)	39/106	40/079	45/122	59/184	47/104
	Calculated Girdle (degree)	54/167	28/026	37/148	29/169	36/160
σ2	Mean Principal Direction (degree)	52/304	63/197	58/317	64/344	70/308
	Mean Resultant Direction (degree)	53/306	69/20 5	58/318	64/344	73/299
	Calculated Girdle (degree)	64/355	79/265	90/047	66/010	77/257
σ3	Mean Principal Direction (degree)	09/197	25/356	07/214	27/175	07/189
	Mean Resultant Direction (degree)	52/142	52/352	23/192	31/173	72/171
	Calculated Girdle (degree)	51/114	56/284	21/143	29/155	63/103

The orientations of the maximum principal stress, σ_1 of the four segments are, I = 33°/105°, II = 13°/090°, III = 33°/118°and IV = 02°/083°. The intermediate principal stress, σ_2 are found to align as, I = 52°/304°, II = 63°/197°, III = 58°/318°and IV = 64°/344°. The minimum principal stress, σ_3 are found to orient as, I = 09°/197°, II = 25°/356°, III = 07°/214°and IV = 07°/189°. It is evident that orientations of the three principal stresses of segments I, III and IV agree well, but that of segment II behave a bit differently. The position (orientation) of σ_2 in segment II falls near that of σ_3 of other segments and vice versa, even if the plunge in II is higher (63°) than those of σ_3 of (nearly horizontal) other segments . The average mean orientation directions of the three principal stresses of the whole section (four segments) are found as σ_1 = 16°/094°, σ_2 = 70°/308° and σ_3 = 07°/189° with minor fluctuation of 10°- 15° on either side. All the aforementioned information is clearly illustrated by the Pi and contour diagrams of the respective segments (Fig. 5.8).

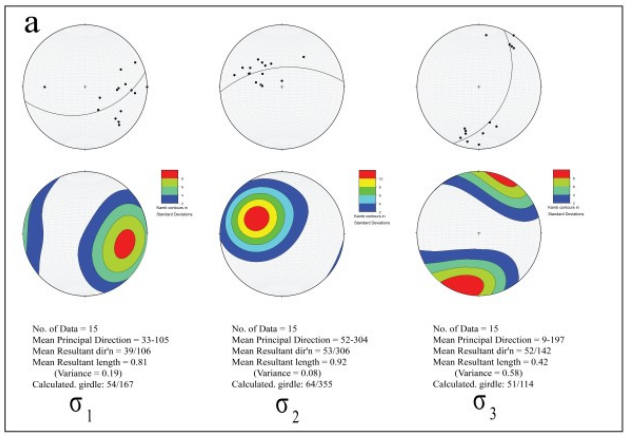

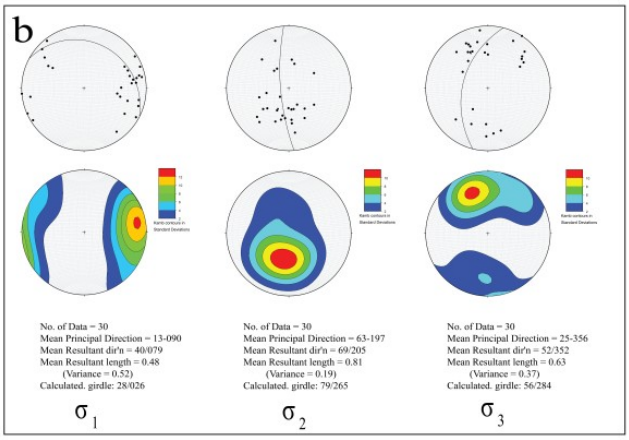

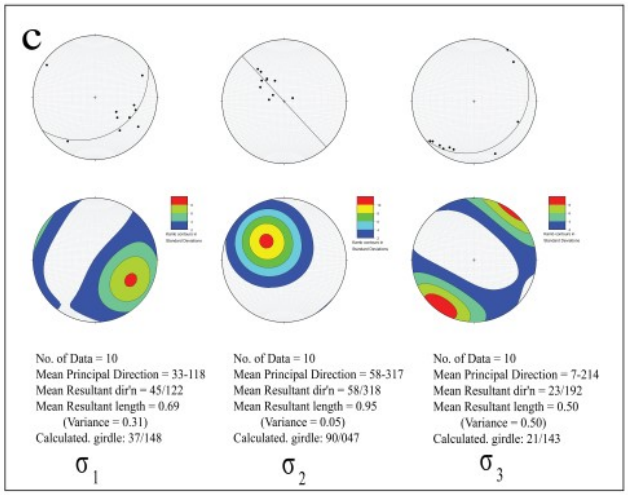

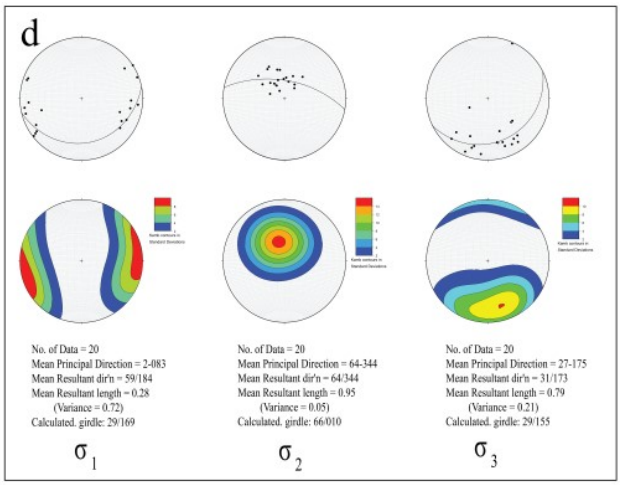

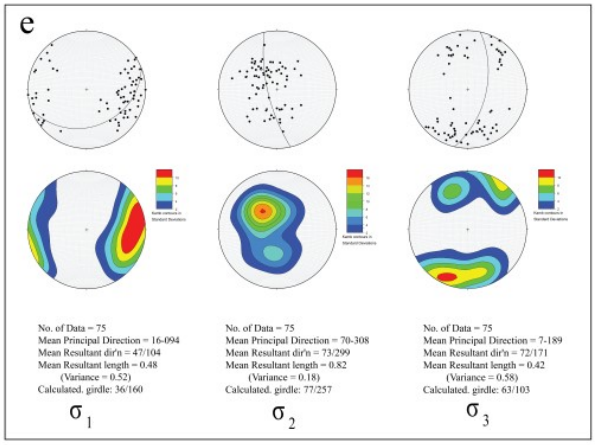

Fig. 5.8: Pi and Contour diagrams of conjugate joints of the section: (a) Segment I, (b) Segment II, (c) Segment III, (d) Segment IV, (e) All Segments.

5.3 Slickenside Analysis

Slickensides are polished and striated surfaces developed on fracture planes by frictional sliding. Slickenside surface is often decorated by lineation parallel to the direction of movement on the surface. Lineation is variously referred to as slickenside lineation, slickenline or slip lineation (Fleuty, 1975). Slickenside data can be analysed to find out the orientations of the three principal stresses of the fault at the moment of slipping/faulting. The basic principle is that using the pitch value of the slickenside, it is properly marked on the stereographic (equal area) projection of the fault plane. Then, the position of σ_2, the intermediate principal stress, is obtained by counting 90° on the fault plane itself. The maximum principal stress (σ_1) and minimum principal stress (σ_3) will lie on a plane normal to σ_2 and passing through the slickenside. In order to get the orientations of σ_1 and σ_3, σ_1 is marked at 30° based on the principle of shear fracturing (Ragan, 1985) with respect to the fault plane. In doing so, however, sense of movement – up and down for normal and thrust faulting, and dextral and sinistral for strike-slip faults should be taken into consideration. Then the position of σ_3 is obtained by counting 90° from the position of σ_1 along the same plane (Fig. 5.9).

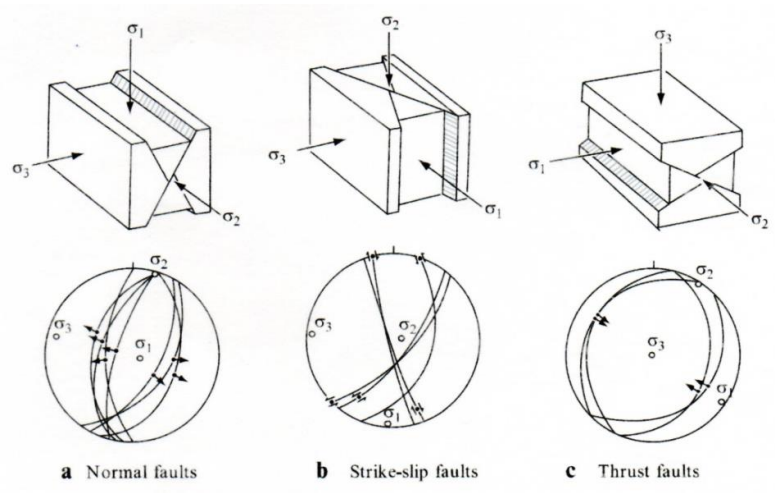

Fig. 5.9: The equal-area stereograms show typical fault and slickenline orientation data for a set of faults within each class. For normal faults and thrust faults, the arrows on the great circles of the stereograms point in the direction of the hanging-wall motion. For strike-slip faults, the arrows on the great circles indicate the sense of shear. After Angelier (1979) in Suppe (1985).

Table 5.4: Slickensides data from different stations of Chumukedima – Piphema section

Sl No	Latitude Longitude	DA (º)	DD (º)	Pitch (º)	Slip-sense	Sigma 1		Sigma 2		Sigma 3	
						Plunge (º)	Trend(º)	Plunge (º)	Trend (º)	Plunge (º)	Trend (º)
1	25°56' 55.2" N 94°01'45.3" E	34	85	80S	Thrust	12	272	6	3	77	119
2	25°56' 55.2" N 94°01'45.3" E	33	70	75S	Thrust	13	261	8	353	75	115
3	25°44' 17.0" N 93°59'07.7" E	57	222	23E	Sinistral	38	98	51	260	9	1
4	25°44' 17.0" N 93°59'07.7" E	78	174	22E	Dextral	6	133	65	236	24	40
5	25°45' 08.0" N 93°57'19.0" E	80	350	10W	Dextral	0	306	76	36	14	216
6	25°44' 28.0" N 93°58'37.0" E	50	140	70N	Thrust	3	126	15	217	74	25
7	25°52' 54.9" N 94°11'12.8" E	82	180	16E	Dextral	6	137	72	244	17	45
8	25°52' 28.7" N 94°02'35.3" E	75	345	20N	Dextral	24	118	65	291	3	27

Sl No	Latitude Longitude	DA (º)	DD (º)	Pitch (º)	Slip-sense	Sigma 1		Sigma 2		Sigma 3	
						Plunge (º)	Trend(º)	Plunge (º)	Trend (º)	Plunge (º)	Trend (º)
9	25°43'39.89"N 94° 1'42.66"E	73	133	30N	Dextral	8	95	55	197	33	360
10	25°44' 18.0" N 93°59'05.0" E	46	136	54E	Thrust	4	292	25	200	65	31
11	25°44' 18.0" N 93°59'05.0" E	42	136	68E	Thrust	5	300	15	209	74	49
12	25°44' 02.0" N 94°00'04.0" E	42	105	63E	Thrust	6	266	17	175	72	14
13	25°44' 27.0" N 93°58'36.0" E	51	116	70E	Thrust	4	102	15	193	74	357
14	25°44' 28.0" N 93°58'35.0" E	75	51	09N	Dextral	4	186	72	83	17	278
15	25°45' 01.0" N 93°57'40.0" E	47	112	55E	Thrust	3	268	25	176	65	5
16	25°45' 02.0" N 93°57'39.0" E	45	124	78E	Thrust	0	295	9	205	81	29
17	25°44' 28.0" N	45	166	60E	Thrust	4	325	21	234	69	65

Sl No	Latitude Longitude	DA (º)	DD (º)	Pitch (º)	Slip-sense	Sigma 1		Sigma 2		Sigma 3	
						Plunge (º)	Trend(º)	Plunge (º)	Trend (º)	Plunge (º)	Trend (º)
	93°58'37.0" E										
18	25°44' 28.0" N 93°58'37.0" E	72	56	10N	Dextral	5	192	69	87	20	284
19	25°44' 28.0" N 93°58'37.0" E	35	157	60N	Dextral	13	316	17	222	69	82
20	25°45' 01.0" N 93°57'40.0" E	49	131	90S	Thrust	4	131	0	221	86	311
21	25°48' 39.0" N 93°48'05.8" E	87	324	77S	Thrust	41	312	13	53	47	157
22	25°46' 38.0" N 93°55'45.0" E	26	339	40W	Dextral	26	122	20	22	56	259
23	25°42' 00.3" N 93°05'40.7" E	49	292	50N	Thrust	3	139	29	231	61	43
24	25°42' 00.3" N 93°05'40.7" E	49	292	65N	Thrust	1	309	18	219	72	42
25	25°44' 16.4" N 93°59'07.7" E	65	187	49E	Thrust	11	159	37	257	51	55

Sl No	Latitude Longitude	DA (º)	DD (º)	Pitch (º)	Slip-sense	Sigma 1		Sigma 2		Sigma 3	
						Plunge (º)	Trend(º)	Plunge (º)	Trend (º)	Plunge (º)	Trend (º)
26	25°44' 16.4" N 93°59'07.7" E	35	163	88W	Normal	80	170	1	74	10	344
27	25°44' 16.4" N 93°59'07.7" E	59	204	36E	Dextral	1	349	44	259	46	80
28	25°44' 16.4" N 93°59'07.7" E	35	183	25W	Dextral	49	287	31	153	24	48
29	25°44' 19.1" N 93°59'03.9" E	50	155	79E	Dextral	5	147	8	238	80	29
30	25°46' 10.0" N 93°47'35.0" E	48	161	65W	Sinistral	0	179	18	88	72	269

Slickensides are not found preserved everywhere covering all the four sections of the studied section. Data of a total of 30 slickensides preserved in the fracture surface could be collected (Table 5.4). So, slickenside analysis is not carried out segment-wise, but for the whole section. They are used to find the position of the three principal stresses. The details of the attitudes of the principal stresses are enumerated in Table 5.5. The slickenside data as plotted in the form of Pi (pole) and Contour diagrams are shown in Figure 5.10.

Table 5.5: The values of the three principal stresses found out from the slickenside data.

No. of Data		**30**
σ1	Mean Principal Direction (degree)	1/126
	Mean Resultant Direction (degree)	52/209
	Calculated Girdle (degree)	10/210
σ2	Mean Principal Direction (degree)	25/216
	Mean Resultant Direction (degree)	56/213
	Calculated Girdle (degree)	87/305
σ3	Mean Principal Direction (degree)	68/034
	Mean Resultant Direction (degree)	69/020
	Calculated Girdle (degree)	89/307

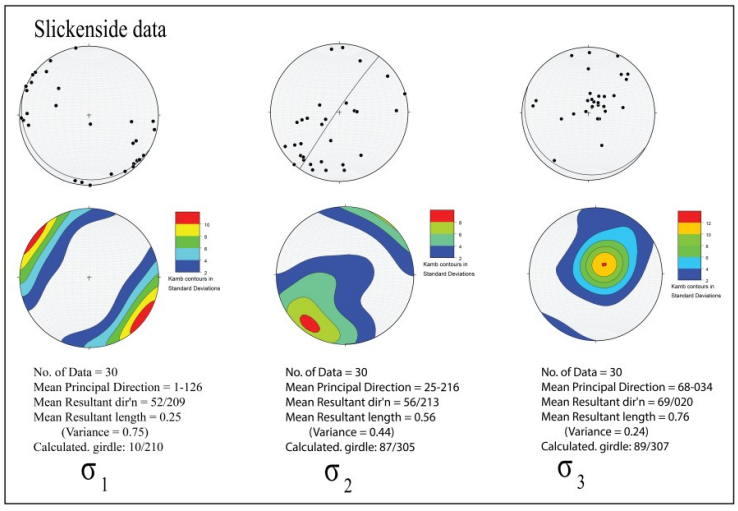

Fig. 5.10: Pole and Contour diagrams of 30 slickenside data from the study area.

In Table 5.5 (with the corresponding illustrations in Fig. 5.10), the orientation of the three principal stresses (mean principal direction values) as revealed by the equal area stereographic projection of the slickenside data are found to be, σ_1 = 01°/126°, σ_2 = 25°/216° and σ_3 = 68°/034°. Since the value of σ_3 is the maximum (near vertical), σ_2 is with moderate plunge amount and σ_1 is almost horizontal, the main controlling mechanism of fracturing (faulting) responsible for causing the striation is reverse faulting where the maximum fault plane dips at 45° and above. All the fault planes along which the 30 slickensides have been recorded are found to have dip amount greater than 45°.

Chapter 6
Estimation of Crustal Shortening

Our earth is ever-changing under the effect of various forces; the effect of plate movement (plate tectonics) causes new crust to be produced at the mid oceanic rifts and old crustal material to be destroyed or recycled at the subduction margins resulting a cyclicity of the crustal material. During this large scale plate movements the crusts are subjected to various tectonic forces, which sometimes, causes extension (normal faulting) and in other cases it causes shortening (folding and faulting).

At the collision plate boundaries various orogenic belts are produced, which are exhibited by a number of folding and thrusting in the area as a result of the lateral compression. This compression is compensated by the vertical thickening which allows the crustal material to move up when there is no space left to move laterally. Along the Indo-Myanmar Ranges the tectonic forces responsible for the generation of the surficial and sub-surficial structures are a result of the interaction and collision of the Indian plate with the Myanmar micro-plate rather than the Eurasian plate (Soibam, 2006). Thus, quantum of crustal shortening is calculated to get an idea about the plate interaction that causes maximum shortening along the compression direction and also to determine the original extent of the study area (Belt of Schuppen).

Shortening calculation is analogous to the estimation of the strain sustained as a result of compressive forces acting on a body. In many areas quantification of shortening is difficult because of many reasons such as tectonic inversion, unavailability of datum surface or decollement depth etc.

Basins which have undergone reversal in subsidence or uplift i.e. places where reactivation of pre-existing structures and fault systems has occurred, such an inversion could affect the structural interpretation resulting in the faulty preparations of cross sections providing an incorrect shortening amount. Area where evidences of strike slipping are observed cross sections across such sections are not recommended as it involves out of section plane movements of materials (Coward, 2014).

Cross balanced sections are representations of the subsurface prepared from the various field data such as the litho-units, thrusts or strike-slips etc. observed the surface. They are prepared based on the assumption of plane strain deformation i.e. there is no gain or loss of material during deformation. It is an important tool utilized by geologists to show the field setting of an area.

Cross balanced sections are also used for the estimation of shortening as they can be unstrained and restored to their original position (Ahlstrom, 1969). It is generally computed using two methods viz; line balancing and area balancing methods. Line balancing method requires good marker horizons and this method is also utilized to calculate the amount of shortening from the various minor structures in the field. In the Belt of Schuppen (BoS) being an imbricate system it is very to ascertain a marker horizon. Therefore, we use minor structures to calculate the shortening of the belt.

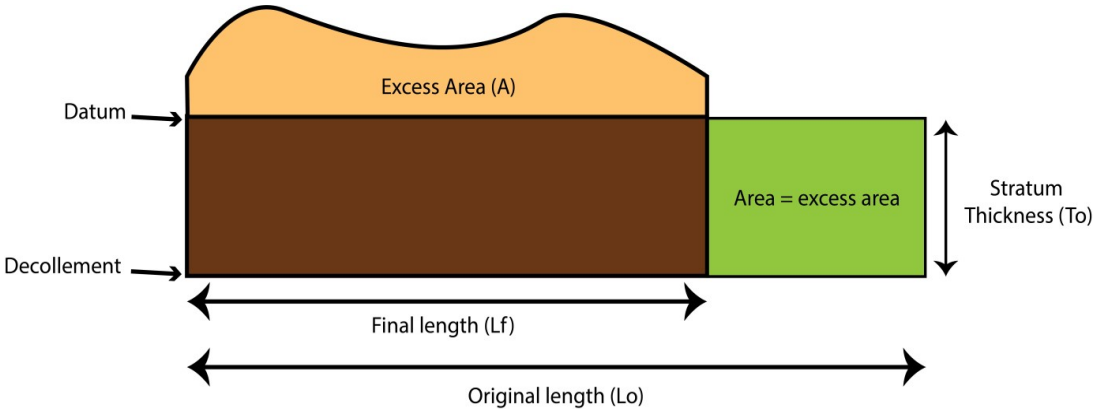

Fig. 6.1: Simple schematic diagram showing how shortening of material is calculated using Area Balancing Method (modified after Hossack, 1979).

In area balancing method (Fig. 6.1) the quantum of shortening can be calculated by dividing the area of section with its original stratigraphic thickness (Hossack, 1979). The formula for calculating original length of the deformed geological cross section was postulated by Elliot (1977) after Gwinn (1970). The relation to calculate the shortening is as follows:

$$L_o = (A/T_o) + L_f$$

Where, L_o = original length

L_f = final length

T_o = depth to decollement or original stratigraphic thickness

A = it is the excess area between the folded bed and the datum (Fig. 6.1)

The initial height of the reference bed (datum) is measured from the height of the same bed in the undisturbed foreland (Hossack, 1979). The initial height of a reference bed could not be ascertained in any section of the Belt of Schuppen due to inability to find a suitable marker horizon as a result of imbricate nature, thus resulting in an inability for accurate determination of the excess area (A). But, Soibam et al., (2015) used values of the total crustal thickness below the mountains and thickness of the crust outside the mountain range after (Coward, 1992) for the calculation of shortening in some section of the Indo-Myanmar Ranges (IMR). The formula used for the calculation of shortening in this method is:

$$\text{Lo} = A \times \frac{T}{H}$$

Where, Lo is original width

A is the area beneath the curve (equivalent with excess area in other shortening methods)

T is the total thickness of the crust below the mountain

H is the crustal thickness outside the mountain range

Mean sea level is used as the datum (seen in their profiles) to estimate the amount of shortening across the Indo-Myanmar Ranges encompassing Nagaland, Manipur and Mizoram. This method of shortening calculation is not applicable for our study areas owing to the short aerial extent of Belt of Schuppen, but not full length of the mountain range. The other reason is that the estimated crustal thickness outside the mountain range which is about 20 km (according to Soibam et al., 2015' calculated shortening along the entire length of the IMR) appears to be much lower when considered only the Belt of Schuppen where the decollement depth is considered to be of 3.6 km as observed from the seismic profiles of the BoS (Choudhuri et al., 2023). The total crustal thickness below the mountain in the Belt of the Schuppen is also not available in the literature. Therefore, an alternative is required to measure the amount of shortening of the area.

Shortening in line balancing (Fig. 6.2) is calculated using simple engineering strain formula which states that the strain in the ratio between the change in final length and original length to the original length. Shortening is expressed in percentage as used

by (Soibam, 1998). A Negative value indicates shortening and positive value suggest extension.

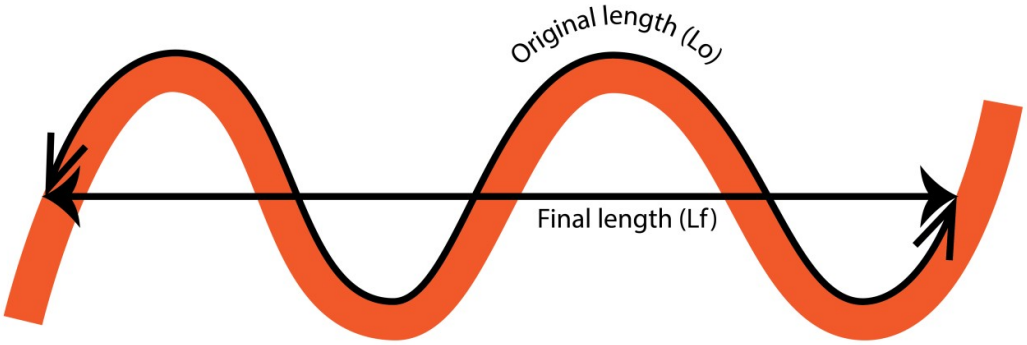

Fig. 6.2: Simple schematic diagram showing how shortening can be calculated from the original length and final length using line balancing method.

$$e = \left(\frac{Lf - Lo}{Lo}\right) \times 100$$

Where, e = strain (shortening or extension in percentage)

Lf = final length

Lo = original length

The Belt of Schuppen, which is the frontal part of the Indo Myanmar Ranges could be the result of the interplay of the general ESE-WNW compression owing to dextral shear deformation mechanism from the interaction of the Indian plate and the Myanmar micro plate (Soibam, 2006), and the effect of E-W trending dextral strike-slipping along the Dauki fault on the south of the belt. The various structures such as fault, folds, strike slips etc. observed in the field are a representation of this tectonic regime. The field observation shows evidences of high degree of shortening in direction parallel to the compressional direction which is perpendicular with the regional trend. The technique of line balancing has been utilized to calculate the amount of shortening from folds and thrust observed in the field. These calculations are made by direct measurements from the field photographs as most of the observed exposures of structures were difficult for physical measurements and in some cases various portions of the structures have been eroded consequently making us compel to draw the projected

continuation for the calculation of shortening. As such, an attempt has been made to calculate the amount of shortening from these structures. Moreover, there are very limited exposures of minor structures from which shortening can be calculated using line balancing method. Thus, amount of shortening have been estimated from four structures (2 thrust and 2 fold minor structures). The minor structures of thrusts from which calculations of shortening were carried out is shown in Figure 6.3. The minor structures of folds from which calculations of shortening were carried out is shown in Figure 6.4. Figure 6.4b shows two consecutive crests respectively of adjacent anticline and syncline developed in shale. Both the crests of the anticline and syncline are found to plunge towards about 350° with an amount of 27°. Another calculation is made from the representation of one seismic profile (Fig. 6.4c) of the Digboi anticline that has been developed just above the Naga thrust. The seismic profile has been taken from the article of Choudhuri et al., 2023. Therefore, this value of shortening can be taken as the value calculated from a known horizon. Thus, this calculated value is used to validate the amount of shortening calculated from the field data.

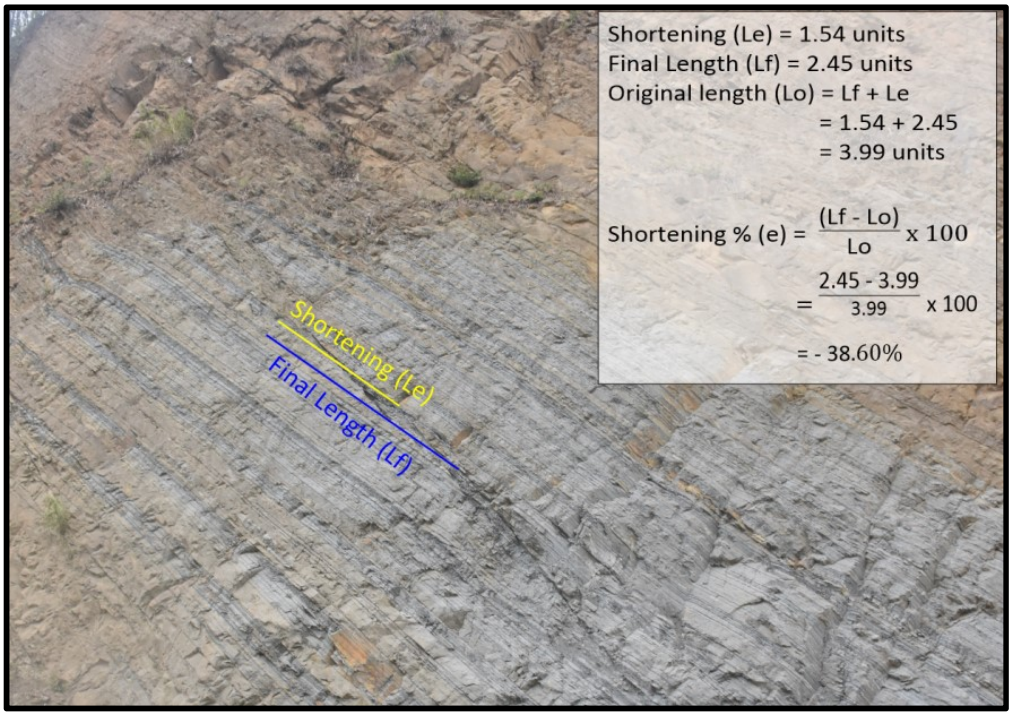

(a)

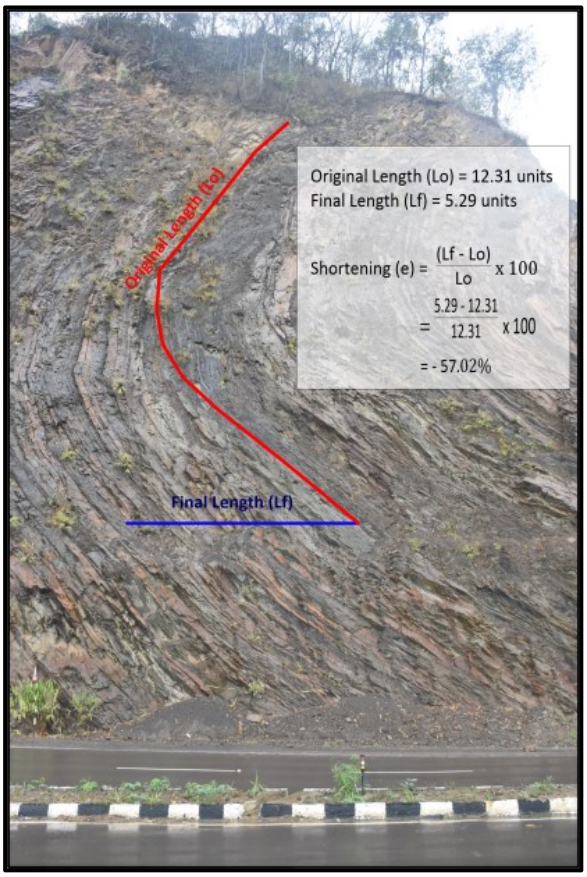

(b)

Fig. 6.3: Photographs showing various minor structures from which shortening is calculated;

(a) calculation of crustal shortening from the exposure of a thrust,

(b) calculation of crustal shortening from another exposure of a thrust.

(a)

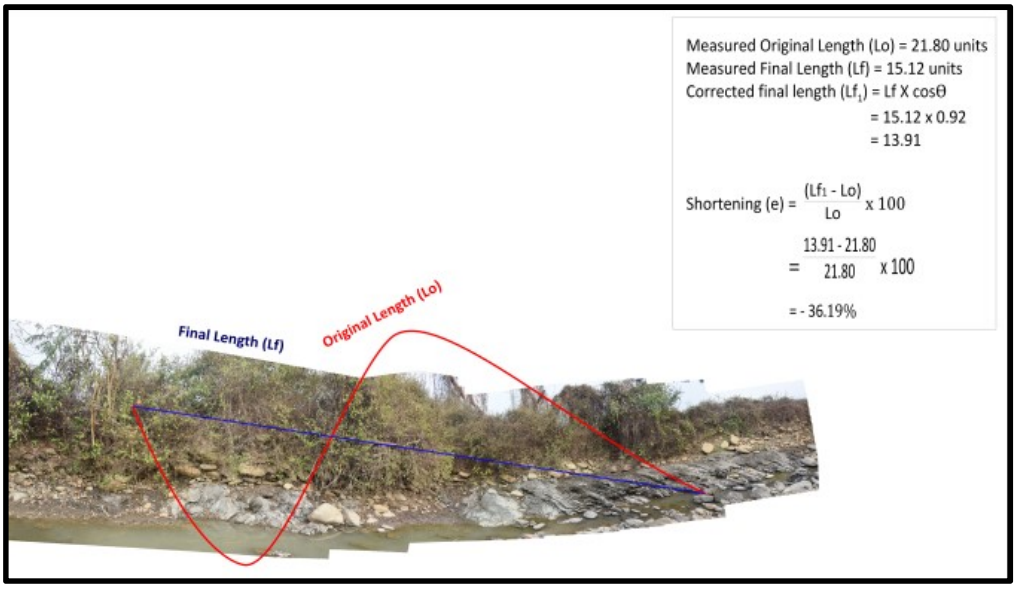

(b)

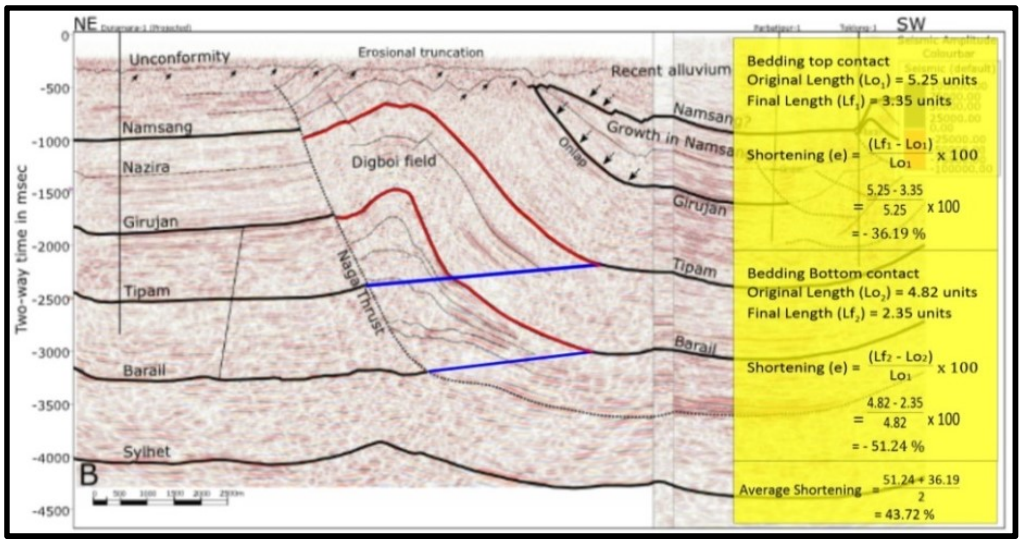

(c)

Fig. 6.4: Photographs showing various minor structures from which shortening is calculated; (a) and (b) calculation of crustal shortening from the exposure of two minor folds, (c) calculation of crustal shortening from a seismic profile (seismic profile from the article of Choudhuri et al., 2023).

The following paragraphs show the calculation of shortening from the aforementioned minor structures.

Shortening calculation from Fig. 6.3a

Final length measured (Lf) = 2.45 units

Shortening measured from the thrusted structure (Le) = 1.54 units

Original length (Lo) = Lf + Le

= (2.45 +1.54) units

= 3.99 units

Therefore, shortening % (e_1) = $\frac{Lf-Lo}{Lo} \times 100$

$= \frac{2.45-3.99}{3.99} \times 100$

$= -38.60\%$

Shortening calculation from Fig. 6.3b

Final length measured (Lf) = 5.29 units

Original length measured (Lo) = 12.31 units

Therefore, shortening % (e_2) = $\frac{Lf-L}{Lo} \times 100$

$= \frac{5.29-12.31}{12.31} \times 100$

$= -57.02\%$

Shortening calculation from Fig. 6.4a

Final length measured (Lf) = 38.49 units

Original length measured (Lo) = 59.04 units

Therefore, shortening % (e_3) = $\frac{Lf-Lo}{Lo} \times 100$

$= \frac{38.49-59.04}{59.04} \times 100$

$= -34.80\ \%$

Correction of shortening value calculation direction w.r.t. the perpendicular direction (for Fig. 6.4b) using Cos θ rule

Final length measured (Lf) = 15.12 units

Corrected final length* (Lf_1) = $Lf \times \cos\theta$ (where is the angle between the direction of the sectional line and the compression direction)

$= 15.12 \times \cos 23°$

$= 15.12 \times 0.92$

$= 13.91$

Calculation of shortening from Fig. 6.4b

Original length measured# (Lo) = 21.80 units

Therefore, shortening % (e_4) = $\frac{LF_1 - Lo}{Lo} \times 100$

$= \frac{13.91 - 21.80}{21.80} \times 100$

$= -36.19\ \%$

* The final length is corrected to accommodate the tilt or deviation of the section away from the regional compression direction using simple cosine trigonometry.

The original length measured is however supposed to remain the same as there is no loss or gain in the material of the beds during deformation (Plain strain deformation).

Average shortening calculated from all the minor structures

$= \frac{e_1 + e_2 + e_3 + e_4}{4}$

$= \frac{(-3\ .60) + (-57.02) + (-34.80) + (-36.19)}{4}$

$= -41.65\%$

Shortening value calculated from seismic profile (Fig. 6.4c)

Bedding Top Contact

Final length measured (Lf) = 3.35 units

Original length measured (Lo) = 5.25 units

Therefore, shortening % (e_5) = $\frac{Lf-Lo}{Lo} \times 100$

$= \frac{3.35-5.25}{5.25} \times 100$

$= -36.19\ \%$

Bedding Bottom Contact

Final length measured (Lf) = 2.35 units

Original length measured (Lo) = 4.82 units

Therefore, shortening % (e_6) = $\frac{Lf-Lo}{Lo} \times 100$

$= \frac{2.35-4.82}{4.82} \times 100$

$= -51.24\ \%$

Average Shortening $= \frac{e_5+e_6}{2}$

$= \frac{(-3\ .19)+(-51.24)}{2}$

$= -43.72\ \%$

Calculation of total extent of the Belt of Schuppen before shortening:

Calculated Shortening: 41.65%

Final Length (Lf) = 18.31 km

Original Length (Lo) =?

We know, e $= \frac{Lf-Lo}{Lo} \times 100$

(- 41.65) $= \frac{100\,Lf-10\ \ Lo}{Lo}$

(- 41.65) Lo = 100 Lf – 100 Lo

100 Lo - 41.65 Lo = 100 Lf

58.35 Lo = 100 x 18.31

Lo $= \frac{1831}{58.35}$

Lo = 31.38 km

* This value is a measure of an aerial extend between the Naga thrust at Chumukedima and the Disang thrust at Piphema measured from Google Earth Imagery (2021)

Table 6.1: Summary of shortening values from various minor structures and other sources.

Sl. No	Figure No.	Location	Shortening	Average Shortening
1	6.3a	25º47'50.56"N 93º48'07.36"E	(-38.60%)	41.65%
2	6.3b	25º45'57.36"N 93º56'29.32"E	(-57.02%)	
3	6.4a	25º45'10.45"N 93º57'19.01"E	(-34.80%)	
4	6.4b	25º36'06.26"N 93º41'14.73"E	(-36.19%)	
5	6.4c	Choudhuri et al., 2023	(- 43.72), (51.24%)	43.72 %
6	Profile 1 to 6	Soibam et al., 2015	(- 30.6%), (- 47.7%), (- 49.4%), (- 49.8%), (- 50.3%), (-60%)	47.96%

The shortening calculated from the various structures in the field gives an average estimated crustal shortening of the area as 41.65%. This value is almost comparable with value of shortening calculated from the seismic profile (Fig. 6.4b), which is calculated as 43.72 %. Soibam et al., (2015) gave an estimated regional shortening (across entire section of IMR) values of 30.6%, 47.7%, 49.4%, 49.8%, 50.3% and 60% respectively from six profiles that pass through Nagaland across the Belt of Schuppen. These values when averaged out (47.96%) give the shortening value of the IMR.

The degree of shortening calculated in the study area is found to be less than the regional shortening value, which could be attributed to the fact that maximum shortening are a result of the thrust slices in an imbricate system due (Shubamenon, 2019). The lesser quantum of shortening in the study area as compared with entire the Indo Myanmar (IMR) could be attributed with the fact that Belt of Schuppen is the frontal part and the maximum shortening could have taken place beyond the Belt of Schuppen toward the

eastern margin of the IMR as seen from the profiles of Soibam et al., (2015) where the maximum peaks are observed in the topographic profiles.

Thus, the study area of the southern part of the Belt of Schuppen shows a shortening value of -41.65% and the aerial extent of the Belt of Schuppen in the study area before tectonic compression is calculated as 31.38 km when the final length is 18.31 km.

Chapter 7
Discussion and Conclusions

7.1 Discussion

The study area is found to have exposures predominantly of the litho-units belonging to various formations of Barail, Surma and Tipam Groups. All the three formations of Barail Group namely Laisong, Jenam and Renji are found exposed in the study area of the Belt of Schuppen (BoS) of Nagaland. But, the Laisong Formation is not found exposed everywhere except in Pimla - Old Jalukie section (Fig. 4.16). In the western side of the entire belt there is no exposure of any litho-unit belonging to Barail Group, but occupied by the exposures of the formations of Surma and Tipam Groups juxtaposed with each other mainly against geological structures predominantly of thrusts. In the middle portion of the BoS particularly in Chumukedima – Piphema (Figs. 4.8 to 4.10) and Pimla - Old Jalukie sections where the belt appears to be wider the youngest group of litho-units like Girujan Clay and Namsang Formation of Dupitila Group are exposed. In these two sections the middle portion is occupied by the valleys respectively of Medziphema and Jalukie intermontane basins. In the valley areas the litho-units like Girujan clay and Namsang Formation are found to cover sporadically by thick piles (Fig. 4.8) of mixtures of water borne clasts of variable sizes ranging from rounded boulders to cobbles embedded in the groundmass of sand (Dihing?). The same water borne recent deposits are found sitting on tops of some exposures of Tipam sandstone (Figs. 4.18 b and c) and Girujan clay occurred in the extreme western margin of the BoS.

In AB segment of Niuland - Zhadima Section (Fig. 4.2) the southern part of BoS is found to be the narrowest. The southern part of the belt lies to the south of approximately N26° latitude. This southern part of the belt is tapered at this segment in such a way that the litho-units of both the western and eastern margins are forming a closure; and gradually becomes wider as moved towards SW and ultimately closed again at about N25.3° latitude. For this segment the calculated π - girdle is found to be 43°/276°, which means that the fold axis is along ESE - WNW. The calculated β - axis is 47°/096°, which indicates that fold axis is plunging with a high angle, which may be attributed to a closure of a fold. In BC segment of Niuland - Zhadima Section, which passes through the litho-units exposed on the eastern side of the BoS the calculated π -

girdle is found to be 83°/221°, which means that the fold axis is roughly along NE - SW. The calculated β - axis is 07°/041°, which indicates that fold axis plunging with about 07° towards NE. The bedding attitudes (Dip - Strike data) of the litho-units along the BC segment (Fig. 4.1) show an anticlinal axis. So, it appears that this part of the southern BoS (south of N26° latitude) is occupied mostly but to a limited extent by exposure of a plunging anticline.

In segment I (AB sectional line) of Chumukedima - Piphema section the calculated π - girdle is found to be 88°/225°, which means that the fold axis is almost horizontal (plunge amount of 02°) and running along NE - SW. For the segment II (BC sectional line) the calculated π - girdle is found to be 70°/267°, which means that the fold axis is plunging with a moderately high angle (20°) and running almost along E - W. The segment II is in the middle portion of the BoS in this particular section. The π – girdle data indicates a possible closure of a fold in this area of the section. The bedding attitudes (Dip - Strike data) of the litho-units along the BC sectional line (Fig. 4.7b) show a synclinal closure. The segment III (CD sectional line) is in the eastern portion of the BoS in this particular section and lies a bit on the southern side of segment II. The calculated π - girdle is found to be 89°/221°, which means that the fold axis is almost horizontal (plunge amount of 01°) and running almost along NE - SW. The π – girdle data indicates that the area is occupied by the litho-units of a limb of a fold whose axis is running along NE - SW.

In Pimla - Old Jalukie section the calculated π - girdle is found to be 85°/039°, which means that the fold axis is having a low plunge amount (05°) and running almost along NE – SW (039°). Here the fold is plunging towards SW. Taking into consideration of the closure of a syncline in Chumukedima - Piphema section and plunging of the fold axis towards the SW in the Pimla - Old Jalukie section it appears that major portion of the BoS on the south of Chumukedima - Piphema section is occupied by the litho-units of a south westerly plunging syncline. The plunge is low. The syncline is most probably extended up to about N25.3° latitude.

The shale and sandstone formations exposed in a river bed at a lower elevation (than the valley) in a river bed just at the eastern margin of Jalukie valley are found folded. The two adjoining anticline and syncline axes preserved in shale are found to

plunge by 27° towards 250°. There is also an exposure of plunging anticline developed in sandstone at the same river bed. The folds are plunging with moderately high angle towards 250°, which means that the resultant force of compression is along 160 - 340°, i.e., along SSE – NNW. This is against the general compression direction of ESE - WNW (Soibam, 2006) of the rest of the Indo-Myanmar Ranges (IMR). This indicates that there is a component of the force pushing towards the east. This eastward pushing force can be attributed to the dextral strike slip motion along the Dauki fault. The eastward motion must have been related to the oblique motion of the landmass (SW-NE) on the east in the latitudinal range of this southern part of BoS before ultimately changing to E-W direction (further south) owing to the dextral strike slip motion of the Dauki fault. In this latitudinal range the general compression direction of the rest of IMR is ESE – WNW (cf. Soibam 2006). But the trend of the BoS is NE-SW, which means that the compression direction of SE-NW. This shows that there is interplay of the dextral motion along the Dauki fault and the ESE – WNW general compression direction of the IMR as a result of which the BoS is made to trend along NE-SW.

The petrography and ICP (MS) data of trace and REE are examined to be able to differentiate and distinguish the different litho-units, which may corroborate with the field setting of the study area. The petrography of sandstone samples is carried out to know the modal proportions of Q, F, R and L so that QFR (Folk, 1980) and QFL (Dickinson, et al., 1983) plots could be constructed. Here, Q, F, R and L stand respectively for Quartz, Feldspar, Rock fragments and Lithic fragments. In QFR plot samples of Surma Group are pigeonholed near the dividing line of subarkose and sublitharenite fields with more enrichment in feldspar and lithic fragments than the samples of Barail Group, which fall in the field of sublitharenite with lesser proportion of feldspar and lithic fragments (Fig. 3.2). At the same time in QFL plot even if all the samples are pigeonholed in the recycled orogenic field there are two groups of rocks (of Barail and Surma Groups) concentrated in different spots (Fig. 3.3). The QFR and QFL plots demonstrate that samples from different litho-units are segregated into different areas of various fields of the respective diagrams thereby rendering clues for confirmation of areas of exposures of different litho-units in construction of geological maps. Thus, petrography turns out to be a very useful tool for understanding the field setting of the imbricate system.

For understanding the trace and Rare Earth Elements geochemistry ICP (MS) analysis is carried out for representative samples of both sandstone and shale (taking into consideration of the respective standards of normalisation) with an aim to render support in the establishment of the field setting of the study area. The spider diagrams for REE (Figs. 3.4a and 3.4b) and UCC (Figs. 3.5a and 3.5b) patterns both for shale and sandstone samples clearly suggest the segregation of samples belonging to different litho-units. The samples belonging to Barail, Surma and Tipam Groups are clustered separately both in the REE spider diagram patterns of shale and sandstone. As in the case of REE, the UCC spider diagram patterns of shale and sandstone, samples belonging to Barail, Surma and Tipam Groups are clustered separately. Thus, trace and REE data analysis also turns out to be very useful tool in the confirmation of different litho-units when preparing the geological map.

The calculated β axis is 02°/043° (Fig. 5.4a) of the joints data in segment I (Fig. 5.1). Hence $\sigma_{1,}$ which should run parallel to the compression direction, should be along 043° + 090° = 133°. Thus, the orientation direction of σ_1 could be considered to be around 130°. The σ_1 direction bisects the roughly 60° measure of angle between the oppositely dipping groups of joints. Thus, majority of joints in this segment are because of shear fracturing i.e., are of Mode II type. From Fig. 5.3a and Fig. 5.5a, it is also learnt that the next prominent set of joints are those running parallel to the compression direction. Since this group of joints parallel to the compression (σ_1) direction could be joints of Mode I type. The parallelism of π girdle of the joints with that of the mean principal orientation of 131° of the beds indicates that orientation of the trends of the planes of joints are perpendicular to the bedding trend of the beds.

From the comparison of β axis directions in Segments I (02°/043°) and II (21°/084°), it appears that strike of majority of the beds in segment II (Fig. 5.1) have been rotated clockwise roughly by 41° (84° - 43°) from their positions in segment I. The segment II just touches the Jalukie-Medziphema intermontane basin (valley). Had the basin been formed because of sagging down of blocks of the bedrocks through various normal faults then the rocks must have been rotated thereby changing their strike directions. Hence, the clockwise rotation of the β axis must have been related with the formation of the valley. The changing of plunge from 02° (Segment I) to 21° (Segment II) supports this proposition. The mean dip amounts of the beds of segment I is 46°, while

that of segment II is 28°. The general decrease in the dip amount from 46° to 28° also indicates that the beds have been rotated. It is learnt that there are some beds (Figs. 5.3b and 5.4b) concentrated at around 040-050°, which are almost similar with the general trend of segment I. This shows that there are still some beds which have not been rotated. We have seen in segment I that the π girdle of the joints is parallel with the mean principal orientation of the beds. It is observed in segment II that even if the π girdle for the whole of 210 joint planes is calculated as 23°/021° (Fig. 5.5b), there are still good proportion of poles concentrated along a line almost parallel with the mean principal orientation (Fig. 5.4b) of the majority of the beds. These poles must have been related with the old joint planes already developed in the rotating bedrock. Thus, older joints are shear fractures of Mode II type that have been developed in similar fashion as in segment I. But, in this segment there is a group of very prominent joint set (of larger proportion as well), which are concentrated along 100-110° (Figs. 5.3b and Fig. 5.5b). These joints are almost controlling the π girdle of whole of the joint planes of this segment (owing to the greater proportion) and the girdle is along 23°/021°. The poles of these joints (Fig. 5.5b) are found not to be parallel with the orientation of the bedding planes (Fig. 5.4b). Hence, this group of joints appears to be a different set, which could have been developed at a later phase. Hence, this new joint set (100-110° orientation) could have been related with normal faulting. Then, normal faulting is supposed to take place because of compression along 100-110°. Thus, the σ_1 direction for the generation of newer groups of joints should be at around 105°. This shows that σ_1 direction in this segment has been rotated anticlockwise by about 20 - 25° from that of segment I. Consequently, the 100-110° orientated joints must have been produced by tensile fracturing and hence are of Mode I type.

The β diagram (Fig. 5.4c) of segment III (Fig. 5.1) shows that the general (average) orientation direction of the beds of this segment is 40°/129° and the β axis being 07°/048°. These attitudes are almost the same with those of segment I where the average orientation direction is found to be 46°/131° and β axis as 02°/043°. The β diagram of this segment also shows that majority of the beds are rotated clockwise by about 10° from the average orientation direction. Very few beds are dispersed anticlockwise by few degrees as well. Hence the larger proportion of the beds of this segment has suffered a little rotation unlike those in segment II from the general average orientation of segment I. There is also very little change in the plunge amount (from 02°

to 07°) of β axis. The joint pattern of this segment (Fig. 5.3c and Fig. 5.5c) is almost the same with that of segment I (Fig. 5.3a and Fig. 5.5a); the only difference is that the proportion of joints oriented roughly along 140-170° is more than that oriented around 060-080° (in segment III, Fig. 5.5c) while the opposite holds good in segment I. It is also seen from Fig. 5.5c that these two clustering directions of joints are roughly divided by another group of joints; the direction being at around 090-110°, which is supposed to be compression direction (by referring to the similar case of segment I). Hence, σ_1 direction in this segment is at around 100°. Consequently, joints oriented roughly along 140-170° and 060-080° are mostly of Mode II type while those aligned along 090-110° are of Mode I type. There are some joints roughly perpendicular to the compression direction as well, in this segment. The π girdle is parallel to the trend of bedding and hence the joints of segment III must have been developed in a similar fashion as in segment I.

The beds of segment IV striking roughly NE-SW and NW-SE are dipping oppositely. The roughly E-W trending beds (clustering along 090-110°) are having few other beds dispersed on both the sides around them. The β axis is 26°/185°. Hence, this segment is occupied either by southerly plunging anticline or syncline. The joints in this segment, at a glance, appear to distribute randomly, but a close observation reveals that the joints cluster (Fig. 5.5d) roughly in three principal directions, 140-170°, 060-080° and 090-110°. These concentration directions are more or less the same with those of segment III, but majority of the joints striking roughly 140-170° are dipping oppositely towards SW as against those of segment III dipping towards NE. Figure 5.5d shows that the principal orientation of the beds of segment IV is 28°/209°; but there are many oppositely dipping beds too whose effect have been subdued in the π diagram as their proportion is very less. The π girdle (Fig. 5.5d) of the joints is 37°/231°. It is also seen that there are limited poles appear to concentrate along an oppositely dipping plane (corresponding to the subdued bedding planes), which should intersect the π girdle at a low southerly pointed plunge with calculated girdle. This plane would run parallel to the trend of the other limb. Hence, all the joints appear to trend almost parallel to the π girdles of the beds. Hence, the joints trending roughly along 140-170° and 060-080° could be of Mode II type. The groups of joints trending roughly 140-170° and 060-070° are separated by a group of joints trending roughly 090-110°. These joints could be of Mode I type. Hence the σ_1 direction in this segment also should be at around 100°.

The orientation of the maximum principal stress, σ_1 of the four segments found out from joint analysis (I = 130°, II = 105°, III = 100°and IV = 100°) almost agrees well with those determined from conjugate analysis (I = 105°, II = 090°, III = 118°and IV = 083°). From the conjugate fracture analysis, it can be argued that fracture systems of BoS are found to be associated with all the three mechanisms of faulting (Fig. 5.7), but mainly controlled by strike-slip faulting (Table 5.2 and Fig. 5.7). It is found that there is influence of normal faulting as well (Fig. 5.7) since σ_1 angle is found moderately high. The fractures associated with normal and thrust faulting other than the general control by strike-slip faulting is evident from Table 5.2 and Figure 5.7 as well. But fractures associated with reverse faulting are relatively very rare.

The analysed data on conjugate fractures can be used to evaluate not only the orientations of the principal stresses but also the internal friction angle (ϕ) of the rocks in which the conjugate fractures are developed. The general range of internal friction angle (ϕ), from the analysis, is found to be between 22°-40° and that of θ, the acute angle between the maximum principal stress and conjugate fracture planes, varies between 25° to 34°; where $\theta = 45° - \phi/2$. Thus, θ ranges between 28.0° to 32.5°. Internal friction angle of shale ranges roughly between18.0°-25.0° while that of sandstone roughly between 26.0°-35.0°. Thus, the conjugate fractures are developed in shale at larger angle (2θ) than that of the siltstone and sandstone, which is owing to the competency contrast between these rock types.

The analysis of slickenside lineation data also implies that the rocks of BoS have experienced all sorts of fracturing mechanism namely normal, strike-slip and reverse (thrust) faulting. But the majority of them are found to have been controlled by the thrust faulting mechanism, where the influence of strike-slip faulting also evident (Fig. 5.10). The slickensides associated with normal and strike-slip faulting other than the general control by thrust faulting is evident from Table 5.4 and Figure 5.10 as well.

The shortening calculated from the various structures in the field gives an average estimated crustal shortening of the area as 41.65%. The degree of shortening calculated in the study area is found to be less than the regional shortening value, which could be attributed to the fact that maximum shortening are a result of the thrust slices in an

imbricate system due (Shubamenon, 2019). The lesser quantum of shortening in the study area as compared with entire the Indo Myanmar (IMR) could be attributed with the fact that Belt of Schuppen is the frontal part and the maximum shortening could have taken place beyond the Belt of Schuppen toward the eastern margin of the IMR as seen from the profiles of Soibam et al., (2015) where the maximum peaks are observed in the topographic profiles.

Thus, the study area of the southern part of the Belt of Schuppen shows a shortening value of -41.65% and the aerial extent of the Belt of Schuppen in the study area before tectonic compression is calculated as 31.38 km when the final length is 18.31 km.

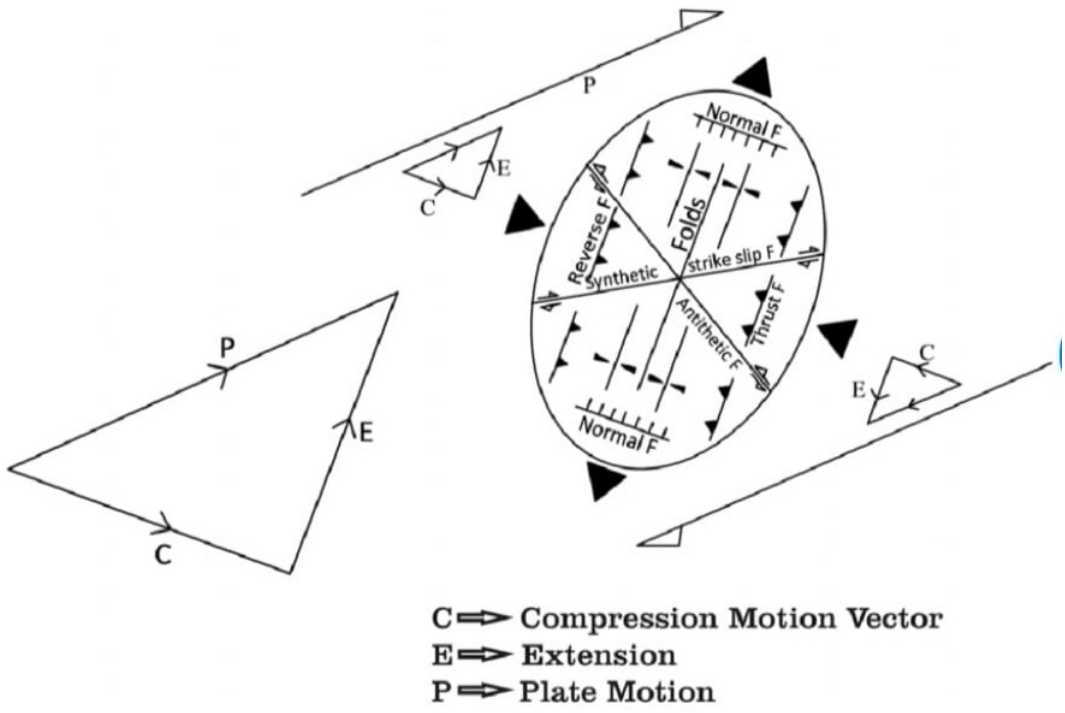

Fig. 7.1: Dextral simple-shear deformation mechanism of the rocks of the rest of Indo-Myanmar Ranges (after Soibam, 2006).

The tectonic features of the Manipur-Naga Hills segment in particular and the Indo-Myanmar Ranges in general are attributed to the dextral simple-shear deformation mechanism as envisaged by Soibam, (2006) (Fig. 7.1). According to this deformation

mechanism, the orientation of the tectonic features in the study area should be aligned in such a manner - the fold axes and thrusts along 020-030º (extension direction); the normal faults along 110-120º (compression direction); the synthetic strike-slip faults along 080-090º and antithetic strike-slip faults along 140-150º (Fig. 7.1). But, this prescribed rule holds good in other areas of the IMR more outside the BoS and lying on the east. In the southern BoS area (from SW end to roughly up to N 26° latitude), the tectonic features particularly the ridge axes and hence the beddings and thrusts are oriented roughly along 045º. The difference in the tectonic features of the BoS and the rest of the IMR is clearly evident in the Google terrain map (Fig. 7.2).

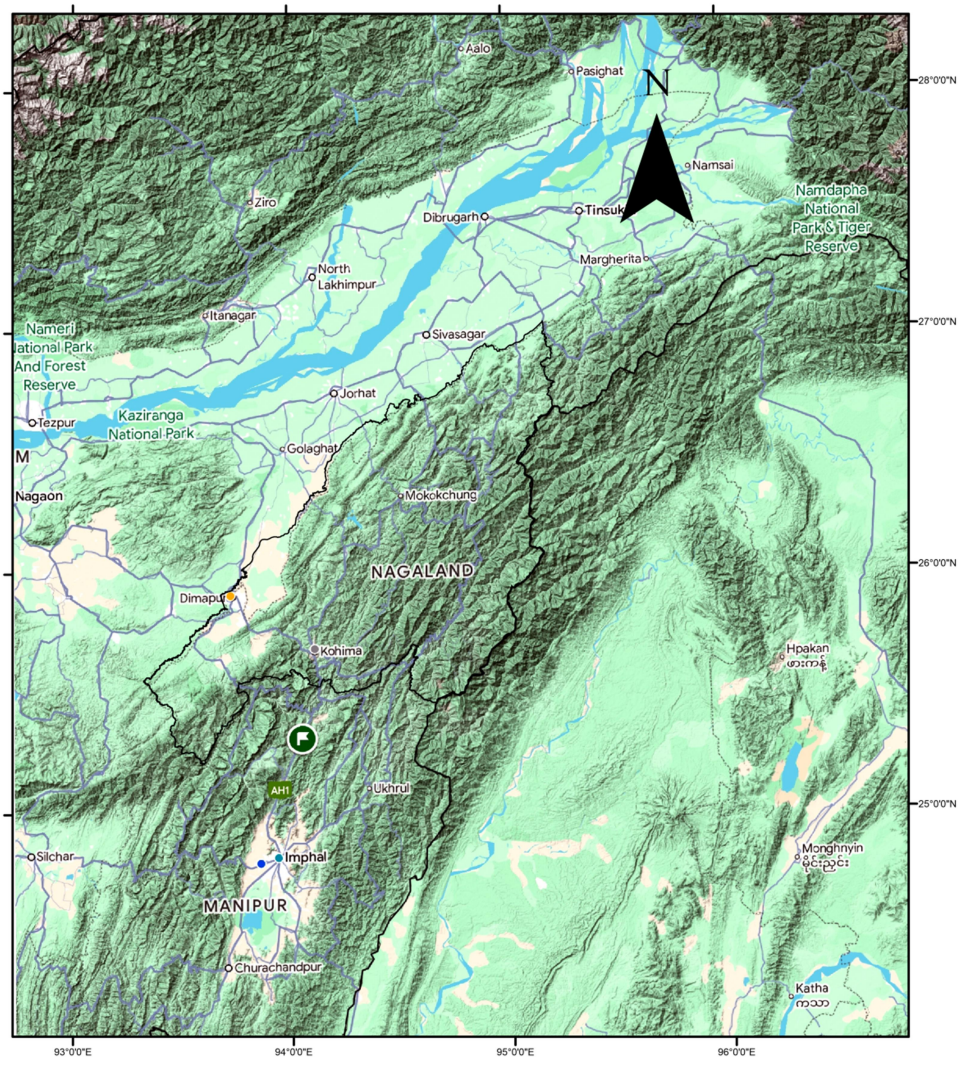

Fig. 7.2: Google terrian map showing the position of Nagaland in the IMR

From the positions of σ_1, σ_2 and σ_3 in the pole diagrams (Fig. 5.5), it is seen that the relative orientations of the maximum principal stress have variable patterns, implying the possible cyclicity of tectonic events, such that is strike-slip faulting replaces the normal faulting as well as reverse faulting. Most interesting observation is the orientation of σ_1, the position of which is found swinging around ESE-WNW to SE-NW. The positions of σ_2 in segments I, III and IV are found to swing roughly around NNW-SSE to NW-SE and those of σ_3 roughly around NNE-SSW to NE-SW. This indicates that the general tectonic shortening in the BoS is along ESE-WNW to SE-NW direction while the extension direction is around NNE-SSW to NE-SW. This is also evident from the close clustering poles of the respective π-girdles of σ_1 and σ_3. In the case of segment II, the orientation of σ_2 is along NNE-SSW while that of σ_3 is along NNW-SSE. The positions and plunges of the three principal stresses and the interchange of positions of σ_2 and σ_3 with respect to those of other segments could be attributed to the reactivation of strike-slip faults as normal fault in segment I, which led to the generation of the Jalukie-Medziphema intermontane basin.

The orientation pattern of the principal stresses of the studied section as a whole suggests that the majority of the conjugate fractures were related to strike-slip faulting where σ_1 and σ_2 lie in the WNW-ESE plane and σ_3 lie in the NNE-SSW direction perpendicular to the WNW-ESE plane. These types of orientation patterns should have a close relationship with the tectonic setting of the IMR.

It is observed that, in general, θ has a larger value for more competent rock like sandstone/siltstone, and a lower value for incompetent rock like shale. However, there are also certain cases where values of ϕ and θ are equal. But in some cases, the value of ϕ is larger for shale and smaller for siltstone/sandstone. This may be due to the hybrid fracturing mechanism, as well as the rotation of the conjugate pairs with respect to the principal stress orientation in subsequent stages of deformation.

Similar to the conjugate fractures analysis, the orientation of the three principal stresses also gives certain type of setting of the study region where, the orientation of σ_1, the position of which is always swinging around ESE-WNW to SE-NW. Whereas the positions of σ_2 and σ_3 swing around NNE-SSW to NE-SW regional extension direction as evident from the parallel nature of the two π-girdles. This particular observation could be

correlated with the general tectonic shortening at around ESE-WNW to SE-NW in the BoS and possible interchange of thrusts to strike-slip and vice-versa.

7.2 Conclusions

Srinivasan (2007) reports that the BoS extends between Dauki fault in the SW and Mishmi thrust in the NE over a length of 500 km. The SW end of BoS moved upwards towards the east along the dextral Dauki fault, while the NE end moved downwards and towards west along the Mishmi thrust, which is also dextral in nature. The E-W oriented dextrally moving Dauki fault turns NNE-ward and extends up to the western limb of southerly plunging Kohima synclinorium (Evans, 1964). The western limb of Kohima synclinorium is well beyond the BoS. Thus, the compressive motion (on account of dextral simple-shear deformation mechanism of the IMR) along WNW direction changes towards W, transforming from thrust to strike-slip motion along the Dauki fault beyond the SW end of the BoS.

Along the latitude of the section of this study area, the regional compression direction of the rest of the IMR beyond the southern part of the BoS should be ESE-WNW. But, in the BoS region along this latitude, the σ_1 swings around ESE-WNW to SE-NW. The interplay of dextral simple-shear deformation of the IMR and dextral strike-slip movement along the Dauki fault could have caused the resultant compressive force rotated clockwise thereby making the southern part of the BoS in this part trend NE-SW differently from that of NNE-SSW of the rest of IMR (Fig. 7.2).

Another important revelation of the palaeo-stress analysis when using each and every conjugate fractures separately is that, even if the bedding tilt correction is applied, the position of σ_1 remains nearly unchanged, since it lies perpendicular to the regional strike, NNE-SSW to NE-SW. But, relative interchanging of σ_2 and σ_3 positions occurs. Therefore, constant compression of the rocks of BoS along ESE-WNW is undoubtedly evident but there is interplay with SSE – NNW compressional force generated on account of dextral strike-slip motion along the Dauki fault.

Joint, conjugate fracture and slickenside analyses reveal that the relative orientations of the maximum principal stress have variable patterns, implying the possible

cyclicity of tectonic events, such that is strike-slip faulting replaces the normal faulting as well as reverse faulting. In some areas of the BoS the strike-slip faults could have been reactivated as normal faults as evident from segment II of the studied section.

The mean orientation directions of the three principal stresses of the whole section (all the four segments) are σ_1 = 16°/094°, σ_2 = 70°/308° and σ_3 = 07°/189° with minor fluctuation on either side. The mean orientations of σ_1 and σ_2 are at an average plunge at 16° and 70° respectively and the orientations distribute more or less uniformly parallel to the WNW-ESE, which is the regional compression direction of the generation of the IMR. Such an observation is also clearly evident from the contour diagrams and the π - girdles. On the other hand, σ_3 has a nearly constant, almost horizontal orientation (Figure 8e) parallel to the extension direction of NNE-SSW. Thus, the stress field of the BoS as a whole has a close relationship with the tectonic setting of the IMR.

When each and every conjugate fracture and slickenside data are analysed separately, it is evident that orientation of σ_1 remains more or less constant (even if swinging in the same quadrant) while that of σ_2 and σ_3 inter-change frequently implying that these faults are formed either by reverse (thrust) faulting or strike-slip faulting. Or otherwise they might have been formed through thrust/reverse faulting, and reactivated as strike slip faulting due to the interplay of dextral slip of the Dauki fault and dextral shear deformation of the IMR along a transitional region between Kohima synclinorium and the BoS. And therefore, all the thrust sheets in the BoS are high-angle faults. Thus, the BoS can be treated as a strike-slip imbricate system rather than as a thrust imbricate system. Tectonically, the formation of BoS is related with the formation of IMR in general.

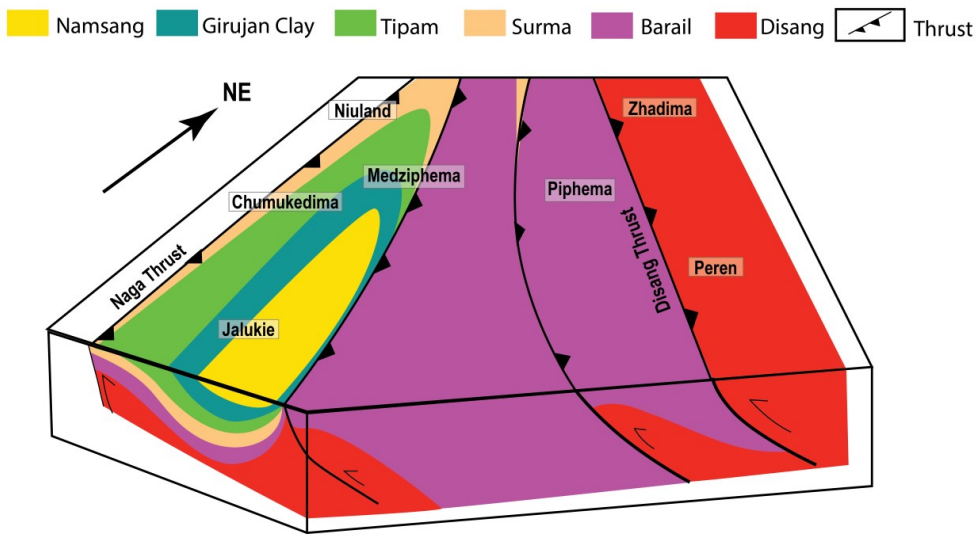

Fig. 7.3 Schematic model showing the southern part (South of 26º N) of the Belt of Schuppen

The studies of the bedding attitude patterns and field setting (Chapter 3) as well as other aspects as discussed in other chapters it is revealed that the northern end of the southern part of BoS near N 26° latitude (near Niuland - Zhadima section) is occupied by a comparatively small anticline. The anticline is found plunging NE with a small angle. But the area on the south of this anticline and the larger portion of the southern part of the BoS (south of N 26° latitude) is occupied by a large syncline. The closure of the syncline on the north is found to expose along the Chumukedima - Piphema section. The syncline is found plunging towards SW. As the litho-units on both the sides of the axial plane of the syncline is dipping in the same direction (towards SW) and since the beds on one limb are not overturned either, it is inferred that along the immediate and adjacent anticlinal axes on both the sides of syncline there has been considerably more overthrusting. There must have been considerable overthrusting on the east thereby concealing the oppositely dipping beds of the eastern limb of the syncline by the thrust sheets obducted along the anticlinal axis and day-lighted by the litho-units of south-easterly dipping beds of the immediate limb of the anticline. The western part of the BoS is occupied by the south-easterly dipping litho-units of the western limb of the syncline. The western limb of the syncline overthrusts the litho-units of the just immediate limb along the anticlinal axis. The schematic model of the southern part of the Belt of Schuppen and the disposition of the different litho-units in the belt is shown in figure 7.3.

BIBLIOGRAPHY

Acharyya, S. K. (2007). Collisional Emplacement History of the Naga-Andaman Ophiolites and the Position of the Eastern Indian Suture. Journal of Asian Earth Sciences, 29, 229-242. https://doi.org/10.1016/j.jseaes.2006.03.003.

Acharyya, S. K. (2008). Tectonic Evolution of Indo-Burma Range with Special Reference to Naga-Manipur Hills. Mem. Geological Survey of India, v. 75, pp. 25-43.

Acharyya, S. K. (2010). Tectonic Evolution of Indo-Burma Range with Special Reference to Naga-Manipur Hills. Memoirs of the Geological Survey of India, 75, 25-43.

Acharya, S. K. and Jena, S. K. (1982). Reference Geological sections from Naga Hill ophiolite belt (I) Between Pedaro Nala (near Zaongar) to Magnetite ridge and Pokphur and (II) Along-Pungro-Luthur- Penkim road Tuensang District, Nagaland. Geol. Surv. India Unpub. Prog. Report.

Acharyya, S. K., Mitra, N. D., & Nandy, D. (1986). Regional geology and tectonic setting of northeast India and adjoining region. Mem. Geological Survey of India, v. 119, pp. 6-12.

Acharyya, S. K., Roy, D. K., & Mitra, N. D. (1986). Stratigraphy and palaeontology of the Naga Hills ophiolite belt. Mem. Geological Survey of India, v. 119, pp. 94-103.

Angelier, J. and Baruah, S., (2009). Seismotectonics in Northeast India: a stress analysis of focal mechanism solutions of earthquakes and its kinematic implications. Geophys. J. Intl., v. 178, pp. 303-326.

Aier, I., Luirei, K., Bhakuni, S. S., Thong, G. T., & Kothyari, G. C. (2011). Geomorphic evolution of Medziphema intermontane basin and Quaternary deformation in the schuppen belt, Nagaland, NE India. Zeitschrift fur Geomorphologie, 55(2), pp. 247.

Apon, M., Notoka, K., & Chang, C., & Ezung, M., & Thong, G., Walling, T., (2024). Analysis of an anthropogenically-induced landslide with emphasis on geological precursors. Results in Earth Sciences. 10.1016/j.rines.2024.100020.

Balasubramanian, A. (2017). Soil Erosion- Causes and Effects. 10.13140/RG.2.2.26247.39841.

Bhattacharjee, C. C. (1991). The ophiolites of Northeast India: a subduction zone Ophiolite Complex of Indo-Burman Orogenic Belt. Tectonophysics, v. 191, pp. 213-222.

Bhattacharjee, C. C. (1997). Tectonism and Sedimentation in the Indo-Burman Sedimentary Basin. Journal of Geoscience, 2, pp. 1-8.

Bhattacharyya, S. and Sanwal, R. (1985). Systematic geological mapping around Fakimile-Thanameir Saramati, district Tuensang, Nagaland. Geological Survey of India, Progress report for the field season 1984-1985.

Bhattacharyya, S. and Sanwal, R. (1986). Systematic mapping around Meluri, Akhegwo, Waziho, and large scale mapping along Satuza, link road to Waziho limestone deposit and around Waziho village, district Phek. Nagaland. Geological Survey of India, Progress report for the field season 1985-1986.

Borah, M. and Choudhury, S. (2023). Seismic Performance of Tall Buildings with Different Structural Systems. In: Fonseca de Oliveira Correia, J.A., Choudhury, S., Dutta, S. (eds) Advances in Structural Mechanics and Applications. ASMA 2021. Structural Integrity, vol 26. Springer, Cham. https://doi.org/10.1007/978-3-031-05509-6_8.

Borgohain, P., Bezbaruah, D., Gogoi, M.P., Gogoi, Y.K., Phukan, P.P., and Bhuyan, D. (2021). Petrography and diagenetic evolution of the Barail sandstones of Naga Schuppen belt, North East India: implication towards reservoir quality. Current Science. doi:10.18520/CS/V121/I8/1107-1113.

Brunnschweiler, R. O. (1966). On the geology of the Indoburman ranges, Journal of the Geological Society of Australia, 13:1, pp. 137-194, doi: 10.1080/00167616608728608.

Butler, R.W., and Bond, C.E. (2020). Thrust systems and contractional tectonics. doi:10.1016/B978-0-444-64134-2.00008-0.

Cadell, H. M. (1889). Experimental Researches in Mountain Building. Transactions of the Royal Society of Edinburgh, 35(01), pp. 337–357. doi: https://doi.org/10.1144/SP490-2019-142.

Chakrabarti, S. K., Singh, H. J., Akhtar, M. D. S., Singh, R. K., Silox, D., Polanco-Ferrer, T., and Polanco-Ferrer, R. E. (2011). Structural Style of the Assam Shelf and Schuppen Belt, A & AA Basin, India. In AAPG Search and Discovery, Article 90118© 2011 GEO India 2011, 2nd South Asian Geoscience Conference, Greater Noida, New Delhi, India.

Chakradhar, M. and Gaur, M.P., (1985). Geological mapping around Jalukie, Kohima district, Nagaland. Geol. Surv. Ind. Progress Report (Unpublished), Field Season 1984-1985.

Chattopadhyay, B., Venkataramana, P., Roy, D.K., Bhattacharyya, S. and Ghosh, S., (1983). Geology of Naga Hills Ophiolite. Geological Survey of India, 2, pp. 59-115.

Choudhuri, M., Routray, P., Jana, B., & Mathur, S. (2023). Timing the Mikir Hill uplift in Assam Basin: Record of stress propagation along the eastern margin of the Indian Plate. Journal of Asian Earth Sciences: X, 9, 100137.

Coulomb, C. A. (1773). Sur une application des regles de Maximis & Minimis a quelques Problemes de Statique, relatifs a l'Architecture, Memoires de Mathematique & de Physique, presentes a l'Academie des Sciences par divers Savans, & lus dans ses Assemblees. 7, pp. 343-82.

Mohr, C. O. (1882). Über die Darstellung des Spannungszustandes und des Defonnation 624 zustandes eines Korper-elements. Zivi lingenieur. 113.

Coward, M. P. (1992). Lecture notes on course for M. Sc. Applied Structural Geology and rock mechanics (1992-93), Imperial College, University of London.

Coward, M. P. (1996). Balancing sections through inverted basins. Geological Society, London, Special Publications, 99(1), 51 -77.

Curray, J.R., Moore, D.G., Lawver, L.A., Emmel, F.J., Raitt, R.W., Henry, M. and Kieckhefer, R., (1979). Tectonics of the Andaman sea and Burma.

Dahlstrom, C.D. (1969). Balanced cross sections. Canadian Journal of Earth Sciences, 6, 743-757.

DeMets, C., Gordon, R.G., Argus, D.F. and Stein, S. (1990). Current plate motions. Geophysical Journal International, 101: 425-478. https://doi.org/10.1111/j.1365-246X.1990.tb06579.x.

Devdas, V. and Gandhi, P. (1986). Systematic geological mapping in Maromi-Akaluto-Suruhuto areas Zunheboto district, Nagaland GSI, Unpub. Progress Report.

Dickinson, W. R. (1970). Interpreting detrital modes of graywacke and arkose. Journal of Sedimentary Research, 40(2), 695-707.

Dickinson, W. R. and Suczek, C. A. (1979). Plate tectonics and sandstone compositions. Aapg Bulletin, 63(12), 2164-2182.

Dickinson. W. R., Sue Beard. L., Brakenridge. R., Erjavec. J., Ferguson. R. C., Inman. K. F., Knepp. R. A., Lindberg. F. A. and Ryberg. P. T. (1983). Provenance of North American Phanerozoic sandstone in relation to tectonic setting. Geological Society of America Bulletin 94(2). doi: 10.1130/0016-7606(1983)94<222:PONAPS>2.0.CO;2.

Dikshit, K. R. and Dikshit, J. K. (2014). North-East India: Land, People and Economy. Advances in Asian Human-Environmental Research. doi: 10.1007/978-94-007-7055-3.

Elliott, S.R. (1977). A theory of a.c. conduction in chalcogenide glasses. Philosophical Magazine, 36, 1291-1304.

Evans, P. (1932). Tertiary succession in Assam. Trans. Min. Geol. Metall. Inst., India, v. 27 (3), pp. 155-260.

Evans, P. (1964). The tectonic framework of Assam. Geological Society of India, *5*, pp. 80-96.

Evans, P. and Mathur, L.P.(1964), 'Oil in India'. International Geological Cong. 22 Session, India, 1964.

Eduard, S. (1885). Das antlitz der erde. v. 1, 2nd ed, Bookseller of the Kais Academy of Sciences.

Fareeduddin and Dilek, Y. (2015). Structure and petrology of the Nagaland-Manipur Hill Ophiolitic Mélange zone, NE India: A Fossil Tethyan Subduction Channel at the India -Burma Plate Boundary. Episodes, 38 (4), pp. 298-314.

Folk, R. L. (1980). Petrology of sedimentary rocks. Hemphill publishing company.

Fossen, H. (2016*).* Structural geology. Cambridge university press.

Fleuty, M. J. (1975). Slickensides and slickenlines. Geological Magazine. 112, pp. 319-322.

Gautam, J. L. and Verma, R. (2007). Seismicity and tectonics of northeast India and northern Burma. Mausam. 58. pp 403-408. doi: 10.54302/mausam.v58i3.1343.

Geological Survey of India, 2011. Geology and mineral resources of Manipur, Mizoram, Nagaland and Tripura. Miscellaneous Publication No. 30 Part IV, Vol-1 (Part-2).

Ghose, N.C. and Agrawal, O.P. (1989). Geological framework of the central part of the Naga Hills Ophiolite, Nagaland. Phanerozoic Ophiolite of India (eds.) NC. Ghose, Sumna Publication, Patna, pp. 165-188.

Ghose, N.C., Agrawal, O.P. and Chatterjee, N. (2010). Geological and mineralogical study of eclogite and glaucophane schists in the Naga Hills Ophiolite, Northeast India. Island Arc, 19: 336-356. https://doi.org/10.1111/j.1440-1738.2010.00710.x.

Ghose, N. C, Chatterjee, N. and Fareeduddin. (2014).A Petrographic Atlas of Ophiolite, Springer, India (2014), pp. 1-234.

Ghosh, S.K., 1993. Structural Geology Fundamentals and Modern Developments, Pergamon Press,

Ghosh, T., Basu, S., and Hazra, S. (2014). Geological mapping of the Schuppen belt of north-east India using geospatial technology. Journal of Asian Earth Sciences, 79, pp. 97-111.

Groshong, R. H., & Groshong, R. H. (2006). 3-D structural geology (pp. 305-371). Springer-Verlag Berlin Heidelberg.

Gwinn, V. E. (1970). Kinematic patterns and estimates of lateral shortening, Valley and Ridge and Great Valley Provinces, central Appalachian, south-central Pennsylvania. In G. W. Fisher (Ed.), Studies of Appalachian Geology: Central and Southern New York (pp. 127–146). New York: Interscience Publishers.

Hobbs, W.H. (1893). The geological structure of the Housatonic Valley lying east of Mount Washington: Journal of Geology, v. 1, pp. 780-802.

Hobbs, W. H. (1894). Note on the English Equivalent of Schuppenstruktur. The Journal of Geology 2. pp. 206 - 206.

Hodgson, R. A. (1961). Classification of structures on joint surfaces. American Journal of Science, 259(7), 493–502. doi: https://doi.org/10.2475/ajs.259.7.493.

Hopgood, A.M. (1987). Imbricate structure. In: Structural Geology and Tectonics. Encyclopedia of Earth Science. Springer, Berlin, Heidelberg. doi: https://doi.org/10.1007/3-540-31080-0_50.

Hossack, J.R. (1979). The use of balanced cross-sections in the calculation of orogenic contraction: A review. Journal of the Geological Society, 136, 705 - 711.

Ibotombi, S. and Khuman, C. M. (2011). Basic rocks of Manipur Ophiolite in the Indo Myanmar hill Ranges, NE India and the Petrotectonic Significance. Journal of Nepal Geological Society. 43. 13-28. 10.3126/jngs.v43i0.24510.

Ibotombi, S., Khuman, C.M. and Subhamenon, S. (2015). Ophiolitic rocks of the Indo-Myanmar Ranges, NE India: Relicts of an inverted and tectonically imbricated hyper-extended continental margin basin?. Geological Society, London, Special Publications. doi :10.1144/SP413.12.

Imsong, W., Thong, G.T., and Sharma, S. (2022). Causes of pulsating evolution of fluvial landforms since the marine isotopic stage-2 in the belt of Schuppen, Nagaland, NE India. Physical Geography, 44, pp. 381 - 404. doi:10.1080/02723646.2022.2064065.

Jain, A. K. and Bhowmik, S. K. (2016). Tectonics and Evolution of the Trans-Himalayan Mountains and Nagaland Ophiolite Belt. Proceedings of the Indian National Science Academy. doi: 10.16943/ptinsa/2016/48471.

Jamir, C., Sharma, N., Sengupta, A. and Ravindranath, N.H. (2012). Farmers' vulnerability to climate variability in Dimapur district of Nagaland, India. Regional Environmental Change, 13, pp. 153-164.

Jamir, M., Chang, C., Jamir, I., Thong, G. and Walling, T. (2022). Landslide susceptibility mapping of Noklak Town, Nagaland, North-east India using bivariate statistical method. Geological Journal. 57. pp. 1-15. doi: https://doi.org/10.1002/gj.4595.

Khuman, C. M. and Ibotombi, S. (2010). Ophiolite of Manipur: Its Field Setting and Petrotectonic Significance. Mem. Geological Society of India. no. 75, 2010, pp. 255 – 290.

Khuman, C. M., & Ibotombi, S. (2022). Source characterisation of the residual lherzolite and harzburgite ultramafics of Manipur Ophiolite Belt in the Indo–Myanmar Hill ranges, NE India. Geological Journal, 57(12), 5294-5307.

Khuman, C., Nagi, K., Ibotombi, S., Sanatomba, H., Aier, A., and Notoka, K. (2023). Structural and Geotechnical Approach of Characterization of the Causes of Meriema Landslide Along the Kohima–Wokha Road Section of the National Highway No. 61, Near Nagaland University-Kohima Campus Approach Road Junction, Nagaland, India. doi:10.1007/978-981-99-6395-9_2.

Mallet, F. R. (1876). Coalfields of Naga Hills. Mem. Geological Survey of India, xii, 2, pp. 269–363.

Marshak, S., & Mitra, G. (1988). Basic methods of structural geology. *(No Title)*.

Mathur, L. P., Evans, P., and International Geological Congress New Delhi, India) (1964) : (1964). Oil in India : a review.

McClay, K. R. (2013). The mapping of geological structures. John Wiley & Sons.

Minster, J. B., and T. H. Jordan (1978), Present-day plate motions, *J. Geophys. Res.*, 83(B11), 5331–5354, doi:10.1029/JB083iB11p05331.

Mitra N. D. & Chowdhury, A., (1970), Geology and coal resources of Nazira coalfield, south of Dikhu river, Tuensang district Nagaland. Rep F.S. 1969-70.unpublished.

Mitchell, A. H. G. and McKerrow. (1975). Analogous evolution of the Burma orogen and the Scottis Caledonides; Geol. Soc. Ant Bull. 86 305-315.

Molnar, P. and Tapponnier, P. (1975). Cenozoic tectonics of Asia: effects of a continental collision. Science, v. 18, pp. 419-426.

Moiya, J. N., Luirei, K., Longkumer, L., Kothyari, G. C., and Thong, G. T. (2020). Late Quaternary deformation in parts of the Belt of Schuppen of Dimapur and Peren districts, Nagaland, NE India. Geological Journal, 55(1), pp. 457-476.

Murrell, S. A. F. (1958). The strength of coal under triaxial compression. Mechanical properties of non-metallic brittle materials, pp. 123-145.

Murrell, S. A. F. (1963). A criterion for brittle fracture of rocks and concrete under triaxial stress and the effect of pore pressure on the criterion. Rock mechanics, pp. 563-577.

Murty, K. N. (1984). Geology and hydrocarbon prospects of Assam Shelf - Recent advances and present status. India. Petroleum Asia Jour.

Nandy, D.R. (1982). Geological set-up of the eastern Himalaya and the Patkoi-Naga-Arakan Yoma (Indo-Burman) hill ranges in relation to the Indian plate movement. Miscellaneous publication - Geological Survey of India. 41-3, pp. 205-213.

Nandy, D. R. (2001). Geodynamics of North-eastern India and the Adjoining Region. Journal of the Geological Society of India. doi: 10.1007/s12594-018-0866-1.

Notoka, K., Chang, C., Ezung, M., Thong, G., Kirha, V., Dzuvichu, K., Miachieo, K., Walling, T. (2025). Appraisal of a Complex Landslide at Kohima Town, Nagaland, India. Journal of Geosciences Research. 10. pp. 14-21. doi: 10.56153/g19088-024-0224-69.

Oldham R. D. (1883). Report on the geology of parts of Manipur and the Naga Hills. Published in the Memoirs of the Geological Survey of India Volume 19, 4.

Park, R. G. (1997). Foundations of structural geology. London: Routledge.

Peach, B. N. and Horne, J. (1907). Geological structure of the North-West Highlands, Geol. Survey Scotland Mem.

Pollard, D. D., & Aydin, A. (1988). Progress in understanding jointing over the past century. Geological Society of America Bulletin, 100(8), 1181-1204.

Ragan D.M. (1985). Structural geology. John Wiley & Sons.

Ramsay, J. G. and Huber, M. I. (1987). The Techniques of Modern Structural Geology. Volume 2: Folds and Fractures. Geological Magazine. 125. 316. doi: 10.1017/S0016756800010384.

Rao, A. R. and Murthy, K. N. (1980). On the origin of Naga thrust, Naga Hills, Assam. Bulletin of the Oil and Natural Gas Commission 17(2): 77-82.

Roy, R. K. and Kacker, R. N. (1980). Tectonic analysis of Naga Hills Orogenic belt along eastern peri-indian suture directorate of geology and mining, Nagaland.

Roy, R. K. and Kacker, R. N. (1986). Cenozoic deformation pattern and mechanism in the Belt of Schuppen and their role in hydrocarbon accumulation: Further exploratory concepts for Assam-Arakan Basin. Indian chapter, IGCP Projects 195 and 197. Meeting. pp. 197-221.

Saini, D.P.M. (2021). Balanced cross sections and structural evolution of Naga Schuppen belt NE India. Shodhganga. http://hdl.handle.net/10603/453301.

Sarma, H. (1985). Systematic Geological Mapping around Pukha-Lungwa-Chenwent-Hyou-Champang areas of Mon district, Unpub. Prog. Rep. GSI for F.s. 1984-85.

Sarma, H. and Bhartiya, S. P. (1978). Systematic Geological mapping around Tuli-Marangkong, Changtongya area of Mokochung district. Nagaland, Geological Survey of India Progress Report for FS 1977-78. (unpublished).

Saxena, S. P., Verma, K. P. and Joshi, A. (1981). Systematic Geological mapping in Tuli-Changtongya-Mopugchukit areas, Mokokchung district, Nagaland. Geological Survey of India Progress Report for F.S.1979-80. (unpublished).

Saxena, S. P. and Yedekar, D. B. (1979). Traverse geological mapping in parts of Tuensang, Mokokchung, Zunheboto, Wokha and Kohima districts. Geological Survey of India Progress Report, Field Season 1978-1979.

Singh, L. S. (2017). Geodynamics and Seismo-Tectonics of North East India: A Review. International Journal of Engineering Technology Science and Research (IJETSR) Volume 4, Issue 9, ISSN 2394 – 3386. doi: www.ijetsr.com.

Singh, S. K., Vidhyadharan, K. T. and Ray, S. B. (1983). Systematic geological mapping of Naga Hill ophiolites in the Phek district, Nagaland. Geological Survey of India, Progress report for the field season 1981-1982.

Singh, R.H., Ibotombi, S., Khaidem, K., Sanasam, S. and Khuman, C.M. (2019). Ichnological Significance of Upper Disang Formation and Lower Barail Formation (Late Eocene to Early Oligocene) of Nagaland, Northeast India, in the Indo-Myanmar Ranges. Journal of the Geological Society of India. 93. pp. 471-481. doi: 10.1007/s12594-019-1202-0.

Soibam, I., (1998), Structural and tectonic analysis of Manipur with special reference to evolution of the Imphal Valley, unpublished thesis of Manipur University.

Soibam, I. (2006). Relative plate motions in and around Manipur and its implications on the tectonics of Indo-Myanmar Ranges. Himalayan Geology 27, 111–122.

Soibam, I., M. Ch. Khuman & Sanasam, S. S., (2015). Ophiolitic rocks of the Indo-Myanmar Ranges, NE India: relicts of an inverted and tectonically imbricated hyper-extended continental margin basin? Geological Society, London, Special Publications, 413:301-331, doi:10.1144/SP413.12.

Spencer, E. W. (1993) Geologic Maps: A Practical Guide to the Preparation and Interpretation of Geologic Maps. ISBN10: 1577664620.

Spencer, E. W. (2017). Geologic maps: A practical guide to preparation and interpretation. Waveland Press.

Srinivasan, V. (2007). Regional structural configuration and seismic pattern of Belt of Schuppen in Northeast India. Journal of the Geological Society of India. 70. 801-814.

Srivastava, R. K. (1983). Systematic Geological mapping around Phokpur-Aipunger-Penkim-Fakimile areas, Tuensang district, Nagaland Geological Survey of India Progress Report for F.S.1982-83. (unpublished).

Srivastava, S. (2017). Lithofacies Analysis of the Palaeogene sediments in parts of Kohima Synclinorium, Nagaland, India: Implications for the Depositional Environment. Himalayan Geology. Vol. 38. 30-37.

Subhamenon, S. S. (2016). Crustal Shortening across the Indo Myanmar Ranges of Northeast India and its tectonic Implications. Shodhganga. http://hdl.handle.net/10603/251262.

Suppe, J. (1985). Geometry and Kinematics of Fault-Bend Folding. American Journal of Science, 283, 684-721.

Tapponnier, P., Peltzer, G. and Armijo, R. (1986). On the mechanics of the collision between India and Asia. - In: Coward, MP & Ries, A.C. (eds.): Collision Tectonics. Geological Society of London. Special Publication. v. 9. pp. 115-157.

Thein, M. (1973). A preliminary synthesis of the geological evolution of Burma with reference to the tectonic development of Southeast Asia. Geological Society of Malaysia, Bulletin 6, July 1973. pp. 87- 116.

Verma, P. K. (2023). Reorienting Techniques. In Optical Mineralogy (pp. 149-174). Cham: Springer Nature Switzerland.

Vidyadharan, K. T., Srivastava, R. K., Bhattacharyya, S., Joshi, A., and Jena, S. K. (1986). Distribution and description of major rock types. Memoirs of the Geological Survey of India, 119. pp. 18-27.

Weijermars, R. (1998). Taylor-mill analogues for patterns of flow and deformation in rocks. *Journal of Structural Geology*, *20*(1), 77-92.